One Step Membrane Filtration

A fundamental study

Haidari, Amir

DOI
10.4233/uuid:4f752da9-ccb7-462a-a5f8-a75b6532fa11

Publication date
2017

Document Version
Final published version

Citation (APA)
Haidari, A. (2017). *One Step Membrane Filtration: A fundamental study*. [Dissertation (TU Delft), Delft University of Technology]. https://doi.org/10.4233/uuid:4f752da9-ccb7-462a-a5f8-a75b6532fa11

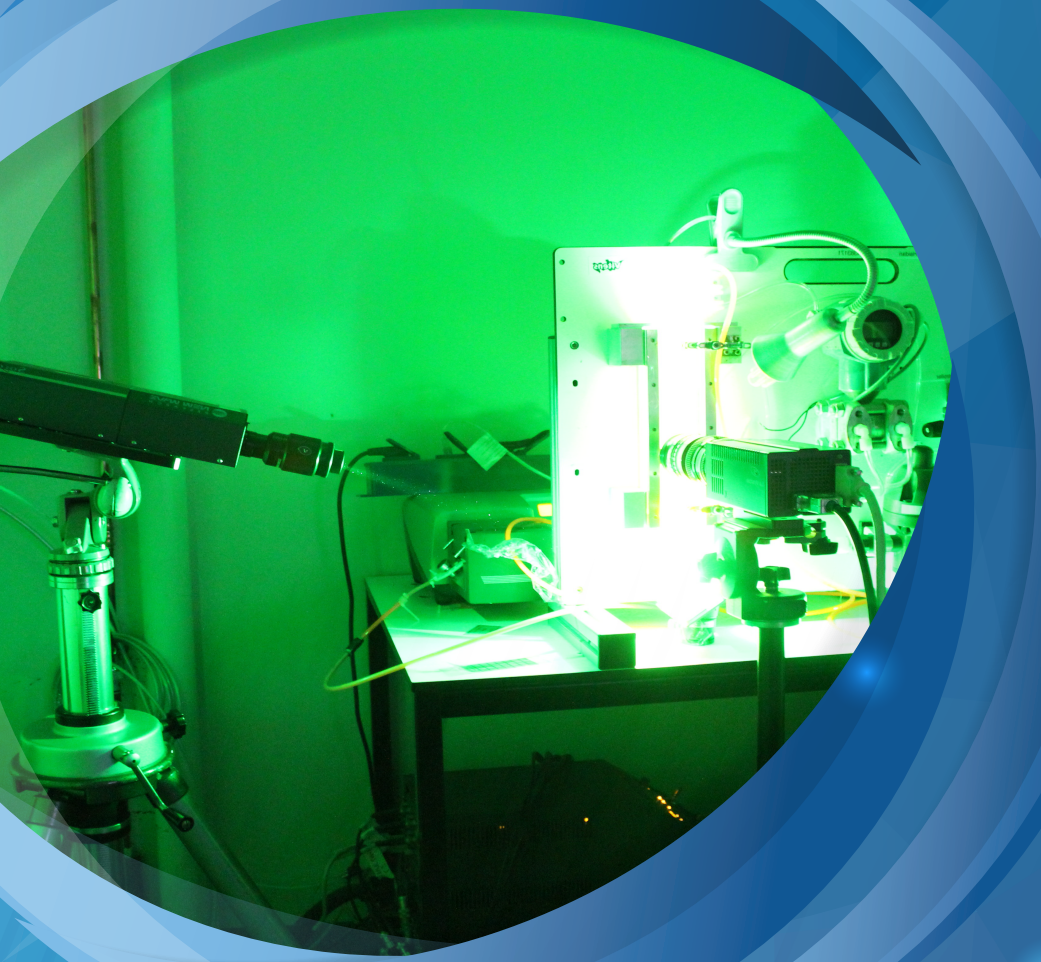

One Step Membrane Filtration

A Fundamental Study

One Step Membrane Filtration

A fundamental study

One Step Membrane Filtration

A fundamental study

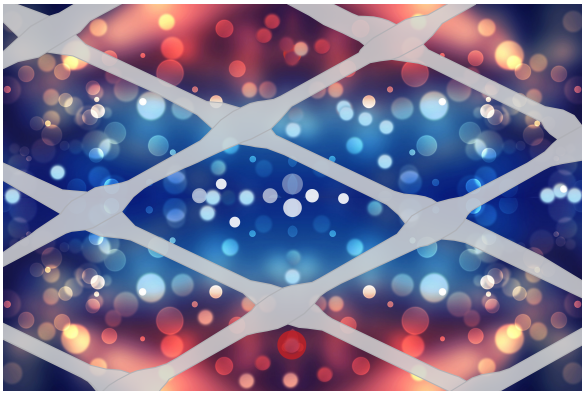

Proefschrift

ter verkrijging van de graad van doctor
aan de Technische Universiteit Delft,
op gezag van de Rector Magnificus prof. ir. K.C.A.M. Luyben,
voorzitter van het College voor Promoties,
in het openbaar te verdedigen op Woensdag 13 September 2017 om 10:00 uur

door

Amir Hoseen Haidari

Faculteit Civiele Techniek en Geowetenschappen (CITG),
Technische Universiteit Delft, Delft, Nederland,
geboren te Herat, Afghanistan.

Dit proefschrift is goedgekeurd door de

promotor: prof. dr. ir. W.G.J. van der Meer
copromotor: dr. ir. S.G.J. Heijman

Samenstelling promotiecommissie:

Rector Magnificus (Voorzitter)	Technische Universiteit Delft
Prof. dr. ir. W.G.J. van der Meer	Technische Universiteit Delft
Dr. ir. S.G.J. Heijman	Technische Universiteit Delft
Onafhankelijke leden:	
Prof. dr. ir. A.J. Karabelas	Centre for Research and Technology Hellas (CERTH)
Prof. dr. ing. M. Wesseling	Universiteit Aachen (RWTH Aachen)
Prof. dr. ir. H.D.W. Roesink	Technische Universiteit Twente (U-Twente)
Prof. dr. ir. A. Verliefde	Universiteit G(h)ent (U-Gent)
Prof. dr. ir. G.J. Witkamp	Technische Universiteit Delft
Prof. dr. ir. L.C. Rietveld	Technische Universiteit Delft, reserve lid

Keywords: Feed spacer; Reverse Osmosis Membrane; Particle Image Velocimetry; PIV; Spiral Wound Modules;

Printed by: Ipskamp Printing, Enschede

Front & Back: De PIV-opstelling die gebruikt werd tijdens dit onderzoek (voorkant), Toranj (een soort art) lijkt op de simulatie van Fibonacci (achterkant)

ISBN 978-94-028-0740-0

An electronic version of this dissertation is available at
http://repository.tudelft.nl/.

I stopped explaining myself when I realized
people only understand from their level of perception

Unknown

Contents

Summary

This study focuses on spiral-wound membrane (SWM) modules, which are the most common commercially available membrane modules for reverse osmosis (RO) and nanofiltration (NF).

While RO membranes can remove almost all kinds of substances from the feed water, they are usually equipped with pretreatment steps for conditioning and modifying the feed water to prevent clogging and fouling of these modules. Energy consumption, fouling and concentration polarization are considered as the primary challenges in these types of RO modules. These challenging factors depend on the feed water quality and they are related directly or indirectly to the design of applied feed spacer in SWM modules. A feed spacer provides a channel between two envelopes from entrance to outlet of a module to let the water flows tangentially over the membrane surfaces from the feed to the concentrate side. Additionally, feed spacers are designed to destabilize the concentration polarization layer; and thereby increase the mass transfer in SWM modules of RO. However, application of feed spacers to efficiently mix the flow comes at the expense of higher energy consumption and fouling formation. Therefore, it is important to understand the hydraulic conditions inside the spacer-filled channels such as those encountered in SWM modules of RO.

Previous RO-studies related to the production of drinking water are primarily performed with the assumption that RO-elements are used for desalination. In contrast to this assumption, the most commercially available configuration RO elements, SWM modules, gained more attention to be used for purification of freshwater resources currently. The main reason of using RO for freshwater purification is that it provides an effective barrier against the continuously emerging micro- and nano-contaminants, which cannot be (easily) removed by conventional treatment technologies. The energy use, scaling and retention in RO are influenced by the concentration polarization. When RO is applied on freshwater, the effects of concentration polarization on the energy use become significantly smaller because the osmotic pressure difference is negligible.

This thesis is divided into two parts. In the first part, this thesis describes a unique brackish water pilot study, which operates without chemical pretreatment. Such pilot study is referred to as one step membrane filtration (OSMF) system. An OSMF-system is an NF/RO-system in which membranes are applied directly to the feed water and operate

without chemical pretreatment.
In the second part, this thesis focuses on the hydraulic conditions of spacer-filled channels and the role of spacer geometry and orientation thereon. The effect of feed spacers on hydraulic conditions is investigated by studying the actual velocity profiles occurring in the spacer-filled channel and the relation between energy losses and spacer geometry.

Particle image velocimetry (PIV) technique is used to determine the orientation and configuration effects of spacers on the actual velocity profiles. PIV is a non-invasive and powerful tool to achieve high-resolution velocity profiles experimentally, which can be used for verification and validation of numerical studies related to spacer-filled channels. 2D and 3D numerical studies have contributed significantly to our understanding of hydraulic conditions in SWM modules of RO. However, these numerical simulations are usually validated with low-resolution experimental methods. PIV measurements from this study, thus, can provide high-resolution experimental data ($7.4 \times 7.4 \mu m^2$) for validation of these numerical studies.

The first results in PIV technique is a simultaneous velocity profile, which is obtained by using each two taken frames at a determined time interval. In this thesis, the simultaneous velocity profiles are used to investigate the variation of temporal velocity at certain locations (points) inside a mesh of a spacer. The spatial velocity profiles that are discussed in this thesis obtained by computing the average of related simultaneous velocity profiles. Chapter 3 describes a detailed explanation about the experimental methods used in this thesis. Summary of chapter 3 is repeated in the experimental section of chapters 5, 6 and 7.

The effect of feed spacers on hydraulic conditions is investigated by comparing an empty channel with a spacer-filled channel, which was filled with a commercial feed spacer (chapter 5). The flow in the empty channel was in a straight line from inlet to outlet and it was steady compared to the flow in the spacer-filled channel. The spatial velocity profiles of spacer-filled channels showed a bimodal shape with a peak at low-velocity ranges and a peak at high-velocity ranges. The low-velocity regimes occurred mostly in regions close to the filaments and a high-velocity regimes occurred at the narrowed parts of the channel or directly after the narrowing parts. The difference between low and high velocity regimes with regard to the velocity magnitude and frequency was higher at a higher flow. Although the increase in velocity magnitude causes generation of a higher shear, it is not necessarily beneficial. That is because the optimal flux as the results of destabilization of the concentration polarization layer will be achieved at a specific velocity. A further increase of the velocity from this optimal velocity will have only a marginal effect on destabilization of the concentration polarization layer, enhancing the flux and consequently production increase.

The hydraulic conditions inside a spacer-filled channel are influenced by configuration as well as orientation of the spacer. The pressure drop, which is measured during this thesis inside the channels with commercial feed spacers was in good agreement with pressure drop from previous mathematical models. Previous studies reported a lower

pressure inside the channels with the cavity spacers than the channels with zigzag spacers. The zigzag or net-type configuration is the common configuration used in SWM of RO. In the zigzag configuration, two layers of filaments with equal average diameter lay on top of each other and make an angle of 45° with each other (hydraulic angle) and with the flow (flow attack angle). In the cavity configuration, the diameter of transverse filaments is smaller than longitudinal filaments. Cavity spacers in this study had a flow attack angle of 135°. The biggest ratio of transverse filaments' diameter to channel height was about 0.6 with cavity spacers. With cavity spacer used in this thesis, the flow was mainly in a straight line from inlet to outlet. The flow disturbance in channels with cavity spacers was at down- and upstream of transverse filaments. The flow acceleration over the transverse filaments of examined spacers was greater for cavity spacers with bigger transverse filaments. In channels with cavity spacers, the velocity was clearly higher at the channel side without transverse filaments than the channel side with transverse filaments. In channels with zigzag spacers, the flow close to the membrane was in the direction of filaments attached to the membrane, i.e. the direction of flow at the top of channel was perpendicular to the direction of flow at the bottom. The flow pattern at the middle of the channel was a combination of flow patterns at the top and bottom. The greater friction losses that were found for spacers with bigger relative height and smaller aspect ratio indicate that the orientation and geometry of transverse filaments contribute to pressure losses. However, it was not possible to find a reliable correlation for predicting the pressure losses based on the geometric characteristics of feed spacers in experimental conditions.

Effect of feed spacer orientation on the flow investigated by using the same commercial spacer at two different flow attack angles. For this purpose, three feed spacers are used with different thickness. The thickness of the top and bottom filaments was the same for each spacer. Pressure drop in the channel with the thinnest spacer was clearly higher at normal orientation (with a flow attack angle of 45°) than at ladder orientation (with a flow attack angle of 90°). The difference between two orientations in the channels with thicker spacers was insignificant. The difference between the lowest and highest the velocity was greater in ladder orientation than zigzag orientation. Commercial ladder spacers with the characteristics described in this thesis are more sensitive to fouling than zigzag spacers because in ladder spacers the velocity becomes virtually zero at the side of the channel where transverse filaments are attached to the membrane.

Samenvatting

Omgekeerde osmose, ofwel reverse osmosis (RO), membranen zijn met een dermate kleine poriegrootte dat zij in staat zijn om vrijwel alle in het water aanwezige componenten te verwijderen. De meest voorkomende membraanconfiguratie is de zgn. spiraal gewonden configuratie ("spiral-wound membrane" ofwel "SWM"). Bij deze configuratie zitten de RO-membranen gewikkeld rondom een centraal geplaatste afvoerbuis. Via deze afvoerbuis (de permeaatbuis) wordt het gezuiverde water (het permeaat) afgevoerd. De in het water aanwezige componenten (verontreinigingen) verlaten via de zgn. concentraatstroom de membraan module.

Hoewel de RO-membranen een uitstekende barrière tegen opgeloste en niet opgeloste componenten vormen, wordt een RO-installatie meestal voorafgegaan door een aantal voorbehandelingstappen om verstopping en vervuiling van de RO-membranen te voorkomen resp. sterk te verminderen. Naast het energieverbruik en het optreden van concentratiepolarisatie, wordt vervuiling dan ook beschouwd als een van de grootste uitdagingen bij toepassing van RO SWM-modules in de drink- en afvalwaterbehandeling. Deze drie aspecten hebben direct of indirect een relatie met de kwaliteit van het te behandelen water (voedingswater) en de configuratie van de SWM-module. Met name de configuratie van de voedingsspacer (feed spacer) speelt hierin een belangrijke rol. De voedingsspacer is een gaasvormig materiaal, geplaats tussen twee membranen, dat er voor zorgt dat het voedingswater evenwijdig (tangentieel) aan het membraanoppervlakte van de invoer- naar de afvoerzijde van het membraan module kan stromen. Tweede functie van deze voedingsspacers is het reduceren van de concentratiepolarisatie en daarmee de stofoverdracht in SWM-modules van RO te verhogen. Echter dit leidt tot een hoger energieverbruik, door een hogere drukval over het voedingskanaal door de aanwezigheid van een voedingsspacer. Daarnaast verhoogt het de kans op vervuiling en verstopping van de module, door dezelfde aanwezigheid van een voedingsspacer in het voedingskanaal. Het is daarom van groot belang om de hydraulische condities in RO SWM-modules nader te bestuderen om op die manier tot optimale configuratie (laag energieverbruik, minimale of geen vervuiling) van een SWM-module te komen.

In het verleden werd met name het gedrag van RO membranen bestudeerd bij het ontzouten van zeewater voor de productie van drinkwater. Echter, tegenwoordig worden de RO-membranen (en dus ook de meest commerciële configuratie van deze membranen, d.w.z. de SWM-modules) ook toegepast voor het zuiveren van zoetwater tot drinkwater.

De toepassing van RO op zoetwater heeft voornamelijk tot doel om de talloze nieuwe micro- en nano-verontreinigingen, die continu aan onze watervoorraden worden toegevoegd en moeilijk te verwijderen zijn met de conventionele verwerkingstechnieken, te elimineren. Het energiegebruik, neerzetting en retentie in zeewater RO-membranen worden beïnvloed door het fenomeen concentratiepolarisatie. Wanneer de RO-membranen op zoetwater worden toegepast is het effect van concentratiepolarisatie op het energiegebruik aanzienlijk kleiner omdat het verschil tussen de osmotische druk van feed en permeaat te verwaarlozen is.

Dit proefschrift bestaat uit twee delen: het eerste deel betreft de beschrijving van een unieke pilot van RO-brakwater die zonder chemische voorbehandeling functioneert. Dit soort pilotstudies waarin de NF/RO-systemen direct en zonder chemische voorbehandeling worden ingezet voor het zuiveren van het invoerwater is bekend als de “one step membrane filtration” systemen (OSMF-systemen).
Deel twee van dit proefschrift heeft betrekking op het analyseren van het gedragsmechanisme van smalle kanalen die gevuld zijn met voedingsspacers zoals de voedingskanalen bij SWM-modules. Het voedingsspacer effect op de hydraulische conditie in het voedingskanaal werd onderzocht door het bestuderen van de relatie tussen energieverliezen en voedingsspacer geometrie en het bestuderen van de werkelijke snelheidsprofielen in de voedingskanalen die gevuld zijn met een voedingsspacer.

De werkelijke snelheidsprofielen worden gemeten en gevisualiseerd voor verschillende configuraties en oriëntaties van voedingsspacers door de particle image velocimetry (PIV) techniek. De PIV-techniek is een non-invasief experimenteel hulpmiddel waarmee snelheidsprofielen met een hoge resolutie worden gemaakt. De PIV staat in de literatuur vermeld als een gewaardeerde techniek die snelheidsprofielen met een hoge resolutie kan genereren voor de verificatie en validatie van de numerieke studies in de spacerskanalen. De studies die worden uitgevoerd met numerieke modellen (2D en 3D) hebben aanzienlijk bijgedragen aan ons begrip van de hydraulische omstandigheden in SWM-modules van RO. Deze simulaties zijn meestal gevalideerd door experimentele methoden met een veel lagere resolutie dan de simulaties. De PIV-metingen die worden uitgevoerd in dit proefschrift kunnen experimentele gegevens met een hoge-resolutie aanleveren die meer geschikt zijn voor de validatie van numerieke modellen.
In de PIV-techniek komt een momentaan snelheidsprofielbeeld tot stand door opnamen van twee opeenvolgende frames. De temporele snelheidsprofielen werden geanalyseerd door het bestuderen van de snelheidsvariaties in tijd voor een beperkt aantal punten in een raster. Een ruimtelijk snelheidsprofiel is verkregen door het berekenen van een gemiddeld snelheidsprofiel uit de momentane snelheidsprofielen. Een gedetailleerde uitleg over deze benaderingswijze is te vinden in hoofdstuk 3 van dit proefschrift.

Het werkingsmechanisme van voedingsspacers werd in de eerste plaats onderzocht door het vergelijken van de hydraulische condities in een smal kanaal zonder voedingsspacer met een die gevuld was met een commercieel verkrijgbare voedingsspacer (hoofdstuk 5). In tegenstelling tot het kanaal met een voedingsspacer, stroomde het water in het lege kanaal in een rechte lijn van de inlaat naar de uitlaat. De figuren van de ruim-

telijke snelheidsprofielen hadden in gevulde spacerskanalen een bimodale vorm met een piek bij de lage snelheden en een piek bij de hoge snelheden. De lage snelheidsregimes traden voornamelijk in de gebieden dichtbij de fibers van de voedingsspacer en de hoge snelheidsregimes vond meestal plaats op versmalde delen van het kanaal of direct erna. Het verhogen van stroming veroorzaakte een groter verschil tussen de lage en hoge snelheidsregimes met betrekking tot de snelheid grootte en frequentie bij een hogere stroming. D.w.z. dat bij een hogere stroming de waarde en frequenties van de tweede piek in de bimodale grafieken groter was. Echter de toename in stroomsnelheid voor het generen van een hogere schuifspanning is niet noodzakelijkerwijs gunstig. Dit komt omdat de optimale permeaat flux als gevolg van een verminderde opbouw van de concentratiepolarisatie-laag, bereikt wordt bij een specifieke snelheid. Een verdere verhoging van de snelheidswaarde heeft dan ook slechts een marginaal effect op de concentratiepolarisatie –laag en daarmee dan ook een gering effect op het verder verhogen van de permeaat flux, respectievelijk permeaat productie.

De configuratie en de oriëntatie van voedingsspacers hebben een significante invloed op de hydraulische condities van een voedingskanaal. De gemeten drukval bij de in dit proefschrift gebruikte commercieel verkrijgbare voedingsspacers kwamen zeer goed overeen met drukvallen berekend op basis van mathematische modellen. Het vergelijken van verschillende commerciële voedingsspacers liet zien dat de drukverliezen in de spacerskanalen met cavity-configuratie lager was dan in de spacerskanalen met zigzag-configuratie. Zigzag of net-type configuratie is de meest toegepaste configuratie van voedingsspacers in SWM van RO. In de zigzag configuratie worden twee series van draden die een gelijke diameter hebben op elkaar geplaatst. De top- en onder draden maken een hoek van 90° met elkaar en een hoek van 45° met de richting van hoofdwaterstroom. In de cavity configuratie hebben de dwarsdraden een kleiner diameter ten opzichte van de hoofd draden. De cavity-spacers in deze studie hadden een stroominvalshoek, de zgn. “flow attack angle”, (de hoek tussen de dwarsdraden en hoofdwaterstroom) van 135°. Van de toegepaste cavity-spacers was er een die draden had met dezelfde diameter in de dwars- en hoofdrichting van de waterstroom en de andere hadden aanzienlijk smallere dwarsdraden dan hoofddraden. Uit het stromingsonderzoek bleek dat de doorstroming in de kanalen met cavity-spacers voornamelijk in een rechte lijn is van de inlaat naar de uitlaat. In de kanalen met cavity-spacers gebeurde de stromingsverstoring stroomopwaarts en stroomafwaarts van de dwarsdraden. De versnelling van water over de dwarsdraden was groter bij cavity-spacers met een grotere diameter van dwars draden. De stroomsnelheden in de kanalen met cavity-spacers waren kennelijk hoger aan de membraanzijde zonder dwarsdraden dan aan de zijde met dwarsdraden.

De stroming in de kanalen met zigzag-spacers is in een rechte lijn van de inlaat naar de uitlaat van kanaal bij lage Reynoldsgetallen (Re<30). Bij hogere Reynoldsgetallen (Re > 30) is stroming aan de boven- en onderkant van het kanaal evenwijdig aan de draden van de zigzag spacers. Dit betekent dat de stroomlijnen aan de bovenkant van het kanaal loodrecht staan op die van onderkant van kanaal. De stromingsrichting in het midden van het kanaal is een combinatie van de stromingsrichting aan de bovenkant en aan de onderkant van de membraan. Er zijn grotere wrijvingsverliezen gevonden voor voe-

dingsspacers met een grotere “relative height” en kleinere “aspect ratio”. Dit wijst erop dat drukverliezen langs het kanaal vooral bepaald worden door de vorm en de geometrie van de dwars draden. Het was echter niet mogelijk om op basis van deze experimentele condities een betrouwbare relatie te vinden die de drukverliezen langs het kanaal op basis van de spacergeometrie kan voorspellen.

Het effect van voedingsspacer oriëntatie op de stroming wordt onderzocht door het gebruikmaken van een aantal commerciële voedingsspacers. In elk scenario blijft de configuratie van een spacer ongewijzigd en wordt de hoek van het raster ten opzichte van de waterstroom (spacer’s flow attack angle) veranderd. Daartoe worden drie voedingsspacers met verschillende diktes gebruikt. In deze spacers was de dikte van de bovenste draden hetzelfde als van de onderste draden. De dunste spacer met een flow attack angle van 45° (normale oriëntatie) toonde een groter drukverlies in vergelijking met dezelfde spacer met een flow attack angle van 90° (ladder oriëntatie). Het drukverliesverschil tussen twee oriëntaties van dikkere spacers was verwaarloosbaar. Het lokale verschil tussen de laagste en de hoogste snelheid was groter in de ladder configuratie van een spacer. Met betrekking tot de vervuiling is de normale oriëntatie beter omdat gebieden met lagere snelheid gevoeliger voor vervuiling zijn.

چکیده

ای نام تو بهترین سرآغاز بی نام تو نامه کی کنم باز ای یاد تو مونس روانم جز یاد تو نیست بر زبانم

المنتهای مایچی (جلزونی) اسمز معکوس و نانو موضوع تحقیقی است که در پیش رو دارید. این المنتها رایجترین المنتهای تجاری اسمز معکوس موجود در بازار می باشند.

در حالیکه غشاهای اسمز معکوس قادر اند که تقریبا تمام انواع ناخالصی ها را از آب جدا سازند با این حال معمولا سیستمهای اسمز معکوس به مراحل پیش تصفیه ای مجهز می شوند تا از آلودگی رسوب و گرفتگی المنتها موجود در این سیتم ها جلوگیری به عمل آید.

مصرف انرژی، آلودگی المنتها و قطبش غلظت از چالش های اصلی در المنتهای مایچی اسمز معکوس می باشند. این عوامل چالش برانگیز توابعی از آب خوراک هستند و بطور مستقیم یا غیر مستقیم با نوع مشبکهای پلاستیکی بکار رفته در کانالهای خوراک ارتباط دارند. یک مشبک پلاستیکی خوراک، بین دو لفاف غشایی از ورودی تا خروجی المنت قرار می گیرد و کانالی را برای عبور آب خوراک به وجود می آورد تا آب خوراک بتواند بر روی هر یک از غشاهای اسمز معکوس به طور مماسی حرکت کرده و به سمت دور ریز المنت برسد. علاوه بر این مشبکهای پلاستیکی خوراک، طراحی شده اند تا لایه قطبش غلظت را بهم شات سازند و بدینوسیله انتقال آب خالص را به درون لفاف ها افزایش دهند. استفاده از مشبکهای خوراک برای مخلوط کردن موثر جریان منجر به افزایش در

مصرف انرژی و ارتقاء کرگتگی های مواد آلی غیرآلی و بیولوژیکی می شود. بنابر این فهمیدن شرایط هیدرولیکی درون کانالهای مشبک دار مانند کانالهایی که در المنتهای ماپچی با آنها مواجه هستیم از اهمیت بسزایی برخوردار است .

تحقیقات قبلی مرتبط با اسمز معکوس برای تهیه آب آشامیدنی به طور عمده با اینسوپیش فرض انجام می شدند که غشاهای اسمز معکوس برای نمک زدایی آبهای شور استفاده می شوند علیرغم اینسوپیش فرض المنت های اسمز معکوس و در نتیجه آرایش ماپچی این المنتها که بیشتر از سایر آرایشها بطور تجاری موجود می باشد اخیرا توجه بیشتری را برای تصفیه ی آبهای استخراج شده از منابع شیرینسازی خود معطوف ساخته اند دلیل استفاده از اسمز معکوس برای تصفیه ی منابع آبی شیرینسازی است که اسمز معکوس مانعی موثر در برابر آلودگیهای میکرومتری و نانومتری که بطور مداوم در حال ظهور در آبهای شیرینسازی می باشند و به راحتی توسط فناوریهای متعارف قابل حذف نیستند بوجود می آورد.

مصرف انرژی، رسوب و بازپس زنی یونها در المنتهای اسمز معکوس تحت تاثیر قطبش غلظت است . هنگامی که از المنتهای اسمز معکوس برای تصفیه ی آب شیرینسازی استفاده میشود، تاثیر قطبش غلظت برروی مصرف انرژی بطور قابل توجهی کاهش پیدا میکند دلیل آن اینست که در اینسازی تفاوت فشار اسمزی در دو طرف غشاء ناچیز می باشد

اینسپایان نامه به دو بخش تقسیم شده است . در بخش اول اینسپایان نامه، یک سیستم تصفیه آب شور منحصر به فرد که بدون پیش تصفیه شیمیایی عمل میکند توصیف شده است . اینسدل که به عنوان سیستم غشایی یک مرحله ای مشهور است به سیستم

اسمز معکوس اطلاق میشود که آب خوراک را بطور مستقیم و بدون هیچ پیش تصفیه شیمیایی بالا میکند. قسمت دوم این پایان نامه به طرز کار کانالهای مشبک دار و نقش مشبکها برروی وضعیت هیدرولیکی این کانالها میپردازد. این قسمت، عمتا اثرات مشبکهای خوراک را برروی وضعیت هیدرولیکی کانالهای مشبک دار مورد بررسی قرار می دهد. این مطالعات بوسیله تحقیق برروی نیمرخهای سرعت و رابطهء موجود بین افت فشار با هندسه مشبکها انجام می شوند.

اثرات گرایش و پیکربندی مشبکها بر روی نیمرخ های سرعتی که به طور واقعی اندازه گیری شده اند (و نه با ساختن مدلهای کامپیوتری) توسط تکنیکی به نام تکنیک اندازه گیری سرعت ذرات بوسیله ی تصاویر (س. ذ. ت)، انجام شده است. "س. ذ. ت" یک ابزار غیر تعرضی و یک روش قدرتمند و موثر برای دستیابی به داده های آزمایشگاهی با وضوح بالا می باشد. از این داده ها میتوان برای تایید و اعتبار سنجی مطالعات عددی در کانالهای مشبک دار استفاده کرد. در روش "س. ذ. ت"، یک نیمرخ سرعت لحظه ای با استفاده از دو عکس گرفته شده با فاصله ی زمانی معین بهم این دو بوجود می آید. نیمرخهای سرعت زمانی با استفاده از تغییرات سرعت در نیمرخهای لحظه ای در چند نقطه ی مشخص از یک مشبک مورد بررسی قرار گرفته اند. نیمرخهای سرعتی فضایی (مکانی) از میانگین سرعتهای لحظه ای حاصل شده اند. توضیحات دقیقتر درباره روش "س. ذ. ت" در فصل سوم این پایان نامه آمده است.

تاثیر مشبک ها بر روی وضعیت هیدرولیکی کانالها بوسیله مقایسه ی یک کانال بدون مشبک و یک کانال دارنده مشبک تجاری،

مورد بررسی قرار گرفته است (فصل پنجم). جریان در کانال بدون مشبک، بطور مستقیم از ورودی به خروجی و با حداقل تغییر مسیر بود. نیمرخهای سرعتی فضایی، شکل یک نمودار دو قله ای را داشتند که یک قله ی آنها در سمت سرعت های پایین نمودار قرار داشت و قله ی دیگر آن در سمت سرعتهای بالاد. رژیمهای کم سرعت بطور عمده در قسمتهای نزدیک به رشته ها رخ دادند و رژیم های پر سرعت در قسمت های تنگ کانال یا بطور مستقیم بعد از این تنگناها. تفاوت بین رژیمهای کم سرعت و پر سرعت با توجه به مقدار و فرکانس سرعت، در جریان های بالاتر بیشتر بود. گرچه افزایش سرعت باعث افزایش نیروی برشی می شود، ولی این افزایش نیروی برشی لزوما همه جا مفید نمی باشد. اینبدان دلیل است که شارژ مطلوب که از بین شاتل لایه ی قطبش غلظتی به دست می آید در سرعتی خاص (سرعت مطلوب) حاصل میگردد. ازدیاد سرعت از این سرعت مطلوب فقط اثر حاشیه ای بر بین شاتل لایه ی قطبش غلظتی، افزایش شارژ و در نتیجه افزایش تولید خواهد داشت.

وضعیت هیدرولیکی کانالهای مشبک دار، بطور قابل ملاحظه ای تحت تاثیر پیکر بندی و گرایش مشبک های موجود در این کانال ها می باشد. افت فشار در مشبک های خوراکی استفاده شده در این پایان نامه بطور قابل توجهی با افت فشار در مدلهای ریاضی استفاده شده در تحقیقات قبلی مطابقت داشت. در تحقیقات نامبرده افت فشار اندازه گیری شده در پیکر بندی های حفره ای کمتر از پیکر بندی های گنگره دار بوده است. پیکره بندی گنگره دار، پیکره بندی ای است که در آن دو لایه رشته با قطرهای برابر بر روی هم قرار گرفته اند و زاویه ی ۴۵ درجه با هم (زاویه ی هیدرولیکی) و با جریان (زاویه ی حمله ی جریان) می سازند. پیکره بندی حفره ای، پیکره بندی است که در آن قطر رشته های عرضی کوچکتر از قطر رشته های طولی می باشد. زاویه ی حمله ی جریان در پیکره

بندی های حفره ای این تحقیق ۱۳۵ درجه بود. بزرگ ترین نسبت قطر رشته های عرضی به ارتفاع کانال در مشبک های حفره ای ۰٫۶ بود.

در مشبک های حفره ای که در این پایان نامه مورد استفاده قرار گرفته اند، جریان آب عمدتا در یک خط مستقیم از ورودی به خروجی بود. در مشبک های مورد بحث، شتاب جریان آب برروی رشته های عرضی با قطر بیشتر، شدید تر بود. در کانالهای دارای مشبک های حفره ای، سرعت آب در سمتی از کانال که برروی غشای آن رشته های عرضی وجود نداشت، به وضوح بیشتر از سمتی بود که بر روی غشای آن رشته های عرضی وجود داشت. در کانالهای دارای مشبک های گنگره دار، جریان آب در نزدیکی غشاها در امتداد رشته های متصل به هر غشا بود. بدین معنی که سمت جریان نزدیک به غشای بالایی، عمود بر سمت جریان نزدیک به غشای پایینی بود. الگوی جریان در وسط کانال ترکیبی از الگوهای جریان در سمت بالادو پایین کانال بود. ضریب اصطکاک بزرگتری برای مشبک هایی با نسبت ارتفاع (قطر رشته های عرضی به ارتفاع کانال) بیشتر و نسبت فاصله (فاصله رشته های عرضی به ارتفاع کانال) کمتر به دست آمد که بیانگر آن است که شکل و هندسهء رشته های عرضی نقشی حائز اهمیت را در افت فشار بوجود آمده توسط مشبک ها بازی می کنند. با این وجود، در شرایط آزمایشی رابطه ای قابل اعتماد بر اساس مشخصات هندسی مشبک ها برای تعیین افت فشار یافت نشد.

تاثیر گرایش مشبک ها بر جریان با استفاده از مشبک های تجاری مشابه در دو زاویه ی حمله ی جریان متفاوت مورد بررسی قرار

گرفت. برای این منظور از سه مشبک خوراک با ضخامت های متفاوت استفاده شده. ضخامت رشته های بالایی و پایینی برای هر مشبک یکسان بود. افت فشار نازکترین مشبک به کار برده شده، بطور واضحی در گرایش معمولی (با زاویه ی حمله ی ٤٥ درجه) بیشتر از گرایش نردبانی (با زاویه ی حمله ی ۹۰ درجه) بود. تفاوت اختلاف فشار بین دو گرایش در کانالهای حاوی مشبکهای ضخیم تر ناچیز بود. تفاوت بین کمترین و بیشترین سرعت در گرایش نردبانی بیشتر از گرایش لنگره دار بود. حساسیت کانالهای دارای مشبک های نردبانی تجاری با ویژگی های توصیف شده در پیشنهادات نامه نسبت به آلودگی بیشتر از مشبک های لنگره دار تجاری استفاده شده است زیرا در مشبک های نردبانی سرعت جریان آب در سمتی از کانال که رشته های عرضی بر روی غشا قرار دارند تقریبا به صفر می رسد

امیر حسین حیدری

سنبله ۱۳۹٦ خورشیدی

Preface

This dissertation is submitted for the degree of Doctor of Philosophy at the Delft University of Technology. This thesis aims to provide a new perspective to developers, researchers and manufacturer of membranes, particularly those who are dealing with the spiral-wound membrane (SWM) modules of reverse osmosis (RO) and nanofiltration (NF). In the remainder of this thesis, the term RO refers to both RO and NF. The small footprint and the simplicity of SWM modules of RO make them attractive to be used as the essential part of water purification systems. Permeate of RO can be engineered to be used as drinking water, feed water for crops in green houses, ultrapure water to be used in industry or manufacturing of pharmaceuticals, etc.

It is my hope that this thesis helps with a better understanding of the hydraulic conditions in the spacer-filled channel and serves as a tool for validation of related computational models.

This thesis has two primary objectives: introducing one step membrane filtration (first part) and providing a deeper understanding of the hydraulic conditions inside spacer-filled channel by a high resolution experimental method (second part). The one step membrane filtration concept aims to reduce the pretreatment of RO to mechanical processes and to use the RO membranes as the only purification step for production of drinking water. In the second part, this thesis provides information about the hydraulic conditions of the spacer-filled channel. The information is gained experimentally by using the particle image velocimetry.

Researches described herein were conducted under the supervision of Professor W.G.J van der Meer in the Department of Sanitary Engineering, Faculty of Civil Engineering and Geosciences of Delft University of Technology, The Netherlands between November 2011- 2016.

This work is to the best of my knowledge original, except where acknowledgment and references are made to the previous works. Neither this nor any substantially similar dissertation has been or is being submitted for any other degree, diploma or qualification at any other university.

Amir Hoseen Haidari
Delft, September 2017

Part 1

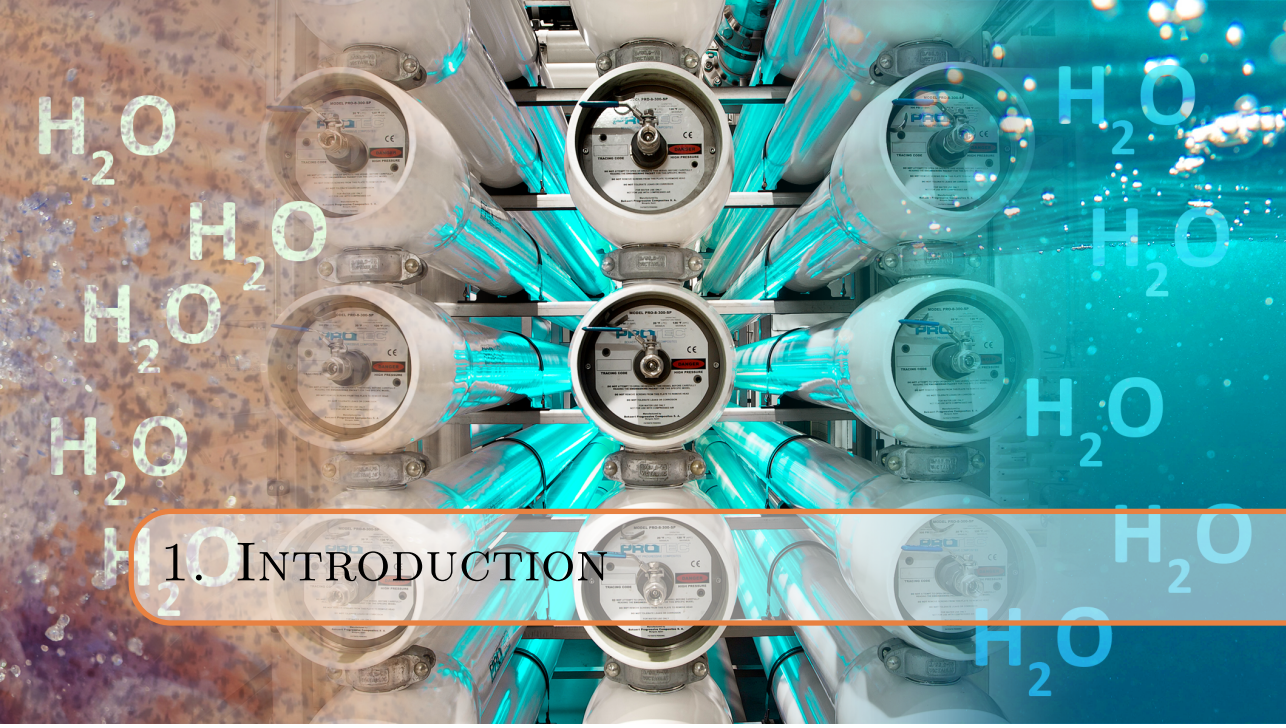

1. Introduction

It is in the nature of water to become transformed into earth
through a predominating earthy virtue;
it is in the nature of earth to become transformed into water
through a predominating aqueous virtue.

Avicenna

1

The rapid growth of the world population has brought several direct and indirect challenges regarding the safe and clean water supply in many corners of the globe. The direct challenge is a higher drinking water demand, which intensifies the pressure on finite fresh water resources. From the limited amount of fresh water (less than 2.5% of total water on earth) only less than one percent can be used for human needs and has to be shared by competing users of different political, social and economic powers. This low amount of water is often threatened by other (indirect) consequences of the rapid increase of world's population such as the climate change and new contaminants. These new contaminants are often harmful at low concentration and a serious challenge for conventional treatment plants.

Currently, membrane technology is being considered as a cost-effective technique to confront many challenges regarding the water purification. The required driving force for membrane separation processes could include pressure, electrical voltage, concentration gradient and temperature. Pressure-driven membranes are commonly used for water treatment. These membranes use a semi-permeable layer as a barrier to separate the feed water into the production stream and concentrate (rejected) stream. The pressure-driven membranes may be categorized with respect to the chemical composition of the semi-permeable layer (e.g. cellulose acetate and polyamide), the pore size of the semi-permeable layer(microfiltration, ultrafiltration, nanofiltration and reverse osmosis), or packing configuration of commercial modules (plate-and-frame, tubular, spiral-wound and hollow fiber). The membrane pore size determines the size of rejected material by the semi-permeable layer. Microfiltration and ultrafiltration can reject the particles, while reverse osmosis and nanofiltration can reject materials as small as molecules and ions. Therefore, in line with the classifications used in the book of "Principles of Water Treatment" [1], in the remainder of this study, the microfiltration and ultrafiltration are referred to as the membrane filtration and nanofiltration and reverse osmosis as reverse osmosis (RO).

RO membranes produce highly purified water to be used in drinking water, dialysis, power generation, pharmaceuticals and medical devices, semiconductors manufacturing, and the paper, sugar, beverage, and horticulture industries as well as in the concentration and reclamation of wastewater [2–11]. RO modules are produced predominantly in the spiral-wound configuration because they offer a good balance between the ease of operation, fouling control, permeation rate and packing density [12–15].The increase of production at low energy consumption is the essential prerequisite to a wider and more efficient application of spiral-wound membrane (SWM) modules of RO and may be obtained by further improvements of the treatment plants design as well as modules design to obtain a higher production at low energy consumption.

Chapter 2 describes a unique design of a pilot plan that uses the available natural hydrostatic pressure as a part of required energy for brackish water RO. The final aim of this pilot study is to examine the feasibility of one step membrane filtration (OSMF). The key concept of OSMF is to reduce the pretreatment of RO to only mechanical treatment, which is controversial to the current trend in designing of RO system. The usual trend is

to design the RO with the highest possible recovery, which often demands an intensive chemical pretreatment and poses challenges with respect to concentrate disposal and membrane fouling. In OSMF concept, membranes work at a recovery that no chemical dosage is required to feed water without increase of energy consumption. The type of feed water, therefore, plays a very important role, e.g. concentration polarization is the main concern in brackish water, biofouling is the major concern to river water and both are issues of seawater.

The production rate of a module can be improved by destabilizing the concentration polarization layer and preventing/controlling of fouling. The concentration polarization occurs due to the reduction of water content as the consequence of water permeation through the membrane. Permeation of water results in the salt concentration increase close to the active surface of membrane sheets and increase of osmotic pressure increase. In addition, the concentration polarization accelerates the onset of fouling [4, 16, 17].

Feed spacers are designed to promote the flow instability and give rise to the mixing of flow close to membrane sheets and destabilization of the concentration polarization layer in SWM modules. However, application of feed spacers comes at the expense of higher energy losses and higher possibility of (bio)fouling formation. Therefore, an optimal design for feed spacer includes a balance between the competing concerns; the energy consumption on one hand and the high productivity thus low concentration polarization and fouling on the other.

Optimal design of the feed spacer for SWM modules of RO would be possible by having a deep understanding of the hydraulic conditions inside the spacer-filled channels. The second part of this study (chapters 3 - 8) aims to elucidate a part of the complex hydraulic behavior of spacer-filled channels at low to moderate Reynolds numbers range (the operating conditions of SWM modules of RO). While computational fluid dynamics (CFD) technique is used by many research groups to gain a better understanding of phenomena inside the feed channel of RO, the number of experimental studies to validate such investigations at a comparable resolution is limited. Particle image velocimetry is referred to a suitable technique for validation of CFD.

The work reported in second part of this thesis uses the pressure drop measurements and 2D-PIV technique to produce data for the analysis and visualization of the dynamics of fluid flow through the narrow spacer-filled channels. The thesis aims to understand and visualize the variations of temporal and spatial velocity patterns and to determine the pressure drop:

- in a spacer-filled channel and in an empty rectangular feed channel of the same size
- in several spacer-filled channels with different configurations of feed spacers
- in several spacer-filled channels with different orientations of feed spacers

In agreement with these aims, the structure of this thesis is as follows. Chapter 3 reviews

previous studies which focused on improvements of SWM modules of RO particularly those as the consequence of feed spacer design. Special attention is given to studies investigating the performance of different spacer configuration and orientation and their effect on the pressure drop, fouling and mass transfer. Chapter 4 describes the methodology used throughout this study for generating and analyzing data from PIV and the differential pressure measured between the feed and concentrate streams. In chapter 5, effects of using a feed spacer inside an empty rectangular channel of the same size is discussed. The feed spacer used for this purpose was a commercial one which is commonly used in seawater RO. The results are compared to previous literature. The relationship between pressure drop and geometry of feed spacer is investigated, and the temporal and spatial velocity profiles obtained from PIV are illustrated in different shapes. Chapter 6 covers the effects of feed spacer configuration on the hydraulic conditions inside several spacer-filled channels. Six spacers are used of which four were net-type spacers and two other cavity spacers. Chapter 7 deals with the orientations of feed spacers. To this aim three spacers of different thickness are used, each at two different orientations; the normal orientation and the ladder orientation. Obtained velocity maps from chapter 6 and chapter 7 are related to the energy consumption and fouling potential of spacers using previous studies. Chapter 8 presents the conclusions and outlook on the results.

2. PURO: Underground RO

Summary

Depletion of fresh groundwater sources as the result of overdraft, salinization and pollution becomes a major problem in parts of the world. Desalination of brackish groundwater by membrane technology, e.g. reverse osmosis (RO), seems to be a promising solution to water scarcity problems. However, energy consumption and concentrate disposal are considered as the main reasons for avoiding RO application. In order to overcome these drawbacks, the PURO concept, which consists of vertically-configured RO unit in an especially drilled well is designed, installed and is going to be tested. The installation operates without any chemical pretreatment and therefore, the concentrate can be injected into a deeper confined aquifer that contains water of similar concentration. To avoid chemical pretreatment, the system operates at lower recovery (50%) than conventional brackish groundwater reverse osmosis (BWRO). Higher energy consumption, as the results of lowering the recovery, is avoided by using natural hydrostatic pressure at the depth that RO is installed and by extracting the permeate water only. PURO consumes about 39% less energy when compared to a conventional BWRO installation of the same capacity. This chapter describes the PURO concept and addresses its advantages and disadvantages. It also provides a rough calculation of water cost for PURO and conventional BWRO with emphasizing on the energy costs.

Parts of this chapter have been published in Journal of Desalination **403**, 208-216 (2017) [18].

2.1. INTRODUCTION

Reliable access to freshwater is one of the fundamental pillars on which a society is built. However, only a tiny fraction of planet's water is directly readily available as freshwater [2, 3].

The shortage of potable water, as consequence of population growth, current consumption patterns and climate changing, will be a major problem in the coming decades and will have the same social impact as that of increased energy prices [4, 6, 19, 20]. Groundwater is by far the most abundant and readily available source of freshwater followed by lakes, reservoirs, rivers and wetlands [3]. When used for drinking water, fresh groundwater sources are preferred to other readily freshwater sources because of the absence of pathogens. However, regions with sustainable fresh groundwater resources are shrinking by the day, throughout the world.

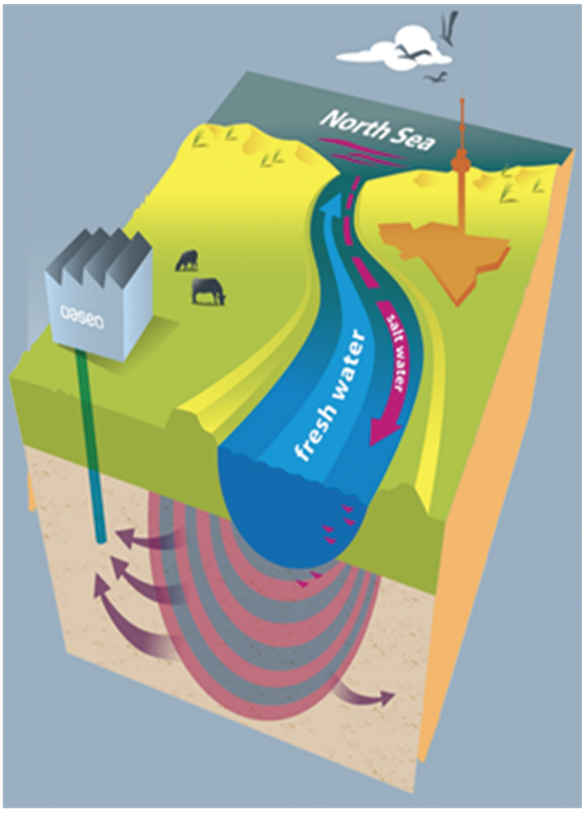

Figure 2.1: Salt water intrusion as the result of climate changing is one of the reasons of using brackish water as a new source for producing drinking water (source of picture: Oasen Water Company)

Salinization of freshwater due to intrusion of the saline water is one of the main problems of freshwater overdrafts (figure 2.1). In countries such as The Netherlands, which are laying below the sea level, over 100 pumping stations are closed due to intruded brackish water and it is expected that over 20% of remaining wells suffer from salinization in coming years [5]. Negative environmental impacts of over-pumping the freshwater are a worldwide problem (United States, Israel and Spain [21]). Artificial replenishment of groundwater by infiltration wells and infiltration through a dense network of ditches and canals [22], is used for years in The Netherlands as a solution for freshwater declination. Although the artificial groundwater recharge is an excellent alternative to natural refilling and is beneficial to environment, it has disadvantages such as considerable footprint and inapplicability of being used in the arid and semi-arid area due to high evaporation rate and operational cost.

2.1.1. APPLICATIONS OF BWRO

Brackish groundwater is referred [23–25] as an appealing alternative to fresh groundwater for future in The Netherlands due to is low content of suspended fines, organic pollutants and pathogenic micro-organisms. Brackish groundwater is theoretically free of xenobiotic substances when compared to fresh groundwater due to its age and the fact that it is not affected by human activities. This makes the brackish water the perfect feed water for RO considering the operation and fouling. Using brackish water is especially interesting for the inland installation, coastal areas with seawater intrusion problems and landlocked countries. Due to utilization of brackish groundwater, the fresh groundwater remains intact and the risk of intrusion of brackish water on the freshwater decreases. The latter becomes more important considering the current trends of climate change. Increase of seawater level as the consequence of climate changing causes seawater intrusion and seepage of brackish water as the final result [26]. However, the brackish groundwater is not directly consumable as drinking water and should be treated. Treatment of brackish water can be done by desalination technologies such as thermal and membrane desalination. However compare to thermal desalination, which is becoming more expensive because of rising energy prices, the membrane processes are becoming more attractive through cheaper material and system development. RO and nanofiltration are commonly used as the main techniques of producing potable water from the saline water.

Agriculture, especially at the sites of highly intensive greenhouses, demands large amount of freshwater with the minimum salt content. Water with minimum salt content is favorable to greenhouses because firstly, it doesn't damage the soil, it doesn't stunt the plant growth, and it doesn't harm the environment and secondly, it is used as the essence of the production of plant food with determined type and the concentration of nutrient for a specific type of crop. Precipitation is generally used as a source of water with low salt content. However, this is not enough to satisfy the water demands and it is only periodically available. In addition, it is foreseen that the natural precipitation in warm periods will decrease and evaporation rate will increase due to global warming leading to greater drought in warm seasons. On top of all, in some countries such as The Netherlands, the open reservoirs that are used for capture of precipitation have insufficient capacity to provide a reliable source during long summers. Therefore, BWRO is intensively used an attractive way of producing low concentrated water for agricultural section [5, 27]. Agriculture of several countries such as Spain (22%) [28], Australia (53%) [29], Israel and The Netherlands is partly depending on the desalinated brackish water. According to Dutch Central Bureau for Statistics, The Netherlands with an area of about 9488 ha of greenhouses (590 ha/million capita) was one of the biggest international exporters of greenhouses' products in 2014. Yet, the actual number of greenhouses that use the BWRO is not known due to illicit use of BWRO by some companies. A study from 2010 [28] shows that only 45% of total RO-concentrate was with permissions and the remaining 55% was illicit.

Despite its popularity, the BWRO is not appealing anymore for European greenhouseholders due to legal issues concerning disposal limitations of the concentrate water. The disposal issue becomes more serious since the announcing of stricter regulations of European Union due to the presence of xenobiotic substances such as antiscalants

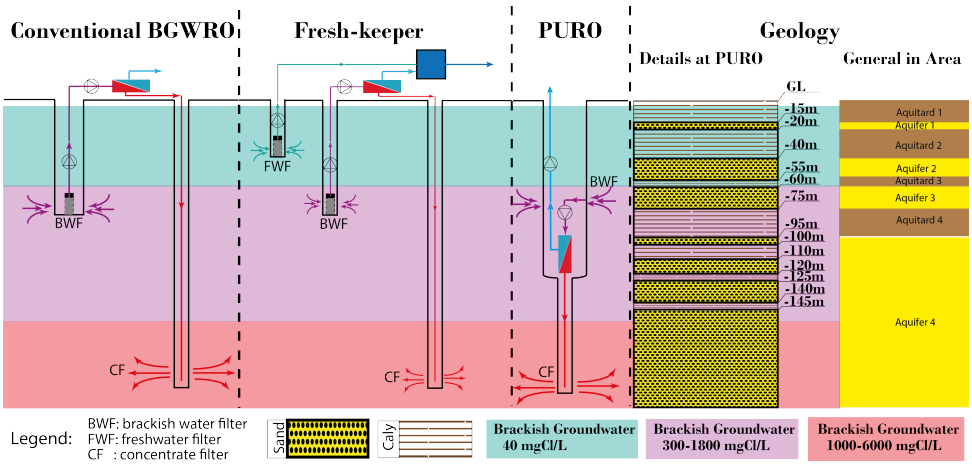

Figure 2.2: Treatment of brackish groundwater with reverse osmosis happens with conventional BWRO methods in The Netherlands (left). However, concentrate disposal into the ground is a problem and hence different new methods are emerging into the market. Fresh-keeper (middle-left) and PURO (middle-right) are two of these emerging technologies from which the latter is at studying stage. Fresh-keeper uses partly freshwater and partly brackish water, while conventional systems and PURO work with brackish water only. Fresh-keeper and PURO operate with a recovery of about 50% to avoid consumption of chemicals in pretreatment in order to have environmental-friendly disposal of concentrate. Fresh-keeper uses the fresh well and PURO uses the RO installation unit in depth to compensate for high energy consumption of BWRO. The hydrogeology at PURO location in details and in surrounding is respectively shown (right). Information is achieved from Oasen Water Company.

in the concentrate stream and uncertainty about the effects of disposal of concentrate into the ground. As the results, investigations for finding solutions for the concentrate disposal problem have drawn attention of many researchers recently. Most of the studies done were focused on decreasing of the concentrate volume by increasing the operational recovery to keep the energy requirements of the RO system at an acceptable range. However, great numbers of these studies end up developing the Zero-Liquid Discharges (ZLD) systems such as evaporative crystallization along with evaporative ponds. A review on treatment technologies of RO-concentrate is provided by Gonzales et al. [30] and Voutchkov [21] mentioned the available alternatives for seawater concentrate disposal. However, the application of ZLD systems is not economically attractive mainly due to a high energy consumption of these systems, especially for BWRO.

2.1.2. NEW TRENDS FOR BWRO IN THE NETHERLANDS

While it is economically prudent to maximize the recovery of BWRO installations, some new studies in The Netherlands are focusing on lowering the recovery in order to avoid the negative effects of presented xenobiotic compounds of concentrate on the target aquifer. The chemicals added in pretreatment step to enhance the recovery of BWRO are the origin of the xenobiotic compounds in concentrate. Fresh-keeper and PURO are two of such studies aiming at no chemical pretreatments of BWRO. The feasibility of Fresh-keeper, particularly concerning the concentrate disposal to a deeper confined aquifer is already proven [23] for The Netherlands and it is in its prestudy phase to be applied in

the state of Florida in US [31, 32]. Albeit, in such studies, to keep the production at the required level, a higher amount of brackish water has to be extracted, which comes at the expense of higher energy consumption. For compensation of energy requirements, in Fresh-keeper concept, the freshwater of the top aquifer blends with permeate of BWRO (figure 2.2). Fresh-keeper installations are mainly used to prevent salinization of freshwater wells and exist of two or three filters at different depth (a filter refers to the casing and filling of a well at the extraction injection point). Each of these filters is located in a separate well to prevent mixing of water during extraction or disposal. Water of top extraction point (freshwater filter) blends with the permeate water of deeper extraction point, which is produced by BWRO. The top extraction point is used to compensate the energy requirements of RO installation. The aim of deeper extraction point is to lower the fresh groundwater extraction. The bottom filter (injection point) is used for disposal of concentrate stream of RO installation in the deeper layer of the aquifer, under an impermeable clay layer to prevent short circuit with top layers. In the new design of Fresh-keeper, all three filters are located in the same well and separation materials are used to prevent mixing of different layers at the well.

Table 2.1: Rough comparison of conventional BWRO with Fresh-keeper and PURO on their strong (+), moderate (±) or weak (−) point in issues related to BWRO.

Concept	Conventional BWRO		Fresh-keeper	PURO
	R=80%	R=50%		
Using freshwater	+	+	−	+
Energy consumption	+	−	±	+
Concentrate disposal	−	+	+	+
Influence of human activities on concentrate disposal	−	−	−	+

PURO is another way of producing freshwater from BWRO at low recovery, which treats the water inside the ground. PURO uses the available hydrostatic pressure at installation depth to decrease the higher energy requirement, which is needed in low recovery BWRO installations. In contrary to Fresh-keeper, PURO uses only brackish water, which leads to preservation of freshwater sources. Table 2.1 summarizes the strong (+) moderate (±) or weak (−) features of different BWRO installations in comparing to each other.

The main part of this manuscript is devoted to compare the PURO with a conventional BWRO. That is mainly done by comparing the production costs. To reveal the advantages of PURO, the manuscript describes how PURO concept is designed and constructed (section 2.2). Then it will be explained how the cost calculations are performed and which parameters are used for calculations (section 2.3). At the end, based on the water cost, the advantages of PURO will be explained (section 2.4).

2.2. PURO: DESIGN AND SPECIFIC FEATURES

The PURO (Put-RO) concept or in well (Put) installed RO consists of PURO well and RO unit. After passing through the cartridge filters, the brackish water will be treated by RO elements with total recovery of 50% and without any pretreatment. The permeate

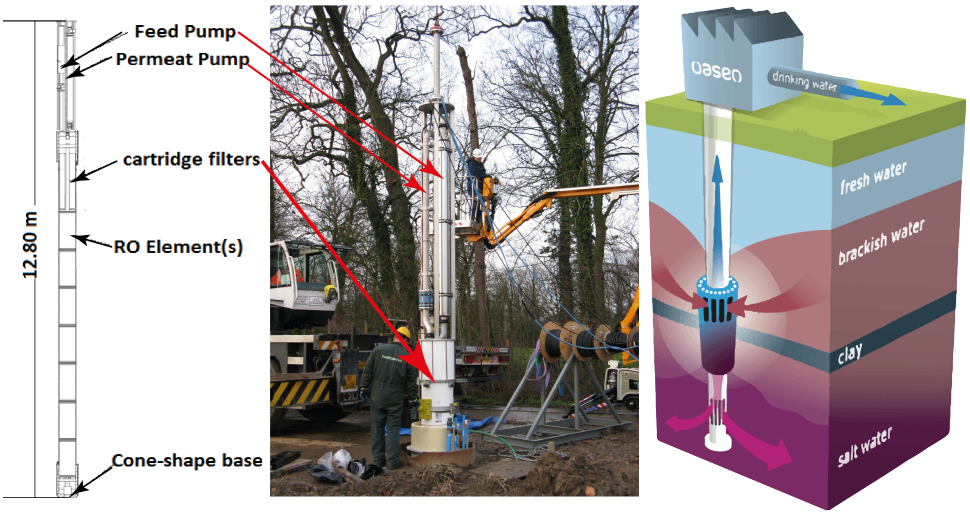

Figure 2.3: Schematic view of PURO inside the ground and simplified hydrogeology of site location (right), actual placing of RO unit inside the PURO well (middle) and a schematic view and positioning of important component of RO unit (left). Feed and permeate pumps are installed on top of the cartridge filters. Deign drawing (left) is from Logisticon water-treatments.

of installation is pumped to the surface to be mixed with the drinking water of the local pumping station during the pilot study and the concentrate, without any xenobiotic substances, is disposed to deeper confined aquifers. Figure 2.3 depicts the schematic view of the PURO (right), shows actual placing of the RO unit inside PURO well middle) and illustrates the schematic view of RO-unit (left). Suitable hydrogeology conditions for water extraction and well injection, local regulations and acceptable local costs for primarily study, drilling, material, etc. are important conditions of the application of PURO concept.

2.2.1. HYDROGEOLOGY AND WELL CONSTRUCTIONS

A simplified hydrogeology at site location, which represents the hydrogeology at most location in west part of The Netherlands illustrated in figure 2.4 and more detailed information of PURO site can be found in figure 2.2 (right). The hydrogeology at PURO site exists of a semi-impermeable layer of clay and peat to a depth of 15 m Below Surface Level (BSL). Underneath is a sandy aquifer, which contains freshwater, to a depth of 26 $mBSL$ and is separated by a major semi-impermeable layer of clay (26–40 $mBSL$) from the second aquifer. At greater depths, down to about 100 $mBSL$, an alteration of (fine) sands and poorly developed impermeable clay layers are found. The boundary between fresh and brackish water is found at the second aquifer (about 60–70 $mBSL$) around which the intake of RO unit is located. The injection filter of the concentrate is located at a depth of 175–200 $mBSL$. At this depth, the salinity of the groundwater is about 1000–1500 mg/l. The temperature of groundwater at the PURO site increases from 12°C at the surface level to 16°C at the depth of 200 $mBSL$. The groundwater table lies about 0.8 $mBSL$.

The PURO well is drilled by the airlifting/reverse circulation method. The diameter of the well decreases from 900 mm (top part) to 500 mm (lower part) at a depth of 125 $mBSL$. The casing or borehole of upper part, which contains the well intake filter and RO unit, is made of a high pressure PVC casing with a diameter of 630 mm. The lower borehole, which meant to infiltrate the concentrate, has a reduced diameter of 200 mm, in a well diameter of 500 mm. The annular space between the well wall and borehole is filled with sieved sandy filter material (0.8–1.25 mm) at the intake and injection point level. The natural semi-impermeable clay layers are restored with special bentonite clay, preventing a shortcut of water flow between the high salinity deeper aquifers and the less salty aquifer at the intake. The constriction at the transition part of the well is used for positioning of the RO unit.

2.2.2. RO UNIT

The RO unit composed of five spiral-wound cartridge filters, a feed pump, a permeate pump, seven RO elements inside a pressure vessel and measurement tools (figure 2.3-left). The unit weighs about 1500 kg at non-operational mode. This will be reduced during the operation mode according to Archimedes' principle due to injection of concentrate that causes the water pressure to rise about one bar [33]. The counter pressure will be increased in the case of clogging of the filter at the disposal point. Positioning and removal of the installation unit in the PVC casing can be done with an 8 cm stainless steel permeate pipe that works as a hanger at the top and eight wheels mounted around the pressure vessel for easy sliding of installation. The visual inspection of the RO-unit and

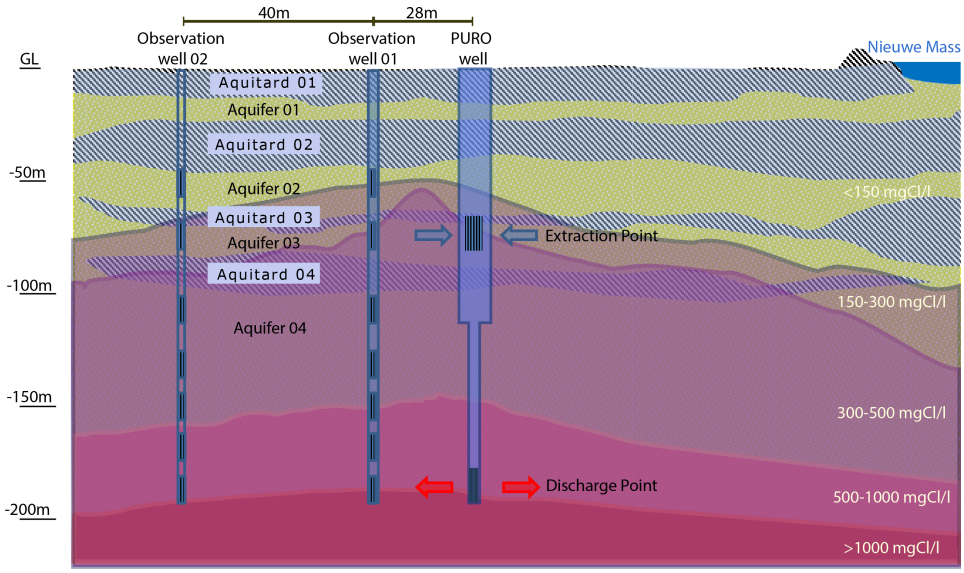

Figure 2.4: Simplified hydrogeology around the PURO and location of observation wells with respect to PURO. Data used for making the scheme are achieved from Oasen Water Company.

eventual cleaning and/or replacement of RO modules and/or cartridge filters will occur every two years, simultaneously during well rehabilitation to minimize the operational costs. Since the replacing-frequency of cartridge filters is higher than RO elements, five parallel cartridge filters are included to prevent frequent hoisting of the unit from the well.

RO MEMBRANES MODULES

8-in. modules are the current industrial standard and most popular elements of spiral wound modules of RO [34, 35] The chosen criterion for design of RO elements is that an element should be as large as possible to obtain maximal production yet small enough to be handled and installed by a single individual [34]. Recently, large-diameter RO elements such as 16 in.(406 mm) and 18 in. (457 mm) have started to emerge in the market. Laboratory experiment [36] and pilot study [37] showed a reduction of costs by the increase of module diameter due to a reduction of system footprint, number of housing, piping interconnection and seals between the modules. Ng and Ong [37] reported no significant improvement of performance in larger modules, but a reduction of about 20–25% in infrastructure, auxiliary parts and pipes costs. Bartel et al. [36] calculated the operating costs for different module diameters and three different water sources: seawater (TDS = 38000 mg/l), brackish groundwater (TDS = 2200 mg/l) and effluent water (TDS = 920 mg/l). A major cost reduction was achieved by increasing the diameter from 8-in. to 16-in. in all three types of water. A further diameter increase did not result in substantial cost reduction. The largest life cycle cost saving in their experiment was determined for the brackish groundwater and lowest for the seawater [36].

In PURO project, well diameter was the decisive parameter for designing the size of RO-elements (16 in.). Also using of one pressure vessel with big elements instead of smaller elements and plenty pressure vessels, was cost effective and more practical during construction, installation and maintenance as shown by former studies [36, 37].

FEED AND PERMEATE WATER

Availability of a structurally isolated aquifer with suitable quality and quantity for BWRO is the main hydrogeology conditions for the application of PURO concept. The composition of feed water should yield a concentrate with low mineral saturation to avoid legal discussion of injection of the concentrate into a target aquifer. The feed water should be also favorable for membrane operation at reduced costs. BWRO systems generally operate at 2000–14000 mg/l of total dissolved solids (TDS) without any problems. The feed water composition of PURO is summarized in table 2.3 (TDS < 1000 mg/l). The RO-unit of PURO operates with recovery of 50% and capacity of 600 m^3/d. Permeate is transported to the surface as the only stream coming from the ground. Possibility of increasing the recovery to evaluate its effects on production, fouling and energy saving will be assess after analyzing the primary results.

CONCENTRATE DISPOSAL

High hydraulic conductivity and storativity of a confined aquifer for long time and low tendency of the clay minerals in the aquifer for mobilization by deflocculating are important characteristics of an aquifer to be recognized as the target aquifer for injection of the

concentrate disposal [24]. Study of Wolthek et al. [23] showed that dispose of supersaturated concentrate of BWRO (a Fresh-keeper installation) with recovery of 50%–75% to deeper aquifers (180 $mBSL$) did not lead to mineral precipitation in the target aquifer. On the other hand, deep well injection of similar pilot plan in other part of The Netherlands, which led to hydrochemical reactions such as cation exchange, precipitation of calcium carbonate and release of magnesium and strontium by dissolution of dolomite suggests that the precipitation of minerals is depending on water quality of extraction and injection point, membrane recovery and texture of the target aquifer [38]. However, monitoring of the water quality of the target aquifer, for a year, showed no significant alteration from native water quality of the target aquifer in both cases [23, 38]. Yet, the clogging of the target aquifer in a long run for a latter study is suggested to be prevented by lowering the pH, for instance by dosage of carbon dioxide or hydrochloric acid into feed water of RO [38]. From studying these results and considering the similarity of hydrogeology and recovery of these studies with PURO, it can be concluded that injection of concentrate into the target aquifer could be without the risk of aquifer clogging by PURO or can be mitigated by lowering the pH of feed water. The investigation of PURO site shows that hydrogeology conditions do not preclude the possibility of precipitation of calcium-related substance at some distance above the injection point (at the depth of 160 $mBSL$), due to finer texture of sand at this depth compare to injection point. Therefore, two observation wells are drilled respectively at distance of 28 m and 68 m (figure 2.4) from PURO well in order to meticulously monitor the water quality and obtain detailed information on the effects of brackish water extraction and concentrate disposal on different aquifers.

2.3. COST COMPARISON OF PURO WITH CONVENTIONAL BWRO

To reveal the advantages of PURO with regard to energy consumption, the unit water cost by PURO is compared with a conventional BWRO of similar properties such as quality of feed water, plant capacity, site conditions, qualified labor and plant life amortization. The unit production cost is a function of process capacity, site characteristics and design future [39]. The unit cost of the water is estimated by dividing the sum of the annual capital repayment and annual operation and maintenance by the volume of water produced during one year. Table 2.2, which is based on the approach of Watson

Table 2.2: Elements of costs analysis for membrane process (based on the method mentioned in desalting handbook for planner by Watson et al. [35]).

Unit cost of water			
Capital costs			Annual costs
Depreciating capital		nondepreciating capital	
Direct capital	Indirect capital		
Well supply	Freight & insurance	Land costs	Electricity
Brine disposal	Overhead	Working capital	labor
Process equipment	Owner's cost		Maintenance & spares
Axillary equipment	Contingency		Membrane replacement
Building			Insurance
Membranes			Chemicals
			Amortization

Table 2.3: Some design criteria, which are used for cost estimation of two scenarios.

Design case	Unit	Conventional BWRO	PURO
Feed Flow (Q_f	m^3/h	50	50
Recovery	%	50	50
Plant capacity	m^3/h	25	25
Pass configuration	–	1	1
Stages configuration in each pass	–	2	1
Number of pressure vessel (Stage 1)	–	4	1
Number of pressure vessel (Stage 2)	–	2	0
Number of element in pressure vessel	–	6	7
Diameter of each element	$Inches$	8	16
Number of elements used	–	36	7
Membrane area	m^2	1472	1122
Amortization period	$Years$	30	30
Number of wells	–	2 wells (one extraction & one injection)	Extraction & injection well in one

et al. [35] and Ettouney et al. [39] is used as the method of calculation of water production costs. However, it should be mentioned that the low capacity of the treatment plant cases high sensitivity of the calculation to small changes. The costs and numbers mentioned in the following parts are only used for clarification of the difference of PURO with conventional treatment plant by the use of most realistic values from two existing projects.

2.3.1. DESIGNING CRITERIA

Table 2.3 summarizes the design criteria used for cost calculations and table 2.4 shows the feed water quality at PURO site. The site conditions, which are associated with availability of feed water intake, brine disposal and pretreatment facilities, are assumed to be the same as both projects are newly designed. Also it has been assumed that construction of specific building is not necessary and will be an available site condition. However, the foot print of PURO is limited to only a recognition part on the ground, while the ground installation requires a bigger footprint. The site conditions will work in advantages of PURO in terms of costs by increasing the capacity. Availability of qualified operators, engineers and management personnel will results in shorter plant downtime and therefore, higher plant availability and production capacity. However, for comparison that is made in this manuscript these costs are assumed to be the same.

The same feed water composition has been assumed for site location of conventional BWRO. Considering the feed water quality (TDS = 981 mg/l) and low operational recovery (50%), it can be assumed that no problem with deep well injection is expected.

2.3.2. FACTORS AFFECTING THE COSTS

The annual fixed charges (annual capital charges) composed of annual depreciating costs and annual non-depreciating costs (table 2.2). The non-depreciating costs consist of the land cost and working capital. The latter is a percentage of annual operation and maintenance. The depreciating costs are composed of direct capital costs and indirect capital costs, which the latter is calculated as a percentage of direct capital costs.

Table 2.4: Feed water quality at extraction location, Ridderkerk The Netherlands (based on data from Oasen Water Company)

pH	7.1	–	
Q_f	50	m^3/h	
Component	Concentration	Component	Concentration
–	mg/l	–	mg/l
Ca	169	CO3	0.26
Mg	34.3	HCO3	280
Na	89.1	SO4	1.6
K	0	Cl	380.15
NH4	3.39	F	0
Ba	0.15	NO3	0
Sr	0		
SiO2	25		
TDS	981.35		

Indirect capital costs and non-depreciating costs together amount to slightly more than 40% of total fixed costs. Consequently, the direct capital cost is the baseline of calculation of fixed charges. Sections 2.3.2 and 2.3.2 respectively describe the assumptions, which are done for calculation of direct capital costs and annual costs. The percentages that are used for calculation of indirect capital costs are mentioned in sections 2.3.2.

DIRECT CAPITAL COSTS

Direct capital costs include the purchase cost of major and auxiliary equipment and construction cost (table 2.5). It is assumed that the membrane cost is about 17 €/m^2. The PURO is designed with one feed pump for the RO unit and one well pump for transporting the permeate water. The conventional BWRO installation is designed with one well pump for extraction of feed water and one feed pump for RO. The finished costs of the well(s), including the casting, were based on the actual projects.

INDIRECT CAPITAL COSTS

Indirect capital costs are generally expressed as percentages of the total direct capital costs. Freight and insurance, construction overhead, owner's costs and contingency costs are considered to be respectively 5%, 15%, 10% and 10% of total direct capital costs [35, 39].

Table 2.5: Values that are used for calculation of direct capital costs.

Parameters	Unit	Value in literature	Reference	Applied Value	
				Conventional BWRO	PURO
Membrane diameter	$Inch$			8	16
Membrane costs	€/ m^2		[39]	17	17
Pressure vessel (PV)	€/PV	950-2000	[40]	1000	21000
Pumps	€	differs	[41, 42]	16400	16500

Table 2.6: Parameters that are used to estimate the annual water costs.

Parameters	Unit	Value in literature	Reference	Applied Value	
				Conventional BWRO	PURO
Electricity	€/kWh	Differs	–	0.098	0.098
Repairs and spares	%$totalcapital$	1%–2%	[35, 39]	1%	1%
Membrane replacement	%/$Year$	3–20	[35, 39, 43]	13%	13%
Insurance	%$totalcapital$	0.5%	[35, 39]	0.5%	0.5%
Annual interest rate	%	5–10%	[35, 39]	6.0%	6.0%
Extraction costs	€/m^3	0.19	–	0	0
Well maintenance	€	–	–	10000	1000
Well rehabilitation	€	–	–	2500	3000

ANNUAL OPERATING COSTS

The expenses incurred after plant commissioning and during actual operation such as labor, energy, chemicals and spare parts are included in the annual operating costs. Table 2.6 shows the assumption used for operational costs. The fourth column of table 2.6 shows the references that some of these values are obtained. Generally, due to automation, a very small teams of engineer(s) and operator(s) are working in RO treatment plant. Since the capacity of the two scenarios is too small, it has been assumed that both units can operate fully automatic. A yearly RO-membrane replacement of 13% is assumed for both cases because a replacement rate of 20% and 5% is reported for membranes used respectively with high and low salinities [35]. The cost of repairs and spare parts, which is mentioned to be less than 2% of total capital costs on annual basis in the literature, is estimated to be around 1% for our study cases. As discussed earlier, no antiscalant will be added and it's assumed that there is no need of chemical cleaning during two years. As mentioned earlier, for chemical cleaning of RO membranes and replacement of cartridge filters, the PURO installation has to be lifted from the well. This is done every two years simultaneously during the well rehabilitation. The amortizations or fixed charges are accounts for annual interest payments for direct and indirect costs. It is obtained from multiplication of these costs with the amortization factor (equation 2.1). In equation 2.1 i and n respectively denotes the annual interest rate and the amortization period and assumed to be 6.0% and 30 years.

$$a = \frac{i \times (1+i)^n}{(1+i)^n - 1} \tag{2.1}$$

2.4. RESULTS AND DISCUSSION

The unit production cost of respectively 0.34 €/m^3 and 0.35 €/m^3 for conventional BWRO and PURO is estimated. The estimated costs are lower than cost ranges that are mentioned in the literature [44–48] because no water extraction taxes, no pretreatment and no post-treatment costs are considered in both situations. The post treatment is assumed not to be necessary because the produced water is not used as potable water and the distance between treatment plant and end user is not bigger than 200 m. The

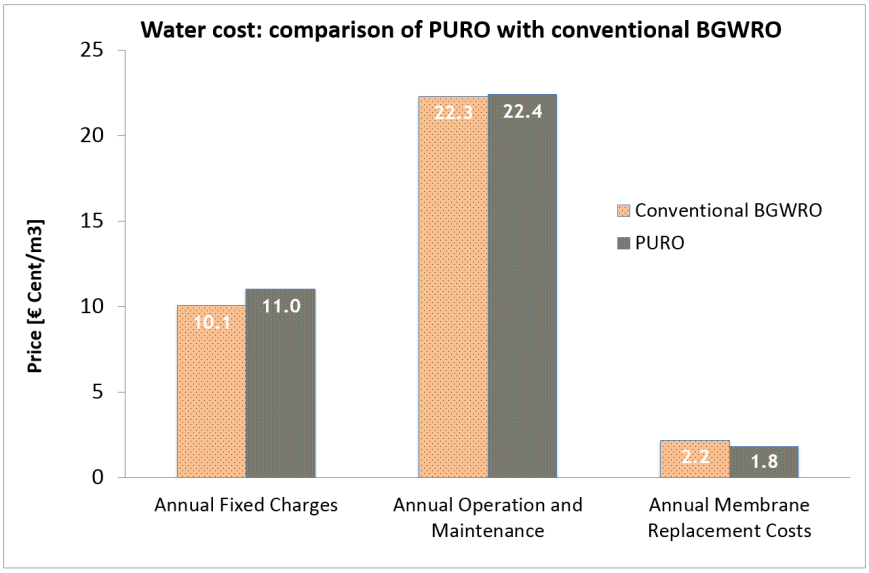

Figure 2.5: Cost comparison of PURO with a conventional BWRO installation. The fixed costs for PURO are higher than conventional BWRO, while the annual operation and maintenance of conventional BWRO is higher than PURO project.

permeate water of PURO aims in blending water of existing treatment plant and permeate of conventional BWRO is used as the main substance of preparing plant foods. Considering the quality of feed water, recovery of the system and new European regulations for concentrate disposal no pretreatment is applied.

The calculations are performed without considering the water extraction taxes due to spatial and temporal diversity of taxes. Generally, in The Netherlands, the central and provincial governments impose separated (respectively 0.19 and 0.01–0.03 € [49]) levies on groundwater extraction. However, since beginning of 2013, only the provincial taxes have to be paid, and governmental taxes are abolished. Since the level of provincial taxes, for current situation, is low compared to other cost elements, they are neglected for water cost calculation. However, for countries that levy charges on groundwater or for the situation that the groundwater taxes law in The Netherlands become effective again, PURO has the advantage of extraction only half of water (when recovery is 50%) to the surface. This means paying half of the water taxes with current regulations.
Figure 2.5 compares the important elements of water cost of PURO with conventional BWRO on a yearly basis. As figure 2.5 shows, the membrane replacement cost of conventional BWRO is slightly higher than PURO since the membrane area (table 2.2) of conventional design is slightly higher but the replacement frequency (table 2.6) of both designs is the same. The expenses incurred after plant commissioning and during actual operation such as labor, energy, chemicals and spare parts are included in the annual operating costs.

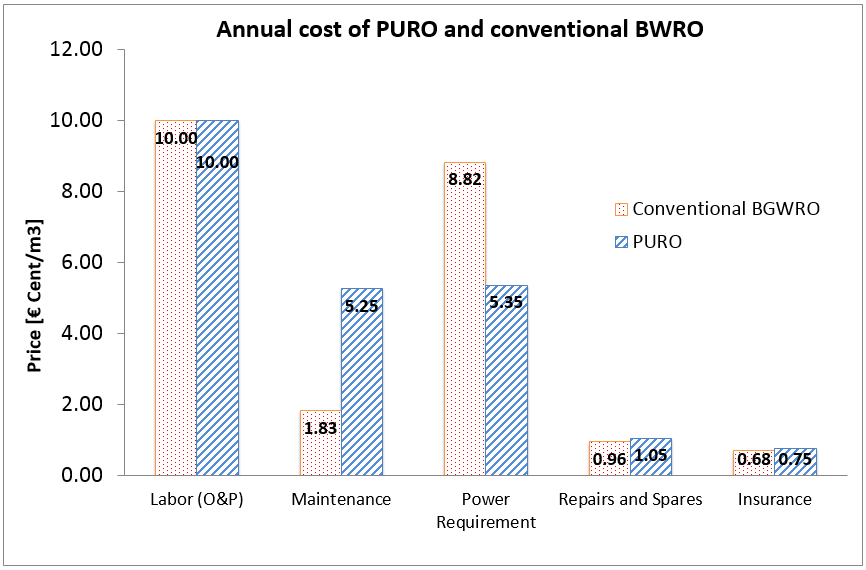

Figure 2.6: Annual operation and maintenance cost comparison (breakdown of annual operation and maintenance block from figure 2.5).

2.4.1. ANNUAL FIXED CHARGES

From the items considered for capital costs only plumbing cost of PURO is lower than conventional BWRO due to fewer numbers of connections with a bigger size in PURO. Construction of well(s) is a major factor of direct capital cost in both scenarios. Despite the construction of two separate wells in BWRO (figure 2.7), the cost of well construction in PURO is slightly higher than conventional BWRO due to complexity of PURO well and lake of experience in constructing of such wells. Considering the capital costs, manufacturing of a unique pressure vessel for PURO to work properly in the brackish water environment and endure the weight of RO installation is one of the major investment costs for PURO when compared to conventional BWRO. The cost of such a pressure vessel was about two times higher than all pressure vessels used for conventional BWRO.

2.4.2. ANNUAL OPERATION AND MAINTENANCE

Comparison of annual operation and maintenance costs shows that the total operation and maintenance costs are comparable for both cases (figure 2.5). A breakdown of operation and maintenance block (figure 2.5) is depicted in figure 2.6. The main differences in annual operation and maintenance costs appear in power utilization and in maintenance. The major cost elements of maintenance costs are hoisting cost of PURO and rehabilitation costs. Rehabilitation cost of PURO is smaller than conventional BWRO, but its maintenance costs is much higher than conventional BWRO, which is mainly caused by hoisting cost of PURO for inspection and maintenance. Figure 2.6 shows that lower energy consumption is the main advantage of PURO. PURO consumes about 39% less energy compared to conventional BWRO of the same capacity (figure 2.7), which is mainly due to more efficient use of available hydrostatic pressure.

In conventional BWRO, the hydrostatic pressure is mainly spent to transport the feed water to surface. At the surface, the water pressure is almost zero and has to be pressurized through the RO-unit (in this case with 9.70 $bars$) to be able to produce permeate water. From the total feed pressure about 1.5 $bars$ will be lost due to resistance of different instruments and the remaining will be lost through the concentrate, unless Energy Recovery Devices (ERD) are used at the concentrate end. However, application of ERD is not common in BWRO because of relatively low feed pressure and low flow rate of concentrate stream [50, 51] when it compares to seawater RO. Besides, the successful application of ERDs in brackish water installation is not yet proved and requires more detailed analysis of the entire RO system.

In contrary to conventional BWRO, the hydrostatic pressure in the PURO will be spent to drive the RO-unit. The hydrostatic pressure available at the PURO site (88 mH_2O) provides major parts (80%) of the operating pressure (110 mH_2O) and the remaining is provided by the installed feed pump (20%).

The extraction pump in PURO transports only permeate to the surface, but does not benefit from the hydrostatic pressure anymore since permeate is pressureless. The energy consumption of extraction pump in PURO seems to be higher than BWRO. That is mainly due to that permeate which has no pressure in PURO and extraction pump in conventional BWRO benefits from the available hydrostatic pressure at the site (50 mH_2O).

In The Netherlands, Optiflux [52, 53] is used for treatment of brackish groundwater in-

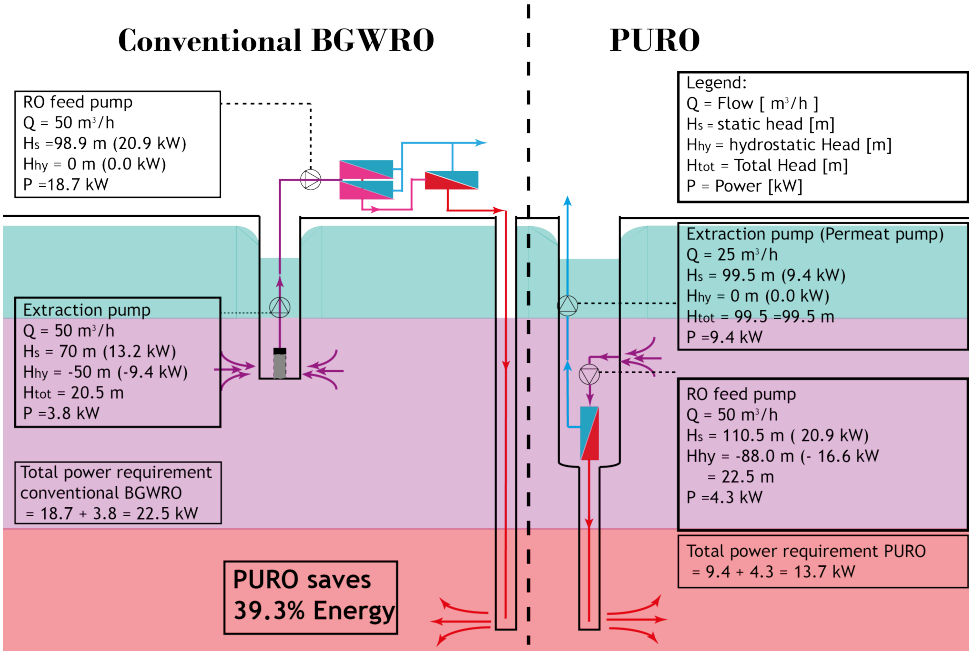

Figure 2.7: Energy consumption for PURO (right) and conventional BWRO (left). Energy consumption in PURO is lower than conventional BWRO and that is the main advantage of PURO when no chemical pretreatment is desired.

stead of the conventional BWRO. In Optiflux concept, the pressure vessel is equipped with a watertight connector in the middle that allows the concentrate to flow back and leave the pressure vessel from both ends and therefore, the pressure vessel acts as two separate pressure vessels with half of elements in each section. An Optiflux pressure vessel containing six elements, for instance, functions as two separate pressure vessels of three elements. In this way the feed pressure required will be reduced due to the reduction of hydraulic losses without extra investment for more pressure vessels. However, even with the application of Optiflux instead of conventional BWRO, PURO has about 28% less energy requirement.

2.5. CONCLUSIONS

Brackish groundwater is becoming an important source of water for inland RO installations due to the climate change as well as overdraft and contamination of fresh groundwater resources. When applying RO for treatment of brackish groundwater, the disposal of contaminated concentrate stream can be prevented by avoiding of chemicals pretreatment of feed water and direct application of feed water to the RO system. However, to prevent scaling of membrane modules, the operation recovery should be reduced. Therefore, more water should be extracted to have the same production capacity. As the consequence of more water extraction, more energy will be required. PURO is a solution to this higher energy consumption of RO systems operating at low recovery. PURO owes its lower energy consumption mainly to an efficient use of available hydrostatic pressure. Suitable hydrogeology conditions, local regulations and local costs for primary study, drilling, material, etc. are important conditions for the application of projects such as PURO. Availability of an aquifer with large quantity of brackish water with a favorable ion concentration for proper feeding of the RO unit and a confined aquifer with high hydraulic conductivity and storativity are the main hydrogeology conditions required for the application of PURO.

Since PURO operates inside the well, a good analysis of the location and feed water, a proper well construction and a good monitoring are essential for PURO. The extra equipment that is required for proper functioning of PURO results in extra investment cost of PURO. Furthermore, the maintenance of PURO is difficult and costly due to limited accessibility of PURO. Despite these higher investment and maintenance cost, the water cost by PURO is comparable with conventional BWRO. Although the production cost of PURO seems to be the same as conventional BWRO, it is a big step toward more energy and environmental friendly desalination of groundwater with RO. It is expected that in the future, the investment and maintenance costs for the PURO installation decrease due to increased experience in making such installations. Also, the application of PURO with higher capacity will reduce the maintenance cost of PURO.

II

Part 2

3. Literature Review

Summary

Spiral-wound membrane (SWM) modules are the most common configuration in reverse osmosis (RO) and Nanofiltration. The enhancement of SWM module design, particularly the geometric design of the feed spacer, can play a crucial role in the cost and a wider application of these modules. In addition to SWM modules feed spacers are also used in flat and sheet configuration of RO, forward osmosis, pressure retarded osmosis, membrane distillation, electrodialysis, etc. The feed spacer influences the flux, pressure losses, and fouling in the membrane process and consequently the product-water unit cost. While there has been a great shift in application of SWM modules of RO toward low salinity sources and the fact that the sensitivity performance of SWM modules of RO is higher at these waters, the configuration and orientation of feed spacers are hardly changed since the first design. A wider use of SWM modules, therefore, requires the adaptation of geometric parameters of the feed spacer to the water source. Improving the feed spacer's design according to the feed water type requires the knowledge of the studies done until now in spacer-filled channels and required investigations in future. This chapter reviews the role of the feed spacer in SWM modules and provides an overview of studies conducted in narrow spacer-filled channels to determine the effect of different geometric characteristics of the feed spacer on hydraulic conditions.

Parts of this chapter have been submitted to Journal of Separation and Purification technology

3.1. INTRODUCTION

Reverse osmosis (RO) has been used as a desalination technique for more than six decades. Historically, RO-membranes were designed for production of drinking water by desalination of seawater and brackish water. Currently, RO is a popular technology for the production of highly purified water used in drinking water, dialysis, power generation, pharmaceuticals and medical devices, semiconductors manufacturing, and the paper, sugar, beverage, and horticulture industries as well as in the concentration and reclamation of wastewater [2–11].

Figure 3.1 outlines the global NF/RO capacity by feed water (A) and by region (B). Although the use of RO for seawater desalination is still dominating the RO-market (figure 3.1-A), there has not been a notable increase in the use of RO for seawater desalination compared to RO application for other feed sources since 2002 [55]. In contrast, there has been an increase of about 40% in use of RO for purification of river water compared to the global installed capacity from 2002 [55]. Figure 3.1-B indicates that RO application for purification of river water happens primarily in parts of the world with rapid industrial growth and strict environmental policy. Given the environmental trends, the application of RO is projected to increase globally in the coming years due to forthcoming environmental regulations in these ar-

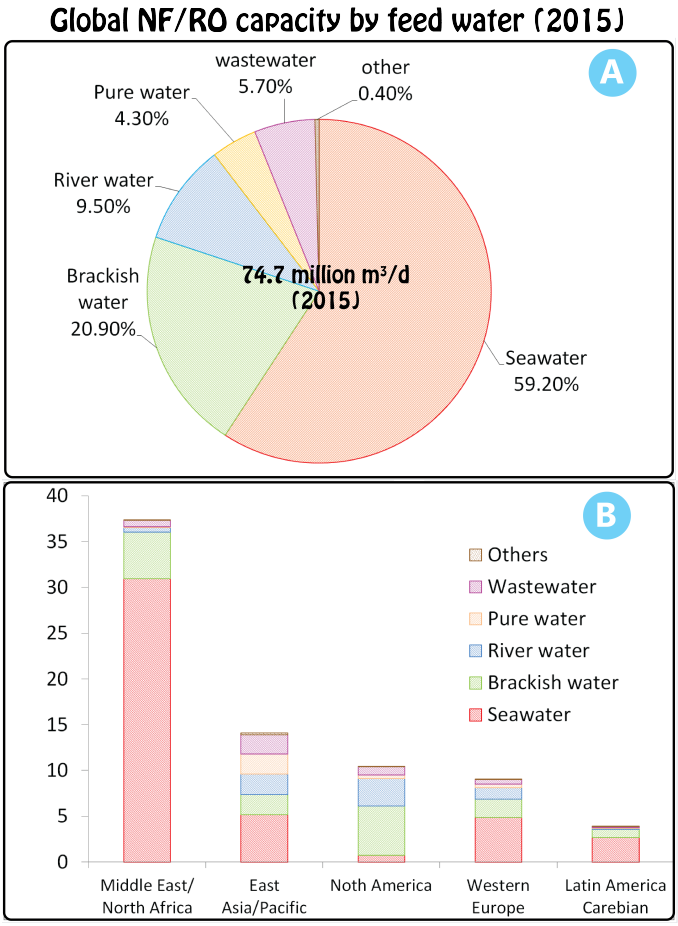

Figure 3.1: Global installed NF/RO capacity by feed water (A) and by region (B). The raw data obtained from DesalData [54]

eas and the influences that these measures would have on other parts around the world.

The spiral-wound membrane (SWM) configuration is predominately applied in NF and RO because they offer a good balance between ease of operation, fouling control, permeation rate, and packing density [12–15]. A wider and a more efficient application of this configuration requires further improvements in different parts of the membrane module. The feed spacer, as an essential part of these modules, has an important role in determining the hydraulic conditions of the feed channel; i.e. pressure drop and cross-flow velocity. The pressure drop is usually associated with the membrane operational cost and the cross-flow velocity with the membrane fouling. Despite numerous studies conducted on the feed spacer in different membrane applications, the modification of the feed spacer in RO has been limited to only a small increase in the thickness of this component.

This chapter will review studies conducted to determine the effects that feed spacers have on hydraulic conditions in the spacer-filled channels such as those that encountered in SWM modules of RO. First, this review provides a general background about SWM module configuration and related improvements and geometric characterizations of the feed spacer in particular. Next, it gives an overview of how feed spacers affect the efficiency and productivity performance of SWM modules with respect to the membrane production, pressure drop, and fouling. Finally, it discusses effects of the spacer geometry on hydraulic conditions of the feed channel. The main aim of this chapter is to provide the reader with an overview about the areas investigated and those that still need attention for feed spacer design in RO. This overview can also be used for other spacer-related membrane technologies working with nonwoven spacers.

3.2. BACKGROUND

In a treatment plant equipped with SWM modules of RO, a membrane block consists of several pressure vessels where each pressure vessel contains 1-8 modules (elements). In cases that there is more than one module in a pressure vessel, the modules are connected to each other through their permeate tube by means of an interconnector adapter(s) [56]. Each SWM module consists of envelopes, a permeate tube, and feed spacers. The envelope is formed by gluing two membrane sheets and the permeate spacer to each other from three sides in a way that non-active surface of membrane sheets face each other and the permeate spacer. Thus, the permeate spacer is inside the envelope and creates a flow pass for permeate water. Additionally, it supports the membrane sheets mechanically against (high) feed pressure [57], and therefore it is made of woven spacers with low permeability to have the required stiffness. This low permeability can have great impact on the pressure drop. However, the pressure drop in the permeate channel of RO is usually neglected by manufactures because SWM modules are historically designed for application in the seawater desalination. Schock and Miquel [58] reported that contrary to manufacturers' claims, the pressure losses in the permeate channel are not negligible. Koutsou et al. [59] confirmed the importance of pressure drop in permeate channel especially for the membrane modules applied on low salinity water. Additionally, they [59] mentioned that stiff and incompressible construction of

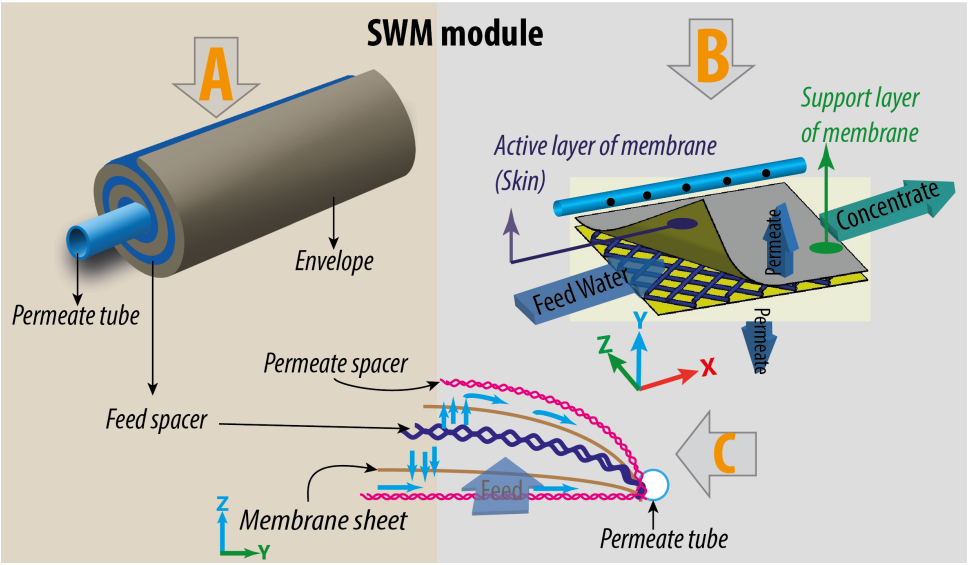

Figure 3.2: A schematic view of SWM module out of the pressure vessel (A), unwrapped situation with only two envelopes (B) and side view of the feed channel (C)

permeate spacer is of importance for seawater desalination due to high applied pressure in these modules.

From its fourth side, the envelope is glued to a perforated tube called the permeate tube. The active layer of each envelope faces toward a more porous spacer than the permeate spacer called the feed spacer. The feed spacer works as a supporting net and keeps the two adjacent envelopes apart [1, 60]; thereby, it provides a passing channel for feed water to move tangentially over the active layer of the membrane [61]. During the flow of bulk through the feed channel, a small portion of water permeates through the membrane and enters the inner part of the envelope, and then the water spirals toward the permeate collection tube. The permeate tube collects and transports the permeate water from envelopes of each element towards the permeate pipe of the pressure vessel. However, a great portion of feed water leaves the feed channel from an outlet, which is positioned against the feed inlet. The outlet stream is called the concentrate stream.

Cost savings in RO would make this technology widely available for sustainable and affordable water production in every corner of the globe. An effective method to achieve this target is to improve the SWM modules because the SWM module is the most applied configuration in RO. These improvements include transformation and consolidation in membrane sheet chemistry, re-evaluation the module design, and optimization of the RO-plant configuration and operation [62]. Among the aforementioned improvements, the impact of module design is most significant. Table 3.1 provides an overview of some improvements regarding the module design of SWM of RO.

Table 3.1: Selected studies addressing geometric improvements made in SWM modules

	Improvement	Results	Ref
Module Design	Using pressure vessels with two lead elements	The shear will be reduced. This results in formation of more a fluffy biofilm. The fluffy biofilm can be removed more easily with mechanical cleaning than impacted biofilm	[52, 53]
	Reducing the number o of elements in a pressure vessel	Linear velocity will be reduced and consequently the pressure losses. This results in productivity enhancement of a module	[52, 53]
		The impact of biomass was reduced on module performance.	[63]
	Diameter of a module	The increase in the membrane diameter results in the reduction of costs due to a reduction of the system footprint, numbers of housing, piping interconnection and seals between the modules	[36, 37]
	Length of a module	An element should be as large as possible to obtain maximal production yet small enough to be handled and installed by a single individual	[34]
		The standard element length is one meter because the industry has commonly made membrane sheets with a width of approximately one meter	[34]
Envelope	Number of envelopes in a module	The optimal numbers of the leaves are almost independent of the concentration, permeability of the membrane, transmembrane pressure (TMP) difference and thickness of the feed and permeate spacers	[58–60]
		The optimal geometry of the SWM module is reach at the highest number of membrane envelopes, when the glue-line is not considered	[58, 60]
	Width of envelope	For a constant membrane area, the highest optimal design is when the width of the envelope is the smallest	[59]
	Thickness	0.2-0.4 mm	[58]
Permeate Spacer	Configuration	Woven	[58]
	Pressure losses	Contrary to manufacturers' claims, the pressure losses in permeate channel are not negligible	[58]
Feed Spacer	Increasing the feed spacer thickness from 0.7 mm to 0.86 mm	0.86 mm thick spacer had a lower fouling tendency, cleaning frequency, and pressure drop	[64]

As mentioned in table 3.1, investigations of the optimal number of envelopes in a module [58–60] agree that the optimal SWM module design can be achieved with the highest number of envelopes when glue-line effect is neglected. It is important to consider the width of the glue-line in determining the optimal number of envelopes because for a higher number of envelopes, it reduces the efficient membrane active area at a higher number of envelopes. The optimal number of envelops in an SWM module of RO including the glue-line has only been determined by practical work of Schock and Miquel [58]. Using a 4-in membrane, Schock and Miquel [58] found that by increasing the width of glue-line, the optimal module design is at a lower number of envelopes. They [58] found an optimal of $4-6$ envelopes for a $4-in$ module with a glue-line width of 40 mm and optimal of $3-4$ envelopes for the same module diameter and a glue line of 80 mm. Manufactures normally produce $4-in$ SWM modules with $6-8$ envelopes. Koutsou et al. [59] and van der Meer et al. [60] referred to the importance of the glue-line but they did not mentioned the optimal number of envelopes including the glue-line.
To the authors' knowledge, Koutosu et al. [59] conducted the only study of the effect of membrane width on module performance. They found [59] that given a constant membrane area (37 m^2 for 8–in membrane), when the width of membrane decrease to its half, the number of envelopes increases, which results in module performance enhancement due to more uniform spatial distribution of the trans membrane pressure. In this study [59] the effect of the glue-line was neglected, which affects the productivity of the membrane. Additionally, it was not mentioned how the increase in the number of envelopes would affect the feed and permeate flow, particularly in area adjacent to the permeate tube. Table 3.1 also shows that a slight increase in the feed spacer thickness causes a lower fouling tendency, cleaning frequency, and pressure drop in the membrane modules. However, the extent of the effect of spacer thickness increase on different factors is not exactly clear from the study because the spacer was chemically enhanced by biocides on top of its thickness enlargement.

3.2.1. MEMBRANE PRODUCTIVITY

Arguably, one of the greatest improvements in the SWM module of RO took place when cellulose acetate membrane were replaced with polyamide and composite membrane. This transformation led to an increase in the productivity of and rejection by SWM modules of RO. For instance, it is reported [62, 65, 66] that compared to 8-in cellulose acetate membranes, the capacity of $8-in$ seawater RO elements made of a polyamide and composite configuration is doubled and the salt passage is decreased about three-fold. The cost of water produced by RO is calculated using ratio of operational and capital expenses to the production capacity. The product unit cost decreases with the increase of production volume at a given set of operating parameters. The production capacity is related to the average permeate flux defined as the flow rate of permeate per unit of membrane area (Equation 3.1).

$$J_{ave} = \frac{Q_p}{A_m em} = NDP \times K_w(Depends\ on\ the\ temprature) \tag{3.1}$$

The membrane permeability for water (K_w), which is also known as the mass transfer coefficient of the membrane for water or the specific flux (J_{SPE}) depends on the temper-

ature (Equation 3.2).

$$K_w = J_{SPE} = \frac{J_{ave} \times TCF}{NDP} \tag{3.2}$$

TCF in Equation 3.2 refers to the temperature correction factor and depends on the choice of reference temperature. Commonly, a reference temperature of 25°C is used as the reference to match the current literature on membrane filtration and the standard test conditions for the membranes as specified by the membrane suppliers. The reference temperature can be based on the local parameters and conditions. For instance, a reference temperature of 10°C is used in some countries and for some specific applications. At a given set of operating parameters, the average permeate flux determines the size of RO train and number of elements required, therefore influencing the capital expenses. The average permeate flux at a constant temperature is determined by using two known parameters: the membrane permeability (K_w) and net driving pressure (NDP). Treatment plants typically work at a constant production rate; i.e. a higher membrane permeability (mass transfer coefficient) results in a lower NDP and required feed pressure. In addition to the NDP and temperature, modifying the membrane sheet or increasing the shear at the boundary layers can improve the membrane permeability. The membrane sheet allows the transport of some compounds and prevent or delay the transportation of others and can have a symmetric or asymmetric configuration [9, 10, 67–74]. The first asymmetric RO membranes produced by Loeb and Sourirajan [75] were made of cellulose acetate and showed up to 100 times higher flux than any symmetric membranes known. The composite configuration of a membrane is made of a fragile discriminating layer with high selectivity (active layer) affixed to a porous support layer (non-active layer) [76, 77]. The support layer protects the ripping or breaking of the membrane sheet, while the active layer is responsible for the mass transport and the membrane selectivity.

PRODUCTIVITY REDUCTION

At a constant NDP, the average permeate flux decreases over time because of the degradation of specific permeate flux (membrane permeability) due to fouling formation [4, 16]; i.e. fouling results in decreased production capacity when a system operates at a constant NDP. The fouling rate is a function of the permeate flux rate relative to the cross-flow rate. A higher average permeate flux causes a higher concentration of particles at the membrane surface and a higher fouling formation rate. Therefore, fouling reduces the average permeate flux and increases the pressure drop of the membrane [78, 79]. The primary fouling mechanisms in RO are related to deposition of inorganic, colloidal and organic materials in addition to microorganism [80] in the feed channel either on the membrane surface or on the feed spacer. The extent and nature of fouling is related to several factors such as feed solution properties (concentration, pH, ionic strength, and component interactions), the membrane module configuration, membrane sheet characteristics (hydrophobicity, charge, roughness, pore size, pore size distribution, and porosity), and operating conditions (temperature, NDP, and cross-flow velocity). In addition to fouling, concentration polarization is another serious concern in the production capacity reduction of a membrane system. Concentration polarization is the consequence of water permeation, causing a higher salt concentration directly

adjacent to the membrane sheets compared to the bulk of fluid. Thus, concentration polarization is not a fouling type, but it reduces the membrane productivity by lowering the permeation of water through the membrane and enhancing the fouling formation [4, 16, 17] on the membrane. For instance, scaling is a consequence of the salt concentration increase as the sparingly soluble salts reach their solubility limit and deposit on the membrane surface [81, 82]. As with fouling, the degree of concentration polarization depends on the ratio of the permeate flow rate to cross-flow and with greater concentration polarization resulting from a higher permeate flow. This is the reason that concentration polarization is worse in the composite membranes, which have a higher permeate flow at the same pressure compared to cellulose acetate and polyamide membranes. Among different types of fouling, biofouling is probably the most difficult type to control because of the complexity of the ecosystems causing it [63, 83–89]. Biofouling is defined as a structured community of bacterial cells adhering to an inert or living surface due to attachment and growth [90–94]. The degree of biofouling is usually determined by measurement of ATP (adenosine triphosphate) for total living biomass [95] and TOC (total organic carbon) for total accumulated biomass [96, 97]. Biofouling can occur with a minimal number of microbial cells that adsorb to a surface and create a conditioning layer for more biomass accumulation [98, 99].

In SWM modules, spacers are regarded as the starting point for biofouling. The biofilm growth favors the feed spacer's junctions close to the module inlet, which leads to a distortion of the flow field and the creation of regions with low-velocity values close to the spacers' intersections [100]. With time, the biofilm accumulates further, eventually clogging a part of the feed channel and spreading the stagnant regions. As a result, the fluid stream through the flow channels is hindered, preferential channels are formed, and consequently, the permeate flow decreases [100–102].

PRODUCTIVITY IMPROVEMENT

Effective fouling control to improve the membrane productivity is possible by having sufficient information about the feed water and a profound understanding of fouling mechanisms and hydrodynamic conditions inside the feed channel. However, the fouling mechanisms are often complex and become even more complicated knowing that a remediation method for one type of fouling mechanism could worsen other types. For instance, increasing the axial flow rate is an effective way of removing the colloidal matter from the membrane surface and reducing the fluid resistance close to the membrane surface (reducing the thickness of concentration polarization layer) due to better flow mixing [103–105], but it is not effective in removal of biofouling. On one hand, the higher flow rate leads to a higher transport of nutrient into the flow cell and higher biomass formation; on the other, the biofilm formed at a higher rate of axial flow is more compact and harder to remove compared to the fluffy biofilm formed at lower shear [102, 106–117]. Consequently, given our current knowledge total fouling prevention seems to be impossible and using a single curative method to combat all fouling types is not practical. Operating the system at a higher shear than operational shear is generally considered an effective way of reducing the fouling and increasing the average permeate flux. A higher shear can be achieved by increasing the axial flow rate, creating flow instabilities, applying two-phase flow, and using a feed spacer. Rotation of the membrane [118] and flow pulsating [119, 120] are possible techniques to make the flow unstable. However,

Table 3.2: Selected studies conducted on mass transfer enhancement

Technique	Specification	Field	Effect of modification on mass transfer	Ref
Multi-layer spacer	3-layer spacer	UF	More turbulence and therefore less fouling and a higher mass transfer was observed	[86]
		ED	20% higher mass transfer was achieved compared to 2-layer	[87]
Two-phase flow	Empty channel	ED	With the increase of the gas to liquid ratio from 0 to 0.9, 70% increase in mass transfer was observed	[97]
	Single-layer net-type spacer		With the increase of the gas to liquid ratio from 0 to 0.9, 50% increase in mass transfer was observed	
	Multi-layer spacer		With the increase of the gas to liquid ratio from 0 to 0.9, no significant increase in mass transfer is observed	
	Using baffles	MBR	A better distribution of bubbles and the size of bubbles was observed. It could be used to lower the fouling and enhance the mass transfer	[98]
Double inlet/outlet cell	Empty feed channel	ED	The mass transfer was the same as single inlet/outlet channel	[97]
	Single-layer net-type spacer		Improvement was less compared to single inlet/outlet channel	
	Multi-layer spacer		Improvement was insignificant compared to single inlet/outlet channel	

these techniques are (i) expensive and (ii) not always easy to apply in SWM modules of RO. Application of a higher axial flow rate as the only method to increase the shear is not economically attractive because the required mixing in the flow, which is needed to effectively decrease the thickness of boundary layer, causes a high pressure drop. Using rotational shear and two-phase flow in addition to the increase of normal axial shear is suggested to be more effective in fouling removal [16, 103]. for example, the rotational shear can be generated by using double inlet/outlet flow cells. Kim et al. [121] and Balster et al. [122] examined the effect of rotational flow on the average permeate flux. These studies [121, 122] found that rotational flow has only a marginal effect on the flux enhancement. The impact of air sparging (two-phase flow) on the improvement of mass transfer was a function of the air/water ratio, bubble size, air distribution patterns, and duration of the air sparging [122–127]. Table 3.2 shows some investigation on the mechanisms of mass transfer enhancement. Periodic membrane cleaning with chemicals and dosing of chemicals in pretreatment are common methods to prevent and control membrane fouling [83, 128–132]. The chemical cleaning, however, is (i) expensive, (ii) of environmental concern (discharge regulations), (iii) not always effective, and (iv) a danger to the membrane lifespan. The price of scale inhibitors and cleaning chemicals alone is reported to be around 5 – 25% of operational costs [82]. Biofouling control is of particular importance in SWM modules of RO is the biofouling control, especially when wastewater, seawater, and fresh surface water are used as the feed.

Table 3.3: Selected studies addressing methods for biofouling control

Method	Suggested mechanism	Effectiveness	Ref
Copper dosage	Copper is thought to be cytotoxic by causing changes in the plasma membrane permeability or efflux of intracellular K^+ during the entry of Cu^{2+} ions	A reduction of biomass concentration to 8000 $pgATP/cm^2$ and pressure drop (18%) with a daily dosage of copper sulfate was achieved	[101]
	Copper can participate in Fenton-like reactions, generating reactive hydroxyl radicals, which can cause cellular damage imparted via oxidative stress		[133]
	Copper is believed to interfere with enzymes involved in cellular respiration and bind to DNA at specific sites		[134]
	Adding copper to water causes a reduction of the contact angle and hence an increase in the hydrophobicity of the feed spacer, which results in a decreased likelihood of biofouling		[132]
Nutrient loading	It is a function of substrate concentration and the linear flow velocity	For a limited substrate load, they attune themselves to this environment by changing their morphology	[117, 135]
Linear velocity	Limiting linear velocity causes less nutrient loading and therefore a lower possibility of biofouling	The formed biofilms were more compact and harder to remove	[102, 117, 136]
Gas sparging	Gas sparging causes an increase of shear	Less effective in SWM than MF and UF	[137, 138]
	It is a function of air/water ratio, bubble size, air distribution patterns and duration of the sparging		[122–127]
		The formed biofilms were more compact and harder to remove	[106, 108, 110, 112, 113, 117, 139]
		Complete removal of biofouling was not achieved. The remaining bacteria on the spacer/membrane caused a rapid regrowth and accumulation of cells	[140]
		Fouling attributed to inhomogeneous air distribution and channeling of the airflow, which can cause incomplete cleaning and an enhancement of scaling.	[124–126, 141]
Feed flow reversal	The feed flow reversal results in re-dissolution of the deposited scale into the solution	The feed flow reversal reduces the impact of biomass on membrane performance and gradually decreases the amount of biomass over time	[8, 63]
Feed flow reversal	Nucleation within the flow channel is due to local pressure differences as well as the presence of rough spots as the nucleation sites. Upon their formation, the bubbles are swept along with the flow due to their coalescing with larger bubbles, and the flow channel will become clean.	Efficiency is higher than air/water cleaning due to that no stagnant bubbles or bubble channeling is formed	[142]
CO_2 nucleation	Rough spots (junctions and filaments of spacers) enhanced the nucleation and subsequent growth of the bubbles	A higher removal efficiency is achieved compared to the air/water cleaning	[142, 143]

Table 3.3 provides a short overview of biofouling control studies. Presently, chemical cleaning is one of the most widely employed techniques for inactivating and removing biomass from RO and NF [130]. This method normally involves dosing biocidal chemicals in the feed water of a membrane system in order to destroy the biofilms [128, 129]. Several biocidal chemical agents have been documented for this use, ranging from acidic cleaning to caustic cleaning and enzymatic cleaning techniques [130, 131]. Multiple studies have shown that a very low dosage of copper [116, 144] and other metals such as silver and gold could be efficient in disinfecting water against microbial biofilms. However, chemical agents are known to reduce the lifespan of the membranes [128]. Additionally, biofilms have a high degree of resistance to many disinfectant, even against antimicrobial compounds such as metal ions [132]. Finally, chemical cleaning could be ineffective due to the effect that it has on other non-targeted fouling types or due to the effect that traces of chemical cleaning has on other locations in the treatment plant. For instance, ineffectiveness of chemical cleaning could be due to residues leakage of chemicals from pretreatment to membrane unit. In this context, it has been shown that systems with continuous chlorination have a higher rate of membrane biofouling [145, 146]. This is most likely due to the formation of assimilable organic carbon (AOC), which serves as indicator of the biological stability of the water, with high levels leading to the biological (re)growth during subsequent return to normal water production through the particulate fouling [92, 101, 147].

3.2.2. ENERGY AND PRESSURE DROP

Studies have shown that energy is a major contributor to the operational costs of RO systems. The required energy for an RO system includes the energy for pumping the feed water, running equipment during pre- and post-treatment, and operating the transfer pumps and high-pressure pumps, among which feed pressure pumps require the most energy to operate [148–150]. The power consumption of a feed pump is a function of feed pressure, recovery and equipment efficiency. At a determined feed pressure, the average flux (J_{ave}) over a module decreases because NDP (Equation 3.3) decreases as a result of the increase in flow friction losses and osmotic pressure of the feed [148].

$$NDP = \frac{J_{ave}}{K_w} = P_{TMP} - \pi_{TMP} = (P_f - P_P) - (\pi_f - \pi_P) = (\frac{P_F + P_C}{2} - P_P) - (\frac{\pi_F + \pi_C}{2} - \pi_P) \tag{3.3}$$

NDP is a measure of available driving pressure to force the water through the membrane from the feed side to the permeate side and is related to the average permeate flux of the system (J_{ave}) and membrane permeability (K_w) [148, 151]. The (available) net driving pressure (NDP) is the difference of the transmembrane pressure and transmembrane osmotic pressure. The pressure losses could be expressed in terms of total pressure drop (ΔP), which is the sum of the pressure drop at successive pressure vessels, interconnections of membrane elements, the permeate channel and the feed channel. The pressure drop in the sequential pressure vessels and successive modules in a pressure vessel can be minimized with an optimal design of the pipes and interconnectors. In an SWM module, usually only the pressure drop in the feed channel (Δp) accounts for the pressure drop calculation. Permeate pressure drop has shown [58] to have potentially more than minor effects on the total pressure losses. Effects of permeate pressure

losses on the feed pressure become particularly important in low salinity water sources, but there is a limited number of investigations in this area. The feed channel pressure drop includes frictions as a consequence of the (clean) channel geometry and frictions as a consequence of fouling. The clean feed channel pressure drop is a function of frictions at the walls and the feed spacer as well as changes in flow directions and flow patterns. Generally, the presence of the feed spacer has greater effects on the pressure drop than the channel walls [152, 153].

3.3. OPTIMAL FEED SPACERS

An optimal membrane module is one with highest production rate at the lowest energy consumption and expense possible. One approach towards the design of such an SWM module is to optimize the feed spacer geometry. Theoretically, an ideal feed spacer is defined as a spacer with the perfect hydrodynamic design [154], i.e. a spacer that neither causes stagnant regions nor blocks the membrane surface area [155]. Stagnant areas cause solids and/or microorganisms to accumulate and/or rejected salts to build up [154, 155] and the resulting smaller membrane surface results in a reduced production rate. In practice, an optimal feed spacer is defined as a design that achieves a balance between competing concerns: the mass transfer on one hand and the pressure drop and fouling on the other. For instance, using a feed spacer in an empty channel causes a mass transfer enhancement [8, 12, 14, 58, 61, 152–159] but at the expense of increased pressure losses along the feed channel [8, 13, 14, 58, 61, 152, 154, 156, 157, 160, 161]. Additionally, the use of a feed spacer in an empty channel reduces effects of concentration polarization but at the expense of the formation of stagnant regions, which are favorable for particle deposition and biomass formation, either downstream [117] or upstream [142] of a spacer. It is reported that feed spacers have a higher impact on the pressure drop (2.5 – 160 times compared to an empty channel) than flux enhancement (2 – 5 times) [157, 162]. Therefore, the optimal feed spacer is the one that results in a the flux improvement without a (significant) increase in pressure losses. It is typically more economically attractive to operate membrane systems with a spacer than without because the benefits of mass transfer often outweigh the disadvantages caused by increased energy losses. Therefore, the main reason for using a feed spacer in SWM modules of RO is to enhance the mass transfer, which is often described by the diffusion model. According to this model, average water flux (J_{ave}) through the membrane is a function of applied pressure over the membrane sheet (NDP), the membrane mass transfer coefficient (K_w) or specific permeate flux (J_{SPE}), and temperature (TCF)(Equation 3.2: $K_w = (J_{ave} \times TCF)/NDP$). The Sherwood number (Equation 3.4), which incorporates the effect of the Reynolds number (Re) and Schmidt number (Sc) is commonly used to predict the membrane mass transfer coefficient (K_w).

$$Sh = K \times Re^a \times Sc^b \times (\frac{Z \times d_h}{L})^c \tag{3.4}$$

The Sherwood number depends on several constants. Table 3.4 shows the common values used for the constants of Sherwood numbers for the empty and spacer-filled channels. Spacer-filled channels with zigzag spacers (diamond shape) are considered to be channels in which the flow direction is changed. Channels with ladder type or cavity

Table 3.4: Constants for the calculation of Sherwood number for empty rectangular-shaped channels and spacer-filled channels

	K	a	b	c	Z	Error	Ref
Empty feed channel	0.66	-1/2	-2/3	0	0	-	
Spacer filled channel without changes in flow direction	0.664	1/2	1/3	1/2	1	30%	[152]
Spacer filled channel with changes in flow direction	$0.664k_{dc}$	1/2	1/3	1/2	2	10%	[152]

type spacers are usually considered to be channels without changes in flow direction, containing one set of filaments parallel to flow and other set perpendicular to flow direction. The last term of the Sherwood number can be neglected in the empty rectangular channels because the constant Z is equal to zero in the empty feed channel. The constant a for the spacer-filled channel is reported to be around 0.5. Da Costa et al. [157] found values range from $0.49-0.66$, Kurada et al. [163] mentioned a value of 0.5, and Schwager et al. [164] reported 0.62. Da Costa et al. [152] investigated the mass transfer coefficient achieved for spacer-filled channels using Equation 3.4 and the constants mentioned in Table 3.4. They [152] found that the mass transfer coefficient differs 30% from the practical value for spacers that do not change the flow direction and 10% for spacers that change the flow direction. In zigzag spacers, which are commonly used in SWM modules, the constant K is related to factor k_{dc}, which is a function of geometrical characteristics of the spacer such as the ratio of filament thickness to the channel height (d/H_{CH}), porosity (ϵ), and hydrodynamic angle (α) (Figure 3.5) [152, 165]. The relationship between the pressure losses and the flow through the channel can be described by determining flow characteristics. However, because the flow characteristics of a spacer-filled channel are too complicated, the friction factor and the pressure drop dependency on the velocity are used to elucidate this relation. The friction factor (C_{td} in Equation 3.5) is defined in terms of three components: the kinetic energy per unit volume of feed, pressure drop per unit length of the flow path and characteristic dimensions of the channel.

$$C_{td} = \frac{2}{\rho \times u_{ave}^2} \times \frac{\Delta p}{L \times d_h} \propto \frac{A'}{Re^n} \tag{3.5}$$

Equation 3.5 is a semi-empirical equation, which means that the pressure drop over the membrane has to be measured in order to determine the friction factor. The friction factor in equation 3.5 is typically expressed as a function of the Reynolds number to a specific power (Re^n) and channel geometry (A'). In the case of an empty rectangular channel, a value of 24 can be assigned to A' [152, 172] .The Reynolds number is a function of inertial and viscous force.

$$Re_h = u_{ave} \times d_h \times \frac{\rho}{\mu} \tag{3.6}$$

The viscous forces are often kept constant in membrane filtration experiments and the inertial forces are a function of the hydraulic diameter, flow density and viscosity. The initial increase of the Reynolds number during steady flow causes slight oscillation, which are superimposed on the steady flow pattern, and flow instabilities appear as a result. A further increase of the Reynolds number causes an increase in the amplitude of the oscillations, which gives rise to flow with considerable mixing [166].
Table 3.5 outlines studies that investigate the effect of the Reynolds number on the hy-

Table 3.5: The effect of Reynolds number on different parameters

Spacer/process	Re	Effect	Ref
Net-type spacers	50	The velocity was on average in flow direction	[166]
	35-45	Numerical study shows that transition to unsteady flow occurs at relatively low Reynolds numbers; i.e. Re = 35–45	[167]
	30	The experimental studies with particle image velocimetry (PIV) shows that unsteady flow for common feed spacer start at low Reynolds numbers (Re = 30)	[168]
	180 – 280	Most geometries started to exhibit oscillations	[166]
	250 – 300	Flow became unsteady and wavy	[166]
	> 300	Flow showed a very unsteady behavior	[166]
	$10 < Re < 100$	Flow separation and boundary layer development play roles in mass transfer enhancement	[169, 170]
	$Re > 100$	Longitudinal and transverse swirling causes mass transfer enhancement due to mixing	[169]
Comparing strip-type shaped promoter or eddy promoters with net-type spacer in electrodialysis		Compared to the strip-type promoters, the net-type promoters were more efficient at the lower Reynolds numbers	[171]
	$Re > 400$	Sherwood number of net-type mesh became equal to or slightly smaller than that of the strip-type promoters likely because the eddy generation mechanism in the net-type spacer is affected by the flow attack angle	[171]

draulic conditions of the feed channel. The hydraulic diameter (d_H) is used to correlated the flow through non-circular or complex channels with constant a cross-sectional area, i.e. hydraulic diameter serves as the characteristic channel dimension [58, 127, 152, 173, 174]. Attempts to relate the hydraulic diameter to the flow behavior by a single equation in the spacer-filled channel had only limited success [173].

$$d_H = \frac{4 \times \epsilon}{\frac{2}{H_{CH}} + (1-\epsilon) \times S_{v,SP}} \tag{3.7}$$

The hydraulic diameter depends on the channel height (H_{CH}), spacer porosity (ϵ), and specific surface of the spacer ($S_{v,SP}$). Equation 3.8 provides a formula for estimation of the spacer porosity (ϵ). In this formula, the porosity is estimated with the channel height or spacer thickness, orientation of longitudinal and transverse filaments with respect to each other and the filaments' geometry.

$$\epsilon = 1 - \frac{V_{sp}}{V_{mesh}} = 1 - \frac{(A_{CT} \times l_{mCT}) + (A_{CP} \times l_{mCP})}{l_{mCT} \times l_{mCP} \times sin\beta \times H_{CH}} \tag{3.8}$$

Equation 3.9 is a simplified form of equation 3.8 for the feed spacers of SWM modules of RO in which the top and bottom filaments have the same average diameter and mesh length.

$$\epsilon = 1 - \frac{\pi \times d}{4 \times l_m \times sin\beta} \tag{3.9}$$

Equation 3.10 represents the specific surface of the spacer ($S_{v,SP}$), which depends on the filaments' geometry.

$$S_{v,SP} = \frac{A_{SP}}{V_{SP}} = \frac{(P_{CT} \times lm_{CT}) + (P_{CP} \times lm_{CP})}{(A_{CT} \times lm_{CT}) + (A_{CP} \times lm_{CP})} \tag{3.10}$$

The average velocity in the spacer-filled channel (u_{ave}) is a function of average feed flow (Q_{ave}) and cross-sectional area of the feed channel (A), which depends on the spacer porosity.

$$u_{ave} = \frac{Q_{ave}}{A_{eff}} = \frac{Q_{ave}}{A \times \epsilon} = \frac{Q_{ave}}{W \times H_{CH} \times \epsilon} \tag{3.11}$$

The actual velocity in the spacer-filled channel should be measured at fully developed flow. The flow becomes fully developed after the entrance length, which is about 2.17 cm for a rectangular empty channel with a ratio of 1/50 of channel height to width (H_{CH}/W) [175]. In a spacer-filled channel with ladder spacers, the flow pattern became periodic typically after three to five transversal filaments [176, 177]. As previously mentioned, the flow through a spacer-filled channel cannot be described easily like the flow through an empty channel and therefore equation 3.5 and/or equation 3.12 is used for a better understanding of the flow regime.

$$dp \propto K \times u_{ave}^{m} \tag{3.12}$$

Equation 3.12 describes how the pressure drop is correlated with the volumetric flow rate. It was believed [173, 178] that the exponent m in equation 3.12 reveals the degree of turbulence in the feed channel. An m-value equal to one was the indication for the laminar flow, a value of 1.75 was the sign for a fully developed turbulent flow and all exponents between these two values were indicators for a transitional regime [173, 178]. However, as mentioned in some studies [142, 154, 179–181], referring to the flow regimes encountered in SWM modules as $turbulent$ is a common misunderstanding because turbulent flow is defined for $Re > 4000$ at which turbulence can be assumed to be isotropic and fully developed while the Re in SWM of RO remains in the laminar flow regimes ($Re < 300$).

3.3.1. ENERGY AND PRESSURE DROP

The desire to enhance the performance of RO together with the development history of these membranes encouraged a vast amount of study related to the role of the feed spacer in determining the hydraulic conditions inside the feed channel of SWM modules. Early studies led to a good understanding of the mechanisms that give rise to concentration polarization, and the recent studies have led to a partial understanding of biofouling mechanisms. The role of the feed spacer in SWM modules of RO has been derived from the function of feed spacers in other fields such as in electrodialysis [121, 154, 182, 183], tubular reverse osmosis [184], electrochemical cells [121, 122, 155, 162, 169, 184–186], and micro- and ultrafiltration processes [14, 152, 156, 157, 160, 184, 187]. In fact, the feed spacers or the flow promoters first became important for membrane mass transport in electrodialysis plants [13, 166]. Most electrodialysis studies are performed in flat flow cells and flat sheet membranes. The working mechanisms and principles of flat flow cells and flat sheet membranes are the same as for an unrolled SWM module, and therefore, flat flow cells are commonly used to study the hydraulic conditions in spacer-filled channels of SWM modules [58, 188]. The curvature effects of SWM modules on the flow can be neglected because the height of feed channels in SWM modules is small enough compared to the channel width [177, 189]. Flat flow cells provide a simple but

Table 3.6: Selected experiments conducted with the visualization techniques for demonstration of the flow around feed spacers

Researcher	Visualization method	Ref
Da Costa et al.	They used injected air bubbles and dye for visualization of flow	[152]
In et al.	They implemented a camera and used ink in water for visualization of laminar flow around the spacers	[196]
Kim et al.	They used ink as the tracer for visualization of the mass transfer in the 3D net-type promoter in electrodialysis	[121]
Geraldes et al.	An aqueous solution of bromophenol blue is used for the visualization of streams in a ladder-type spacer	[197]
Vrouwenvelder et al.	A solution of potassium permanganate ($KMnO_4$) is used for visualization of the flow in a flow cell	[79]
Schulenburg et al.	They used nuclear magnetic resonance imaging (NMRI) to show the distribution of the spatial distribution of biofilm and mapping of the velocity field	[100]
Creber et al.	UNMRI is used to show the effect of different chemicals on cleaning of RO and NF	[193]
Willems et al.	They used particle image velocimetry (PIV) to visualize the effects of two phase flow in spacer-filled channels	[141]

effective method for studying flux, pressure drop, fouling and flow pattern visualization in feed channels [14, 152, 154, 157, 190, 191] in a shorter time and with lower material expenses compared to a full-scale module. Usually, flow cells with permeate production ability are used for studying the flux and concentration polarization and cells without permeate production are for studying biofouling because the formation of biofouling is not affected by the permeate production [192]. Additionally, feed water ranging from low to high concentration of inorganic substances is used to investigate the concentration polarization and (in)organic fouling and tap water with sodium acetate or a special ratio of combined sodium acetate, sodium nitrate and sodium phosphate ($C:P:N$) is used to study the biofouling [79, 80, 100–102, 116, 117, 140, 161, 193–195]. Visualization is an important method in determining the fluid condition in SWM modules of RO. In previous studies, the velocity profiles utilized were a rough calculation of the actual velocity profile. Additionally, interactions between multiple ionic components in the feed solution was neglected in those studies [198]. In more recent studies, the velocity profiles and pressure losses in spacer-filled channels are predicted with numerical models [15, 60, 142, 179, 195–204] for which excellent reviews are available [13, 180, 199]. Computational fluid dynamics (CFD) is a common numerical technique in membrane processes for simulation, visualization and analysis of fluid systems. The main advantages of CFD models over experimental methods are lower material costs and the higher ability to control specific process parameters e.g. the inlet feed velocity, feed concentration, and temperature [198]. The primary challenge for such models is that there are limited direct experimental studies on the detailed velocity profile with resolution at the range relevant for CFD studies to support them. Table 3.6 summarizes some visualization studies of the flow pattern in spacer-filled channels. Experimental methods such as injected dyes and particle depositions [121, 174, 197] give good results for mapping the velocity profile albeit at much lower resolution than numerical studies. Electrochemical methods [141, 200], in which numbers of electrodes are embedded into the channel wall, are more often used for visualization in membrane technology. A disadvantage of electrochemical measurements is that they can only be performed in the absence of the membrane in order to accommodate the electrodes [141].

Particle image velocimetry (PIV) (figure 3.3) is a non-invasive visualization method that offers reasonable spatial and temporal resolution without the need of limiting electrodes. A detailed description of the technique can be obtained from Raffel [201] and Adrain [202]. In membrane technology, PIV can be used to determine the particle deceleration and dead zones as well as for creating fluid velocity mapping in fouling studies. However, despite the advantages of PIV, this method is not commonly applied in SWM modules and there is only a limited number of studies available [141, 153, 203] using this technique. In addition to challenges regarding the verification and validation of numerical studies, it is difficult to match the geometry of feed spacers used in most CFD studies with the geometry provided by manufacturer, e.g. intricate properties such as the torsion and protrusion between two nodes are difficult to generate. Also, simulation of fouling is a time-consuming and challenging job and need its own experts [198].

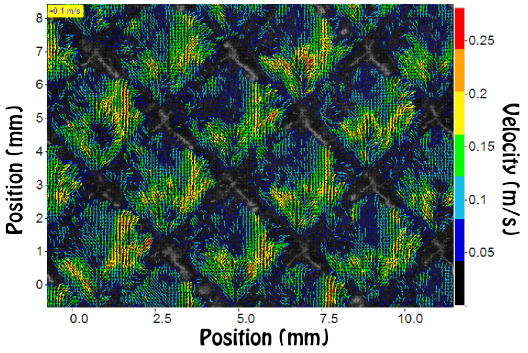

Figure 3.3: Fluid velocity mapping measured and created by PIV inside a feed channel of SWM of RO membrane. A clean spacer (28 $mils$ = 0.7 mm) and a clean membrane coupon were used for this experiment. The inflow was about 16l/h and the average cross-flow velocity around 0.16 m/s. The average particle diameter was 10 μm. Deceleration of particles occurs close to nodes and spacer filaments, which are also the places that show the highest fouling by autopsy. The highest velocity is found over the filaments and directly downstream of filaments.

3.4. GEOMETRY OF FEED SPACERS

Figure 3.4 illustrates different feed spacer configurations that are used in the membrane filtration process. Spacer A is the most common configuration used in SWM modules of nanofiltration and reverse osmosis. Other configurations are used in microfiltration, ultrafiltration, electrodialysis, membrane bioreactors, etc. A feed spacer in SWM modules of RO typically has a net-type shape and is made of polypropylene. The extruded meshes in these spacers have a two-level structure where the cross filaments are welded in a nonwoven way on top of each other and make an inner angle of 90° with each other (β). The feed spacer in RO (figure 3.5) is oriented in at an angle of 45° with the flow (the flow attack angle). The top and bottom filaments have almost an equal average diameter. Along each filament in a mesh, the diameter is neither constant nor perfectly round. In other applications, such as ultrafiltration, the spacer could consist of thinner filaments perpendicular to flow and thicker filaments parallel to flow (figure 3.4-B) [64]. Table 3.7 shows some studies done on the effect of feed spacer configuration in different fields.

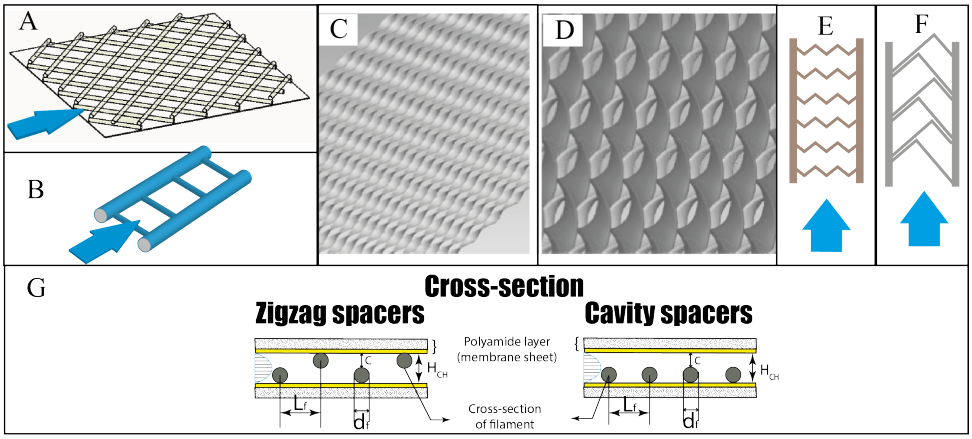

Figure 3.4: Typical spacer design: rhombus diamond-type (A), ladder-type (B), mono-layer helix (C), double-layer helix (D) [205], zigzag-type (Corrugated) (E), herringbone spacer (F). The ladder-type spacer (B) with two possible cross-sections; zigzag-type (left) and cavity-type (right) cross-section. The possible geometrical parameters are c/H_{CH}, adaptive height (d_f/H_{CH}), and aspect ratio (L_f/H_{CH}). L_f is the distance between two filaments, H_{CH} is the channel height, d_f is the average diameter of the filaments and c is the gap between the membrane and the cross filament

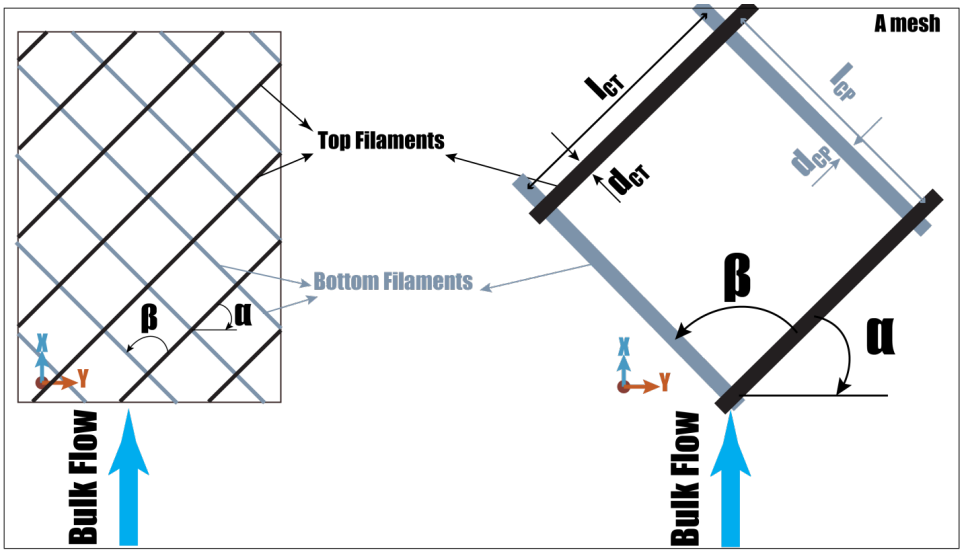

Figure 3.5: : The extruded meshes in spacers of SWM modules of nanofiltration and reverse osmosis are made of two layers, which are constructed in a nonwoven way.

Table 3.7: Selected studies comparing different configuration of feed spacers

Studied configuration	Field	Results	Ref
Eddy promoter is compared with net-type spacer	ED	The effectiveness of the eddy promoters was only achieved at a high Reynolds number while the efficiency of the net-type promoters was achieved for the whole range of Reynolds numbers	[171]
Cavity configuration is compared with zigzag configuration (aspect ratio=5)	-	The unsteady flows in the channel begin at a Reynolds number of 250 – 300 for both spacers used in this study	[196]
Zigzag spacer (Corrugated) with net-type spacer	UF	• The pressure drop was lower in the zigzag spacer than the net-type spacer • Flux enhancement was a function of feed water properties • Zigzag spacers had a better flux enhancement compare to net-type spacer for feed water without fouling	[159]
Zigzag spacer (Corrugated) with net-type spacer	UF	The pressure loss and the permeation rate were constant over time for the zigzag spacer, but the net-type spacer showed an increase in the pressure loss over time due to blockage of the spacer mesh	[204]
Ladder-type spacers with the staggered herringbone	ED	• The staggered herringbone were better spacers for enhancing mass transfer • The configuration with one herringbone filament provided better enhancement than a group of herringbone filaments because of the complete rotation of the flow	[4]

3.4.1. MODIFIED FEED SPACER MATERIAL

Feed spacers are manufactured from a variety of materials. Feed spacers in SWM of RO are made of semi-crystalline thermoplastics such as polypropylene and, to a lesser extent, polyethylene. Feed spacers made of the same material could differ from each other based on the material density, i.e. a polyethylene feed spacer could be low-density polyethylene, polyethylene, or high-density polyethylene. To the authors' knowledge, no investigations have been conducted on the effects that plastic type could have on the pressure drop and fouling of membranes. For instance, it not yet known how the feed spacer stiffness could affect the fouling and different cleaning methods.

Most studies on feed spacer materials used additives to make feed spacers more resistance to biofouling [58, 102, 116, 144, 161]. Most of these studies found that the surface modification to reduce adhesion of microorganisms to the spacer and membrane is not adequate to prevent or limit biofouling [116, 144, 161]. Additionally, the surface modification did not have a significant impact on the feed channel pressure drop [116, 144, 161]. Unsuccessful application of modified spacers in biofouling prevention is due to the finding that coated surfaces could only kill microbes under initial conditions, after which the dead layer of the microorganisms will form and cover the antimicrobial coating compounds, preparing the surface for a second layer to be built on top of exposed or even lysed microorganisms.

Araùjo et al. [116] reported that biofouling prevention was not successful with use of a copper-coated feed spacer because the coating agent toxicity became ineffective due to extracellular polymeric substances secreted by microorganisms. This occurs when some microbial strains with a higher resistance to the metal coating first colonize on the coating metal and make the conditions favorable for other microorganisms to accumulate by covering the coated metal with their extracellular polymeric substances. Tsuneda et al. [90] showed that the extracellular polymeric substances are responsible for bacterial adhesion to the solid surface by measuring the polysaccharides using techniques such as FTRI (Fourier transform infrared) spectrometry. Polysaccharides are known to constitute the largest portion of extracellular polymeric substances and are related to cell adhesion during initial stages of biofilm formation [90]. In addition to the ineffectiveness of antimicrobial metals in prevention of biofouling, these antimicrobial metals can potentially leach into the permeate. Moreover, their function in presence of binding inorganics when applied in full-scale operation has not been investigated.

In addition to the coating of spacers with antimicrobial metal, surface-confined macromolecules known as polymer brushes are also being used to modify the feed spacers. In this technique, the feed spacer surface becomes hydrophilic. Hydrophilic surfaces are known to be resistant tot the adhesion of bacteria and proteins [206], i.e. polymer brushes reduce the friction between the modified feed spacer and microorganisms and consequently the microbial adhesions [207–209]. Araùjo et al. [116] compared a system containing a biostatic modified feed spacer and membrane with an unmodified system under the same operational conditions. The modified feed spacer was infused with of 0.5 $wt\%$ triclosan, an anti-biofouling compound. The results showed the same pressure drop and accumulated biomass in the hydrophilic-modified and unmodified systems [116]. The malfunctioning of the biostatic hydrophilic system was related to rapid leaching of the active compound due to high shear forces, which disrupted the structure of

absorbed polymer brush layers and destroyed the complex coacervate-brush structure [210].

3.4.2. FILAMENT CROSS-SECTION

Feed spacers are usually composed of filaments with rounded cross-sections. This is the case in spite of results that have shown [211, 212] rounded cross-sections are less effective in destabilization of the concentration polarization layer and enhancement of mass transfer compared to other cross-sectional shapes such as a rectangle or triangle. Ahmad et al. [211] found in a CFD-study that spacers with triangular or rectangular cross-sections more effectively destabilize the concentration polarization than those with a rounded cross-section. They found that spacers with triangular cross-sections were the most effective spacers for destabilization of the concentration polarization layer. Icoz et al. [212] determined that spacers with hexagonal and square cross-sections enhance heat transfer better than spacers with rounded cross-sections. Amokrane et al. [213] compared the oval and elliptic shaped filaments with rounded filament and found a higher pressure drop in the system with rounded filaments. Additionally, oval and elliptic cross-sections resulted in a thicker concentration polarization layer and lower mass transfer. Filaments with rounded cross-section are typically preferred because in contrast to the mass transfer, the pressure drop caused by rounded cross-section filaments is lower than other cross-section shapes [212, 214]. The lower pressure drop can be translated into a lower pumping energy, which is one of the primary design considerations for membrane systems. However, due to manufacturing difficulties, the cross-section in an SWM module of RO is not uniform over the whole length. It is thinner between two nodes than at the nodes themselves, bulges out and has slightly twisted shape. The non-uniform shape of the filaments could result in particle deposition [12, 215]. It is proposed [12] that the main region of deposition would be around the point where the attached filaments bulge outward.

3.4.3. FILAMENT TORSION

As mentioned in the previous section, spacers in SWM modules of RO usually have torsion in filaments between two nodes of a mesh, which can result in the formation of longitudinal and transverse vortices, a more powerful destabilization of the concentra-

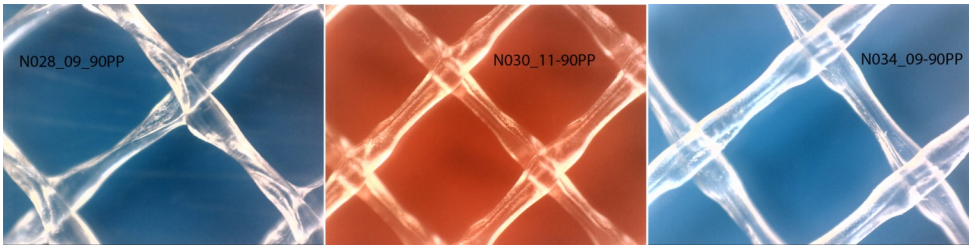

Figure 3.6: Three standard spacers used in SWM modules of RO with a thickness of 0.71, 0.76 and 0.86 mm respectively from left to right. A turning-liked filament can be observed on the most left spacer but not on the other ones.

tion polarization layer and consequently a higher mass transfer. The torsion region of filaments is more obvious in thinner spacers than thicker ones (figure 3.6).
In heat transfer studies, modifying spacers by winding helical bars around cylindrical filaments or by using twisted tapes thought to enhance the mixing efficiencies of vortices close to the membrane walls [170]. However, these types of vortices occur mainly in the bulk of the flow, while the resistance against the mass transfer is greatest at the membrane walls [170]. Based on this, Li et al. [170] and Balster et al. [169] examined the torsion efficiency of spacers.
Surprisingly, Li et al. [170] found that spacers with modified filaments caused lower mass transfer than nonwoven net spacers. Balster et al. [169] found that spacers with twisted filaments have a higher mass transfer than unmodified spacers. However, in the study by Balster et al. [169] the geometric configuration of the spacers was not identical. Therefore, it seems that further investigation is required to elucidate the actual effect of torsion on not only the mass transfer but also on the pressure drop and fouling.

3.4.4. LOCATION OF TRANSVERSE FILAMENTS

The position of transverse filaments in ladder and cavity spacers with respect to the channel height appears to be important for the mass transfer, energy usage, and fouling formation.
Geraldes et al. [197] investigated the formation of a concentration polarization layer on the membrane with respect to the position of transverse filaments in the channel height. Two scenarios were investigated: (i) in the first system, the transverse filaments were adjacent to the membrane and (ii) in the second system, the transverse filaments were placed on the impermeable layer on the opposite side of the membrane. The study assumed that the permeate flux along the membrane was uniform because both the osmotic pressure of the feed solution and the apparent rejection coefficient were low. A lower degree of concentration polarization was observed in the first scenario, where the same concentration polarization pattern was observed for each transverse filament, showing two maxima that appear in the base of each transverse filament. The first maximum, which was much higher, appears at the base of the filament positioned at the upstream of the inter-filament distance [197]. A PIV study showed that these are the locations with the lowest cross-section velocity [153].
However, the authors were unable to identify any experiment studies showing the effect positioning the transverse filaments at the middle of the channel with some distance from the top and bottom membrane (submerged spacer) on parameters such as concentration polarization, pressure drop and fouling. Cao et al. [191] discussed the effect of a ladder type submerged spacer through modeling. Using spacers with a transverse filament diameter 1/3 of the channel height (d_{CT}/H_{CH} =1/3) at a Reynolds number between 120−480, the study [191] found that in contrast to zigzag spacers and ladder spacers, the flow in submerged spacers is symmetrical towards both membrane sheets, i.e. the mass transfer on both membrane sheets could have a similar magnitude.

3.4.5. HYDRODYNAMIC ANGLE (β)

The hydrodynamic angle is defined as the inner angle between two adjacent filaments facing the feed flow. The hydrodynamic angle ensures the generation of swirling in the

feed channel albeit at the expense of an increase in the pressure drop [152, 216]. The maximum cost [157] and a maximum flux [152] are achieved by applying a spacer with a hydrodynamic angle of 90° because a spacer with the hydrodynamic angle of 90° generates dominantly transverse vortices with an axis perpendicular to the flow direction [216]. Spacers with a hydrodynamic angle of 45° cause a degree of channeling either along the membrane surface or along the channel roof, which causes a flux reduction of 16-25% [157].

3.4.6. SPACER ORIENTATION

The spacer orientation is defined as the manner in which the flow attack angle faces the feed flow. Da Costa et al. [157] studied the effect of spacer orientation on the pressure drop and found that spacers with filaments parallel to the axis of the flow channel have a lower pressure drop and are therefore more economically attractive. Fimbbres-Weihs and Wiley [217] conducted a numerical study to show that the 45° orientation promotes mass transfer to a greater extent than that of the 90° orientation due to the absence of a fully formed recirculation region and an increase of wall shear by increase of the Reynolds number. Neal et al. [12] showed in an experimental study that flux in microfiltration membranes increases by increasing the flow attack angle concluding that spacers with a flow attack angle of 45° have the best performance. That is attributed to two factors: (i) the tested spacer was made of two layers of nonwoven filaments with an hydrodynamic angle of 90°, and positioning of the spacer for the highest possible angle (90°), and (ii) on one membrane wall means the lowest possible angle of attack (0°) on the opposite membrane wall.
Neal et al. [12] studied the effects of spacer orientation on fouling for three scenarios: (i) when the transverse filaments were attached to the membrane and perpendicular to the flow (the 90° orientation), (ii) when the transverse filaments were attached to the membrane and parallel to the flow (0° orientation) and (iii) when the attached filaments were arranged at 45° of flow deposition (normal orientation). At 90° orientation, particles were deposited in a transverse band across the entire spacer cell, and the deposition region was displaced from the transverse filament by a zone of no deposition. The clear space between the edge of the filament and the deposition zone was attributed to the presence of recirculation eddies behind the transverse filaments. In the 0° orientation, particles were deposited by applying a higher flux, and deposition was concentrated around the attached filaments, which were parallel to the flow. In the normal orientation, deposition occurred mainly in the center of the cell. The location of the deposition was related to the shape of the filaments which were not uniform cylinders but instead wider at the center and edges.

3.4.7. SPACER THICKNESS (CHANNEL HEIGHT)

The height of a spacer-filled channel is determined by the thickness of the feed spacer. The channel height filled with nonwoven spacers is equal to the spacer's height at nodes where the transverse and longitudinal filaments cross each other. Theoretically, the spacer's height at each node is summation of a transverse and a longitudinal filament. Such estimation for channel height is used in most computational studies related to the nonwoven spacers. In practice, however, the spacer height at nodes is slightly smaller

than the summation of transverse and longitudinal filaments because filaments at nodes are embedded within each other.
The increase of spacer thickness at a constant filament length results in a reduction of the porosity, the specific surface area of the feed spacer and average velocity but an increase of the hydraulic diameter of the spacer. However, it is difficult to determine the effects of feed spacer thickness increase on the pressure drop by using theoretical formulas only.
The channel height determines the fouling formation at the membrane surface. At a constant flow rate, the cross-flow velocity in channels with thicker spacers is lower than channels with thinner spacers. A lower velocity means a thicker concentration polarization layer, a higher chance of particle deposition and a higher chance of scaling but a decreased chance of biofouling. The lower cross-flow velocity results in a lower nutrient load and consequently a lower biomass accumulation, a lower initial feed channel pressure drop and a lower increase of the feed channel pressure drop. The results of laboratory work [161], a pilot plan study [218] and a full-scale study [36] reveal that initial pressure drop decreases with the increase of feed spacer thickness. However, it should be noted that at a constant feed flow rate, the amount of biomass accumulation in channels with thinner spacers is the same as channels with thicker spacers because the amount of nutrient is constant [36, 161, 218]. In addition to the cross-flow velocity, the fouling will also be affected by the flow distribution pattern, which is a function of spacers' geometry, configuration, and orientation.
Additionally, the membrane specific area is primarily determined by the feed spacer thickness. Membranes with larger specific area produce larger quantity of water. Therefore, the spacer should be as thin as possible to have the largest possible membrane specific area and production rate but as thick as possible to cause the lowest possible pressure drop and fouling rate.

3.4.8. NUMBER OF FILAMENT LAYERS

Standard nonwoven spacers are made of two layers of filaments on top of each other. One study argued that spacers with three filament layers are capable of increasing the flux without covering additional membrane area, which led to lower capital and processing costs [219]. A comparison of 2-layer and 3-layer spacers of identical mesh length and hydraulic diameter showed that the 3-layer spacer operated at a higher flow instability range than the 2-layer spacer (lower Reynolds number power, n in equation 3.5: $C_{td} \propto A'/Re^n$) but at the expense of higher pressure losses [219]. Li et al. [170] used multi-layer net-type spacers to investigate the effects of these type of spacers on the formation of the concentration polarization layer, process performance and cross-flow power consumption. They [170] concluded that the performance of multi-layer spacers was better than that of standard nonwoven spacers. One particular design of multi-layer spacers with standard nonwoven spacers in the outer layers and twisted tapes in the middle-layer showed an increase of 30% in Sherwood number compared to standard nonwoven spacers for the same cross-flow power consumption [170]. The same design showed 40% less power consumption at a constant Sherwood number compared to the standard nonwoven spacer.
The multi-layer spacer designed by Balster et al. [169] was made of a standard net-type

spacer in the middle and two thin net-type spacers on the outside. This designed obtained 20% higher mass transfer compared to a standard nonwoven spacer at the same power consumption.
The selected studies did not investigate the effect of the multi-layer spacer on the particulate fouling and biofouling.

3.4.9. INTER-FILAMENT DISTANCE AND FILAMENT THICKNESS

Da Costa et al. [14] reported that the mass transfer in the presence of spacers is a function of two mechanisms: (i) the friction generated by the mixing of fluid streams crossing each other at an angle, which is determined by the hydrodynamic angle of spacers and (ii) the friction created by wakes of fluid formed past transverse filaments. Under similar conditions, the second mechanism appears to be dominant and depends mainly on the filament shape and thickness [14], specifically demonstrating that thicker filaments had a higher impact on the mass transfer of the surface to which they are attached and are more likely to promote mass transfer on the opposite wall compared to thinner filaments. In a CFD study, Karode and Kumar [220] showed that spacers with unequal filament diameters caused a lower pressure drop and induced an unequal shear rate on the top and bottom faces of the flow channel. Such unequal shear rates at the top and bottom faces would be expected to have an adverse impact on the membrane module performance because of different mass transfer characteristics and fouling for adjacent membrane leaves. The study also found that a higher overall bulk instabilities flow would not necessarily result in higher shear rates at the top and bottom faces.
Shrivastava et al. [4] used ladder type spacers with a square cross-section in electrochemical flow cells to measure the current. The study reported that by decreasing the inter-filament spaces, the current transfer increased at the detached membrane and decreased at the attached membrane. The increase at the detached membrane is due to an increase in the number of filaments, an increase of the velocity above these filaments and an enhanced mass transfer. The decrease at the attached membrane is caused by reduction of the effective membrane area, which was occupied by the filaments.
It is common in the literature to use dimensionless values instead of filament diameter and inter-filament length. Relative height (d_{CP}/H_{CH}) and aspect ratio (l_{CP}/H_{CH}) are dimensionless terms that describe the ratio of filament height and inter-filament distance of transverse filaments to the channel height, respectively.

RELATIVE HEIGHT (d_{CP}/H_{CH})

The flow instabilities, are among others parameters, also a function of relative height and aspect ratio. Most nonwoven spacers are made with a relative height of 0.5. Geraldes et al. [177] showed that flow instabilities occur at $150 < Re < 300$ in a rectangular channel filled with a ladder-spacer that had a relative height of 0.5. Another finding of the study was that for a constant Reynolds number and aspect ratio (l_{CT}/H_{CH}), the decrease of relative height from 0.5 to 0.25 resulted in lower friction losses while the increase of relative height from 0.5 to 0.75 resulted in generation of a secondary recirculation region of significant dimension. This secondary recirculation region constituted a third type of flow structure, which was not observed for relative height of 0.25 and 0.5. The third type of flow structure mentioned by Geraldes et al. [177] is likely a reason for mass transfer

increase at thicker filaments mentioned by Da Costa et al. [14].

ASPECT RATIO

Cao et al. [191] suggested that reducing the transverse filament distance will reduce the distance between shear stress peaks. This was beneficial for the membrane mass transfer because the reduced distance between shear stress peaks introduced a larger shear stress near the membrane wall and increased the number of eddies. Geraldes et al. [177] used ladder spacers with three aspect ratios, specifically 1.9, 3.8 and 5.7, to investigate the effect of mass transfer and friction losses. The friction number is decreased by decreasing the number of transverse filaments per unit length because of the decline of total drag of the fluid flow. In fact, all three contributors to the pressure drop in the cell (friction at the wall, friction at the surface of the filaments and friction due to the drag of the filaments) decrease with a reduction in the number of transverse filaments.

A higher flow instability close to the membrane wall indicates a higher mass transfer. Karode and Kumar [220] and Geraldes et al. [177] showed that an increase in aspect ratio (l_{CT}/H_{CH}) caused higher flow instabilities. Geraldes et al. [177] found that flow instabilities occur at lower Reynolds numbers for spacers with a constant relative height and greater aspect ratio. For instance, it was shown that the Reynolds numbers at which the instabilities start were $250 < Re < 300$, $175 < Re < 200$ and $150 < Re < 175$ for aspect ratios of 1.9, 3.8 and 5.7, respectively. In and Ho [196] reported that flow instabilities begin at a Reynolds number of 250 – 300 for zigzag type spacers and the cavity spacer with an aspect ratio of 5.

A high aspect ratio (l_{CT}/H_{CH}) led to the condition that the region of the recirculation zone, which occurs downstream of transverse filaments, did not reach the subsequent filament. Geraldes et al. [177] reported that for a constant relative height, the recirculation zone did not reach the subsequent transverse filament at aspect ratios 3.8 and 5.7.

Amokrane et al. [163] examined the effect of aspect ratio (d_{CT}/H_{CH}) for zigzag, cavity and submerged spacers with a constant relative height of 0.5 ($d_{CT}/H_{CH} = 0.5$). The study found that for aspect ratios (d_{CT}/H_{CH}) of 2 and 4, the flow remained stable in zigzag and cavity spacers but became unstable in submerged spacers. An addition finding was that the mass transfer through the membrane decreased in all three types of spacers by increasing the aspect ratio (d_{CT}/H_{CH}).

3.4.10. SPACER POROSITY

In SWM modules of RO where the top and bottom filaments are the same, the porosity is determined by knowing the aspect ratio (l_{CT}/H_{CH}) and hydrodynamic angle. Numerical methods showed a decreased pressure drop due to an increased aspect ratio and increased hydrodynamic angle [167]. Equation 3.8 indicates that both an increase in the rate of l_{CT}/H_{CH} and a decrease in the hydrodynamic angle can translate into increased porosity. Therefore, an increase in the porosity results in a decrease of the pressure drop on one hand and an increase of flux due to greater active membrane area on the other. Da Costa et al. [157] reported that an increase of 70% in the porosity of a spacer led to a minor flux drop of 2 – 10% and minor pressure drop enhancement.

Table 3.8: Summary of geometric effects of the feed spacer on the hydraulic conditions of the spacer-filled channel.

Investigated parameter	Specification	Results			Ref
		Pressure drop	Flux	Fouling	
Material	Adding metals	No remarkable changes	No noticeable change	Lower biofouling only in initial stages	
	Polymer brushes	No remarkable changes	No noticeable change		
Filament cross-section	Round filaments compare to other shapes	Lower pressure drop	Lower flux	-	
Filament torsion	-	-	Flux enhancement due to destabilization of the boundary layer	-	
Hydrodynamic angle in UF	UF90°	Highest pressure drop	Highest flux	-	
$230 < Re < 1661$	UF45°	-	16-25% lower flux due to channeling	-	
Orientation of feed spacer	45° versus 90°	45° had a higher pressure drop	45° had a better mass transfer	At 90° orientation, particles are deposited in a transverse band across the entire spacer cell, and in the normal orientation, deposition occurred primarily in the center of the cell	
Spacer thickness	Increase from 0.7 to 0.86 mm	Lower pressure drop in thicker spacer	-	Lower fouling in thicker spacer	
Number of layers	-	Higher turbulence and pressure drop	Higher flux	-	
Relative height					
Aspect ratio	Increase of aspect ratio	Lower pressure drop	-	-	
Porosity	Increase of porosity	Minor decrease in pressure drop	Minor decrease in flux (2 – 10%)	-	

3.5. CONCLUSION

In this chapter, we reviewed the effect of geometric design on the performance of SWM modules, generally, and the effect of feed spacer design on the hydraulic conditions of narrow feed channels and performance of SWM modules of RO in particular. Several researchers demonstrated the noteworthy effect of velocity on the fouling, the permeate production and pressure losses. The velocity in a spacer-filled channel is mostly affected by the feed spacer geometry. Therefore, it is crucial to understand how each parameter in spacer geometry affects the hydraulic conditions of the feed channel in order to be able to enhance the performance of the feed spacer and consequently the SWM modules.

This review shows that using a single type of spacer in SWM modules of RO for different applications is not beneficial and instead, it would be more advantageous to use a specific feed spacer for a particular type of feed water. For instance, the net-type spacer employed in the current SWM modules of RO is suitable for water with high salinity rather than water with low salinity at a determined recovery. This is because the net-type spacer can destabilize the concentration polarization layer to a reasonable extent by means of proper flow mixing, which also results in high pressure losses. However, the ratio of pressure losses to required feed pressure is almost negligible when applied to water with high salinity (high osmotic pressure). In contrast, the ratio of pressure losses to feed pressure becomes significantly higher in water with low salinity (low osmotic pressure) for which concentration polarization is not the main problem. In contrast, the ladder-type spacers are more suitable for use with low salinity water such as river water because they have lower mixing ability and lower pressure losses compared to net-type spacers. The lower resistance of the ladder-type also spacers makes them more suitable to be cleaned with air-flow, by which the higher shear forces remove the particles and biofilms.

The detailed design of an optimal spacer for a specific type of feed water is possible by numerical studies and valued experimental studies with resolution in the range of numerical studies to validate them. There is a limited number of experimental techniques that can be used for validation of numerical studies in SWM modules of RO because the experimental studies often have a much lower resolution than numerical studies. Particle image velocimetry (PIV) is one of the techniques that can be used for validation of numerical studies.

4. Experimental

Summary

Studies in the following chapters (chapters chapter 5-7) involve the flow and pressure drop measurements, respectively, for the friction losses calculation and velocity visualization. The flow is measured by a mass flow meter, pressure drop with a differential pressure meter, and velocity with the planar particle image velocimetry (PIV). PIV is a non-intrusive optical measurement technique used for diagnostics of the flow. In planar PIV, two velocity components are measured simultaneously because only a single camera was used. In this thesis, the two measured velocity components were the velocity parallel to flow (Ux) and velocity perpendicular to flow (Uy). The third component of velocity; i.e. the velocity component in the direction of channel height (Uz), was not measured in this thesis. The velocity is measured asynchronously at three heights inside the channel. The field in front of the channel (Z3), relative to the camera position, called also "close to the observation window". That is because the front part of the flow cell was made of Plexiglas, which made it possible for the camera to detect the flow pattern. The field at the rear part of the channel (Z1), relative to the camera position, called also "close to membrane" because in contrary to the actual feed channel that has two membrane sheets, the flow cell had only one membrane sheet. This membrane sheet was located at the rear part of the flow cell to make it possible for camera to capture pictures.

Parts of this chapter have been published in Journal of Water Research **106**, 232-241 (2016) [153].

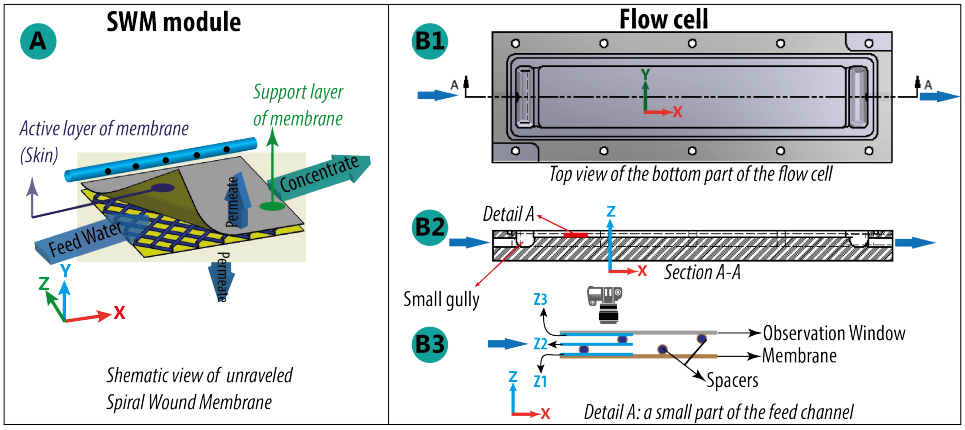

Figure 4.1: A shows the schematic view of unraveled Spiral Wound Membrane (SWM) module and B shows the bottom part of the flow cell in top view (B1) and side view (B2). Detail *A* is a part of the flow channel and shown in B3. The field $Z3$ is close to camera and the observation window, $Z2$ at the middle of the channel and $Z3$ far from the camera and at the rear part of the feed channel. Small gullies at the inflow and outflow provide homogeneity of the flow through the channel.

4.1. INTRODUCTION

The experimental setup is shown in figure 4.2. A solution with fluorescent particles (02) flows through a pump (03) and a mass flow meter (04) to a flow cells (05). A magnetic stirrer (01) ensures that particles remain in suspension. The pressure drop

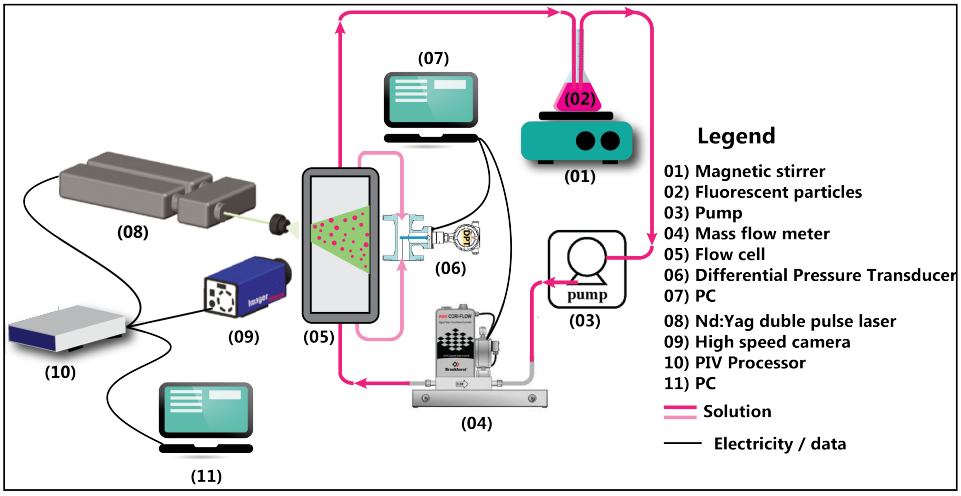

Figure 4.2: Experimental setup. The setup can be divided into two parts. One part is used for measurement of the flow, density and temperature, which are used for calculation of average velocity and friction losses. The other part is used for visualization of the flow and velocity inside the feed channel.

over the flow cell is measured by means of a differential pressure transducer (06). Simultaneously, the laser (08) emits two lights with a short time interval and a high-speed camera (09) takes two images (11). The friction losses are calculated by obtained values from mass flow meter. The captured images are used to determine the temporal and spatial velocity maps (13) inside the channel by using a special algorithm (Davis 7.2).

4.2. TRACERS

The solution contains suspended fluorescent particles (Dantec, Ulm, Germany) to provide velocity information in the fluid. The velocity measurement in PIV technique is a function of two fundamental dimensions of the velocity; the shifting distance and the time. The measurement technique is indirect in a sense that camera detects the movements of particles instead of the fluid. Therefore, the tracers (seed or particles) properties should be in a range that significant discrepancy between the fluid and particle motion is avoided and particles represent the dynamical flow characteristics. The Stokes number (equation 4.1) is a dimensionless number used to determine the degree to which particles follow the flow. In other Words, the Stokes number determines particles' repose time to the flow response time. A Stokes Number much greater than 1 ($S_{tk} \gg 1$) describes particles that remain unaffected by the fluid velocity change and continue their original trajectory. For Stokes values much smaller than one ($S_{tk} \ll 1$) the particles response time is less than the time characteristic associated with the flow, i.e. that particles have ample time to respond to changes in flow velocity [221] and simply follow the flow.

$$S_{tk} = \frac{\tau \times U_{ave}}{d_f} \tag{4.1}$$

The relaxation time (equation 4.2), or particle response time, is the required time for particles to respond to a change of the fluid's velocity when the surrounding fluid velocity changes. For instance, when encountering an object, the fluid velocity, around the object, changes and particles follow the fluid and flows around the object.

$$\tau = \frac{d_p^2 \times \rho_p}{18 \times \mu} \tag{4.2}$$

Relaxation time is calculated from the diameter of the particle (d_p), particle density (ρ_p) and dynamic viscosity of the surrounding fluid (μ). The fluorescent particles in this study had a mean volume-distribution size of 10 μm and a density of 1.19 g/cm^3. A simple estimation shows that the response time of these particles at 20°C is estimated to be around 6.5 $\times 10^{-6}$ seconds. Such a response time is much smaller than the time scales of any realistic liquid. For the same response time, the Stokes number was around 5 $\times 10^{-3}$ for the thinnest spacer used in these studies (28 mil spacer: 0.71 mm spacer). Flow with a Stokes number much less than 0.1 ($S_{tk} \ll 0.1$) has a tracing accuracy error below 1% [221], indicating that the tracing accuracy in studies done is less than 1%.

In addition, to the fluid-mechanical requirement, the particles have to scatter enough light in order to be visible to the camera. The particle image intensity can be improved by increasing the scatter light power or choosing the proper seeding particles. It is usually

more effective and economical to choose the proper seeding particles than increasing the laser power. In general, the scattering light is a function of the ratio of the refractive index of the seed particles to that of the surrounding medium, the particles size, their shape and orientation. Moreover, light polarization and observation angles play important roles in scattering the power of particles. Therefore, a compromise is required between reducing the particle size to improve the flow tracking and increasing the particle size to improve the light scattering. Typical particle dimensions are in the order of tens of micrometers for fluids [221].

Particles used here were coated with Rhodamine-B to absorb the incident light and re-emit it at a higher wavelength. In combination with the $Nd:Yag$ laser, the coated particles not only scattered the laser light but also emitted orange-red light ($550-680\ nm$). This technique made it possible to separate the tracer particles from other scattering objects, such the observation window, membrane and feed spacer. This is done using a cutoff filter (Lavision, Grove, UK), which is centered around the emission wavelength of the particles ($\lambda = 545\ nm$). The cutoff filter passes only the emitted fluorescent light from the tracer particles and accordingly blocks the high background light level, as the consequence of application of the spacer and membrane (the wavelength of the incident light) and in this way improves the quality of the final result (vector maps).

4.3. FLOW RATE

Experiments were performed with the same set of flow rate in all configurations and orientations of feed spacers. This means that a different average velocity (equation 3.10) has been generated for each spacer at a particular flow rate. A range of flow rates made it possible to choose the same average inlet velocity during comparison of scenarios. The average velocity, which also known as the effective velocity in some literature [180, 217], is calculated by dividing the velocity of the empty channel (superficial velocity) to the porosity of the feed spacer (equation 3.10). The flow rate of the main liquid is controlled and measured by using a mass flow meter (Bronkhorst Instruments, Ruurlo, The Netherlands) of which the specifications are mentioned in table 4.1.

Table 4.1: Specifications of M14 mini-Cori-Flow (Bronkhorst), which is used to control the mass flow toward the flow cell.

Flow			Accuracy		
Minimum g/h	Nominal g/h	Maximum g/h	Flow ± % of flow	Density $\pm kg/m^3$	Temperature $^\circ C$
1000	10000	30000	0.2	5	0.5

4.4. FLOW CELL

It is common to use flat flow cells in studies related to hydraulic conditions of thin spacer-filled channels such as those of SWM modules of RO. A flat flow cell provides a simple but effective method of studying concentration polarization, biofouling, flux,

and pressure losses of SWM modules under various operating conditions such as different feed pressure, feed velocity and feed concentration [14, 152, 154, 157, 190, 191]. Reducing material expenses and investigation times as well as the ability to visualize the flow are the main advantages of using flat flow cell over a SWM module. The effect of curvature on the flow in SWM modules is insignificant and can be neglected when simulating these modules with flat flow cell because the feed channel height in SWM modules is very small [189, 197].

Flat flow cells are often used in studies related to hydraulic conditions in spacer-filled channel. For instance, the test cell used by Shen et al. [160, 187] and Light et al. [156] was composed of two separate plates with an overall dimension of 61 cm long and 19 cm wide. The top plate was made of Plexiglas (2.5cm thick) to facilitate viewing of the flow pattern and the bottom plate was made of polyvinyl chloride (5.1 cm thick). Two inlet ports were at the front end, and a similar pair of outlet ports was at the rear. The pressure gauges (the pressure tap holes) were located at the beginning, middle and end of the test section. The pressure tap holes were positioned in the middle of the channel width. The permeate outlet of the cell was designed at the bottom of the cell. A small O-ring was used to prevent mixing of permeate and concentrate. A large O-ring was used to seal the top and bottom test cell plates. The channel width was 10.2 cm and the channel length was 52.1 cm [156]. Flat Sheet Monitor (FSM) is another example of the flat flow cell, which is developed by the Vitens water company in collaboration with Kiwa, the Dutch water research institute. The body of FSM is made of stainless steel and its cover lid from Perspex. Membrane Fouling Simulator (MFS) is a downscaled version of the FSM, which is more suitable for transport, positioning and consequently use in the laboratory.

In this study, MFS-like flow cells are used to measure the velocity and the pressure drop. The flow cell (Demo, Delft, The Netherlands) was operated without permeation because the permeate flow in RO is small compared to cross-flow velocity. Additionally, previous studies have shown that effects of permeate production on pressure drop are insignificant [98, 192]. The membrane coupon and the spacer are located within the flow channel (L = 200 mm, W = 40 mm and H = 0.7 mm). The flow channel is embedded in the bottom part of the flow cell (L = 260 mm, W = 85 mm, H = 55 mm). In contrary to the spacer-filled channel experiments in which the total height of the flow channel was filled with the membrane and spacer, the empty channel experiments (Chapter 4) were car-

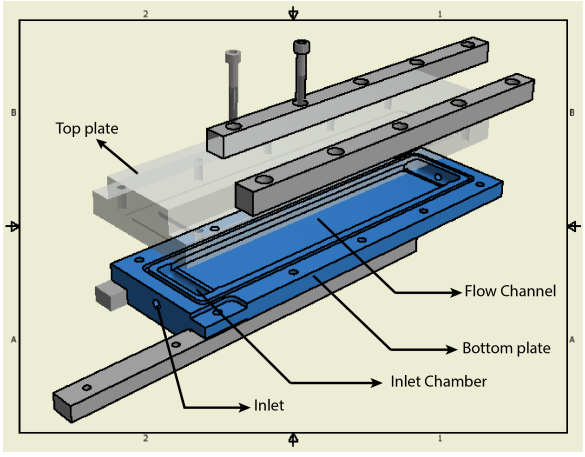

Figure 4.3: The flow cell used in this study. The feed channel is embedded in the bottom plate. The top plate is made of transparent material for visualization purposes.

ried out with only the membrane coupon (Trisep-AMC1) inside the feed channel. Each experiment was carried out at different flow rates and a constant temperature.

4.5. PRESSURE METER

Differential pressure transmitter (Deltabar S PDM75 Endress & Hauser, The Netherlands) is used to measure the pressure drop between inlet and outlet of the flow cell. The transmitter uses a metallic measuring diaphragm. The separating diaphragms are deflected on both sides by the acting pressure. The filled oil transfers the pressure to a resistant circuit bridge (semiconductor technology). The deferential-pressure-dependent change of bridge output voltage is measured and further processed.

4.6. MEMBRANE COUPON

Several membranes (figure 4.4) are used at the beginning of this PhD-study to investigate effects of membrane roughness on the velocity patterns without any feed spacers. The results of these studies are not being shown in this thesis. Trisep-ACM1 is used in all the performed experiments, i.e, in the empty and spacer-filled channel because it has the lowest average roughness among the tested polyamide membranes.

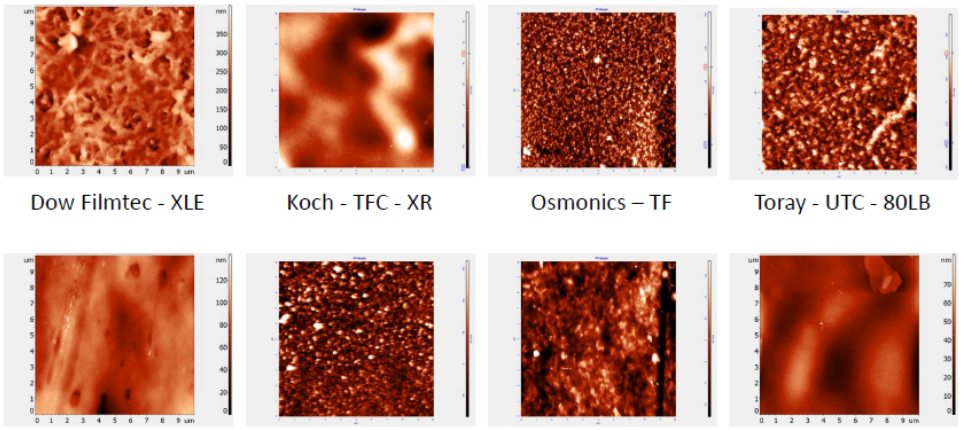

	Roughness (average)	Root Mean Square (RMS)
Dow Filmtec-XLE	38.637 nm	49.547 nm
Koch - TFC - XR	21.933 nm	33.178 nm
Osmonics - TF	19.073 nm	23.596 nm
Toray - UTC - 80LB	59.465 nm	74.901 nm
Osmonics -CA	5.425 nm	7.251 nm
Trisep-X201	34.708 nm	46.003 nm
Trisep-SB50	10.440 nm	13.782 nm
Trisep - ACMI	16.451 nm	21.012 nm

Figure 4.4: SEM images for determining membrane coupons roughness. In the remainder of this thesis, the membrane coupon refers to Trisep-ACM1. The latter has the lowest average roughness among polyamide membranes.

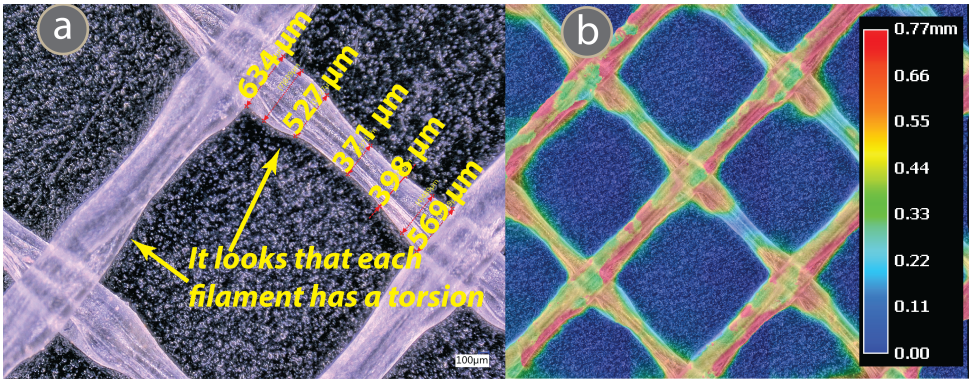

Figure 4.5: The typical commercial feed spacer, nonwoven and 31 mil (0.76 mm) thick. Image "a" shows dimensions of a filament. Image "b" shows the position of the spacer with respect to the membrane surface. The figure shows an uneven filaments' cross-section over their length. Moreover, a slight torsion is visible in each filament. These types of geometrical details are normally not incorporated in the computational models.

4.7. FEED SPACERS

The studied spacers were commercial nonwoven polypropylene (PP) spacers. The geometric data of these spacers are mentioned in related chapters. For each spacer the porosity (equation 3.7) and the hydraulic diameter (equation 3.6) are calculated. For calculation of average velocity (equation 3.10), it was assumed that the thickness of a filament is the same over its length in a mesh while, in reality, the thickness of a manufactured filament varies over its length. In contrary to general assumption that the channel height is twice the filament diameter, we measured the filament thickness and channel height in laboratory because the channel height is slightly smaller than the twice the filament diameter. The channel height is determined by the thickest part of the spacer, which is at spacer nodes. The thickness of spacer nodes is smaller than twice the filaments thickness because the top and bottom filaments are slightly embedded in each other (figure 4.5).

4.8. LASER

Experiments are done by using a laser light because the laser is able to emit monochromic light with high-energy density, which can easily be bundled into a thin light sheet. Laser sheet made it possible to illuminate and record the tracers without chromatic aberration. Diode laser $Nd:Yag$ (neodymium-doped yttrium aluminum garnet) from Litron-Optical (table 4.2) is the semiconductor laser that is used for the PIV measurements in this thesis because semiconductor lasers have usually a compact size. Additionally, this type of laser can supply a very good beam quality because the heating is considerably reduced in this type of laser. The mentioned laser is classified into class four lasers.

Table 4.2: Specifications of laser (Nano S 65 – 15 PIV) used in PIV setup.

Energy at 532nm	Repetition Rate	Beam diameter	Pulse length at 1064nm	Divergence	Pulse stability	Jitter
mJ	Hz	mm	ns	mrad	± %	±ns
65	0-15	4	6-8	2.5	2	<0.5

4.9. CAMERA

Imager Pro X 2M (Lavision, UK) is used in these experiments for taking images. The camera is equipped with an interline transfer chip with progressive scan readout. A minimum inter-frame time of 110 ns makes this camera suitable for PIV installation. The interline transfer chip makes the camera more sensitive in the blue-green region of the light spectrum. General specifications of the camera are mentioned in table 4.3.

Imager pro X 2M is a CCD-based camera. A CCD-camera is equipped with a CCD electronic sensor, which can convert light (i.e. photons) into electric charge (i.e. electrons). A CCD sensor is composed of an array of many individual CCDs, either in the form of a line (e.g. in a line scan camera), or a rectangular or other specialized form. A distinctive CCD element in the sensor is called a pixel.

Table 4.3: Specifications of Imager Pro X 2M

Description	Specifications	Description	Specifications
Double shutter	Two images with the minimum inter-framing time	Maximum Quantum Efficiency	typ. 55% at 500 nm
Inter-frame	110 nS	Full Well capacity	40000 e^-
Dynamic range A/D	14 bit	Blooming Suppression	> 300×
Interface	Camera link	Readout rate	40MHz
Number of pixels	1600 × 1200	Frame rate	29 frames/s
Pixel size	7.4 × 7.4 μm^2	Binning	
Sensor format	12.2 × 9 mm^2	- horizontal	1, 2
Spectral range	290 – 1100 nm	- vertical	1, 2, 4, 8
Operating temperature	5 – 40°C	Cooling Peltier	to 10°C

4.10. PIV DATA ACQUISITION SYSTEM

During the PIV-measurements, the fluorescent particles inside the channel are illuminated by a laser (Nano S, $Nd:Yag$ laser, Litron laser, UK) with two light pulses of a short interval. A high-speed camera (Lavision, Grove, UK) is recorded two frames exposed by the laser light pulses. The time interval between two pulses (two frames) was adjusted to the particles-displacement in order to reduce the number of pairing losses. The time interval was varied from 150 – 2500 μS depending on the flow rate inside the channel and presence of the spacer. Each of the captured frames is divided into small interrogation areas. An embedded algorithm in the software determines the shift of intensity pattern in each of these small areas. The logarithm uses the information from every two captured sequenced frames and a mathematical method such as Fast Fourier Transfer (FFT) to determine the quantity and direction of tracers in the solution. The

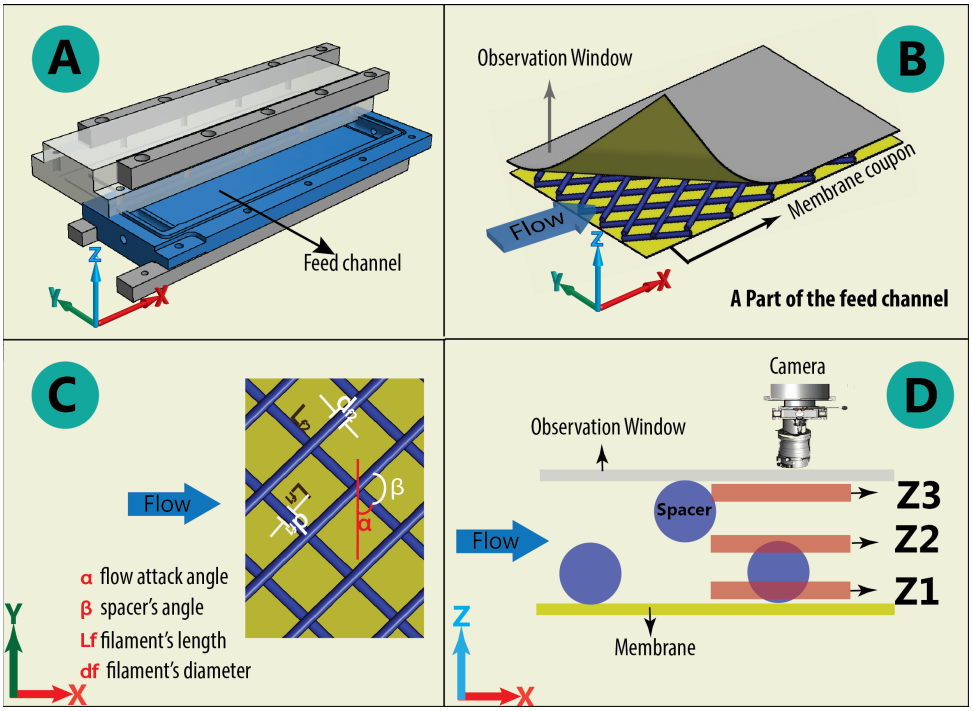

Figure 4.6: The flow cell ($L = 260\ mm$, $W = 85\ mm$, $H = 55\ mm$) is made of a Plexiglas at the top, which serves as an observation window. The flow channel ($L = 200mm$, $W = 40mm$, $H = 0.7\ mm$) is embedded in the bottom part of the flow cell (A). A membrane coupon and the feed spacer are placed in the feed channel under the observation window (B). Definition of the spacer nomenclature used in this study (C). Definition of the focusing depth of the camera (D).

controlled time interval and calculated displacement are used for calculation of the velocity vectors. In order to limit the effects of boundaries (entrance, edges and exit) on the flow and to ensure a fully developed flow, the frames are taken at about 100 mm from the inlet and $15mm$ from each edge of the cell.

PIV-images captured at three different heights inside the feed channel: close to the camera (Z3), middle of the channel (Z2) and far from the camera or close to membrane sheet at the bottom of the feed channel (Z1) (figure 4.6). Since the thickness of the laser sheet light (2 mm) is greater than the thickness of feed channel, the entire channel height is illuminated. That is a common situation in μPIV [141] which is solved by fixing the camera focus at a specific distance from the lens and moving the object [141, 222]. In this study, the camera focus was fixed at a specific distance from the lens and the camera moved on the translation stage because moving the object was not possible. The translation stage made it possible to move the camera 50 μm in each step. The camera was initially placed such that particles in the middle of the channel and close to membrane were barely in focus (Z3). Then the camera is moved to the next positions (Z1, Z2) with translating stage. The setup's depth of field was about 0.14 mm. For each specific flow rate and depth, 50 pairs of images (100 frames) were taken (figure 4.7a) with the time

interval of about 30 mS. An instantaneous (momentary) velocity map is calculated for each pair of frames, which results in 50 instantaneous velocity maps (figure 4.7b). These 50 images are used to compare the temporal variation of velocity inside the feed channels. An average of these 50 pictures (figure 4.7c) is used to study the spatial variation of velocity inside the feed channel.

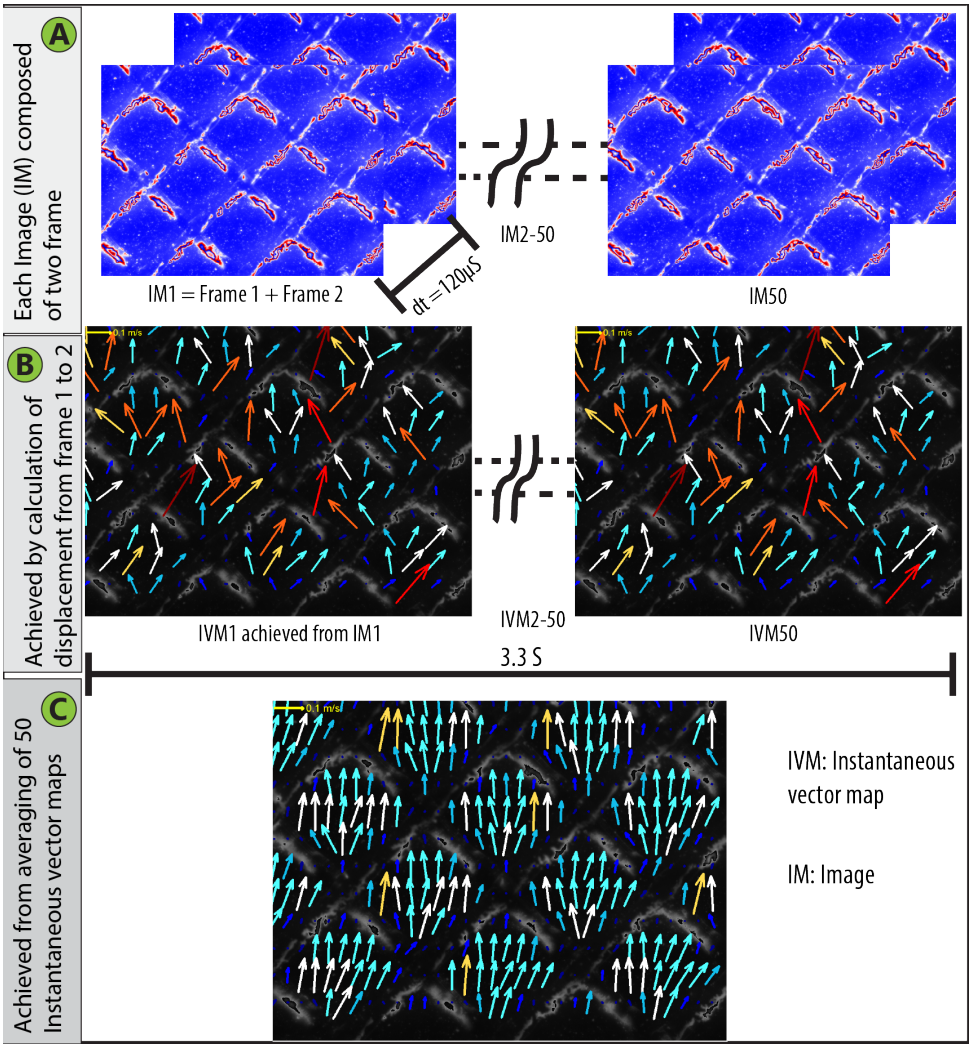

Figure 4.7: PIV measurement and data analysis: 50 pairs of images are taken, with a time interval of 120 μS between two frames of each pair of pictures and time interval of 0.06 s between each pair (a). Using each pair picture, the instantaneous velocity of the respective pair is calculated (b). Average of all 50 velocity maps is presented as the average velocity(c).

5. Empty and spacer-filled channel

Summary

It is widely accepted that our understanding about the membrane process increases by investigation of the hydraulic conditions of membranes. While numerical studies have been broadly used for this purpose, the experimental studies of a comparable resolution are scarce. In this study, we compared the pressure drop, the temporal and the spatial velocity maps of a spacer-filled channel and an empty channel of the same size to determine the effect of presence of the feeds spacer on hydraulic conditions. The velocity maps are obtained experimentally by using of the particle image velocimetry (PIV) technique. Application of the feed spacer caused 2 – 8.5 higher pressure drop increase in the experimental conditions in this research. The flow had a spatial distribution in the form of a unimodal symmetric curve of normal distribution in the empty channel and a bimodal asymmetric curve in the spacer-filled channel. The bimodal curve indicates the presence of high- and low-velocity zones. Additionally, the low-velocity zones showed also a lower variation of velocity in time, which indicates the high fouling potential of these locations. The results from this study may be uses for validation of numerical studies.

Parts of this chapter have been published in Journal of Water Research **106**, 232-241 (2016) [153].

5.1. INTRODUCTION

Application of reverse osmosis (RO) for purification of water increases continuously. Spiral Wound Membrane(SWM) modules of RO (RO) are the most applied configuration in drinking and wastewater. The feed spacer as one of the main parts of the SWM modules of RO plays an important role in hydrodynamic inside these modules. In addition to SWM modules feed spacers are also used in flat and sheet configuration of RO, forward osmosis, pressure retarded osmosis, membrane distillation, electrodialysis, etc. The feed spacer acts as a stabilizer by separating the membranes' leaves and forming of the feed channel. Alternatively, it disrupts the flow and enhances the flow mixing between the bulk of the fluid and the fluid adjacent to the membrane surface. The latter improves the mass transfer, albeit at the expense of increases in energy losses [14, 61]. The benefits of mass transfer enhancement often outweigh the disadvantages caused by increased energy losses such that it becomes more economically attractive to operate membrane systems with spacer than without [155, 157, 180]. The former studies have shown that current feed spacer could themselves become a source of fouling, particularly biofouling [63, 79, 98, 101, 102, 116, 117, 192, 223]. The biofouling becomes more highlighted in surface freshwater or municipal wastewater than the saline water resources because of the lower potential of freshwater for creation of the concentration polarization. Therefore, design of feed spacers to promote the flow instabilities simultaneously with minimizing of energy losses and fouling will contribute enormously to improvement of a membrane's configuration. The design of an optimal feed spacer requires a deep understanding of the flow conditions through studying the flow velocity map, deceleration locations and flow distributions in the feed channel. This can be done experimentally or by using of computational simulation.

Computational techniques provide high-resolution velocity maps in the range of micrometers (μm^2)and have relatively lower costs and risks compare to experimental methods. However, application of these numerical techniques may be associated with difficulties such as matching of exact geometry of the modeled-spacer with reality, simulation of fouling and accurate verification and validation of these models. Many numerical studies are done with simplified spacer geometry, while geometrical details of the filaments in the feed spacer have remarkable effects on the hydrodynamics of channel and the fouling. For instance, Neal et al. [12] showed experimentally that particle deposition occurs around the point where the attached filaments to membrane bulge outward. While advances in the technology such as the 3D-printing provide a promising solution to this difficulty, the fouling process, as one of the main phenomena taking place in membrane systems, remains as a complicated and time consuming part to be incorporated into numerical models [180]. According to Fimbres and Wiley [180], and Schausberger et al. [224], the fouling models that are developed before them [224–226] could not be used as a reliable predictive design tool. As mentioned by former studies [180, 227], the verification deals with mathematics of the model, while validation deals with its physics. Oberkampf and Trucano referred in their study [227] to the five most common sources of the numerical errors that could be present within a model. These numerical errors result is defining a different set of equations than the system of partial differential equations, that the transport equations defined, and consequently, not

accurate verification of the model [180]. Validation is one of the main difficulties that most computational studies within the field of membrane science face. Therefore, some researchers [141, 180] recommended applying of direct, non-invasive, high resolution experimental methods such as the particle image velocimetry (PIV).

To the authors' knowledge, PIV is used only by Gimmelshtein and Semiat [203], and Willems et al. [141] for flow investigation inside the SWM modules of RO. Gimmelstein and Semiat [203] studied the liquid flow in spacer-filled cells in the velocity ranges from $0.06 - 1.3\ m/s$. Willems et al. [141] investigated the liquid velocity profiles of water and water-air mixture in spacer-filled channels. Gimmelstein en Semiat [203] showed that the bulk of fluid flows in a straight line from inlet to outlet with only small deviations near the filaments. Willems et al. [141] found that liquid flows mainly parallel to the spacers' filaments and therefore, the direction of flow changed 90° over the height of the channel. Willems et al. [141] related the disagreement of their findings with those of Gimmelshtein and Semiat [203] to that in their setup the spacer filled the whole height of channel whereas in the study of Gimmelshtein and Semiat 20% of the height of the feed channel was empty. Willems et al. [141] found that the liquid velocity was unsteady in one phase and two phase flow, which was in agreement with different studies [167, 205, 228, 229] done with computational fluid dynamics (CFD).
Because of the limited availability of PIV-studies in the spacer-filled of RO and the empty channel (slit) of the same size, we studied the flow of water through the empty and spacer-filled channel at Reynolds' numbers (Re) below 250 to provide a visual aid for a better understanding of the flow inside SWM modules of RO. To this end, first the terms that are used throughout this chapter are explained and then the setup and measurement methods are described. After that, the effects of introducing of a typical feed spacer of RO to an empty feed channel on the pressure drop are investigated. In the next section, the temporal velocity acquired from the PIV measurement is studied as these types of information are scarce in literature. After that, the spatial velocity is measured, and the results are compared to the available experimental data and the CFD studies. Finally, the effect of increase of Reynolds number on velocity pattern inside the spacer-filled channel is studied.

5.2. MATERIAL

In this chapter, we compared the effect of using a feed spacer inside an empty channel of the same size. The specification of the empty and spacer feed channel are mentioned in table 5.1.

Table 5.1: List of some studies done on mass transfer enhancement

Id	Channel height	Filament length	Spacer angle	Porosity	Hydraulic diameter	Material
Unit	(mm)	(mm)	(O)	(%)	(mm)	(-)
Empty channel (Slit)	0.76mm	NA	NA	100	1.50	Without spacer
Spacer-filled channel	0.76mm	2.33	89.5	87	0.88	polypropylene

5.3. RESULTS

5.3.1. PRESSURE DROP

The driving force in SWM modules of RO is strongly influenced by feed channel pressure losses, which increase due to application of feed spacers [58, 61, 152] and formation of fouling. The pressure drop of a spacer-filled channel depends on the viscous drag on the spacer, the form drag, the kinetic losses or eddies due to directional flow changes and the viscous drag on the channel walls [152]. All of these components are related directly or indirectly to the average velocity in direction of the flow (U_x) albeit with different magnitude. The flow condition (if a flow is laminar or not) is determined by defining the relation between the pressure drop and the power of average velocity m (equation 3.12). Da Costa et al. [157] suggested that for laminar flow m should be around one and for turbulent around 1.75. However, in turbulent flow the Reynold's number (Re) is far above the Re in the SWM modules of RO. Therefore, as it has been suggested [179, 180], it is better to talk about the disturbance inside the flow as eddies rather than turbulence. Figure 5.1 shows the effects of the increase in the flow rate (A) and the average velocity (B) on the pressure drop per unit length of channel. The pressure drop measured here is the total pressure drop, which consists of the pressure drop as the consequence of connecting the tubes to the pressure transducer, pressure drop at the boundary layers and pressure drop due to the presence of the feed spacer. The pressure drop in the spacer-filled channel was (0.27 $bars/m$ for an average velocity of 0.16 m/s) in the expected practical range of a single SWM module of RO (0.2 – 0.3 $bars/m$ for an average velocity of 0.16 m/s). The effect of only the feed spacer on the pressure drop is calculated by subtracting the pressure drop of the empty channel from the spacer-filled channel. This difference was respectively 0.008 and 0.31 bar/m for the lowest and highest flow rate applied. The power m was increased from 1.63 to 1.74 by considering only the spacer.

5.3.2. PIV MEASUREMENTS

SPATIAL VELOCITY PATTERN

Figure 5.2 illustrates the spatial average velocity of the spacer-filled channel at different levels; close to the membrane (Z1), at the boundary of the top and bottom filaments (Z2) and close to the observation window of the flow channel (Z3). The measurements of each level were performed at a different momentum but with the same inlet velocity. The flow was aligned with the direction of the filaments at Z1 (close to the membrane) and Z3 (close to window). The flow at Z2 (middle of the channel) had a pattern such as the mixed image of the flow at Z1 and Z3. These results were in accordance with the results achieved by the Willems et al. [141] for a single-phase flow in the spacer-filled channel. The flow pattern at the middle of the channel was the same as the flow pattern observed by Lau et al. [229] when they used a spacer of 1.0 mm thick with a flow attack angle of 45° and a Re of 600 (fig. 07 in their work). However, the length of filament is not mentioned in the provided literature. While, the presented results in figure 5.2 correspond to the highest average velocity only, the flow patterns remained the same by decreasing of the average velocity to 0.06 m/s (figure 5.3). However, by further decrease of the velocity, the flow pattern deviated more from the flow pattern shown in figure 5.2

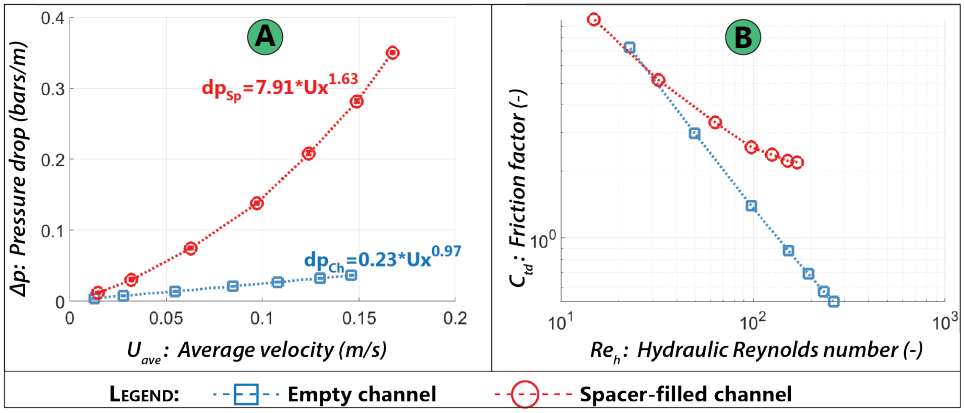

Figure 5.1: Effects of the increase of average velocity on the pressure drop (A) and increase of Reynolds number on friction losses (B) in the empty and spacer-filled channel of the same height 0.762 mm (30 $mils$). The slope of empty channel is -1, which indicates a totally laminar flow. The slope of spacer-filled channel is slightly different. In the spacer-filled channel, the flow is not turbulent because the Reynolds number is much lower than the Reynolds number in turbulent regime.

5

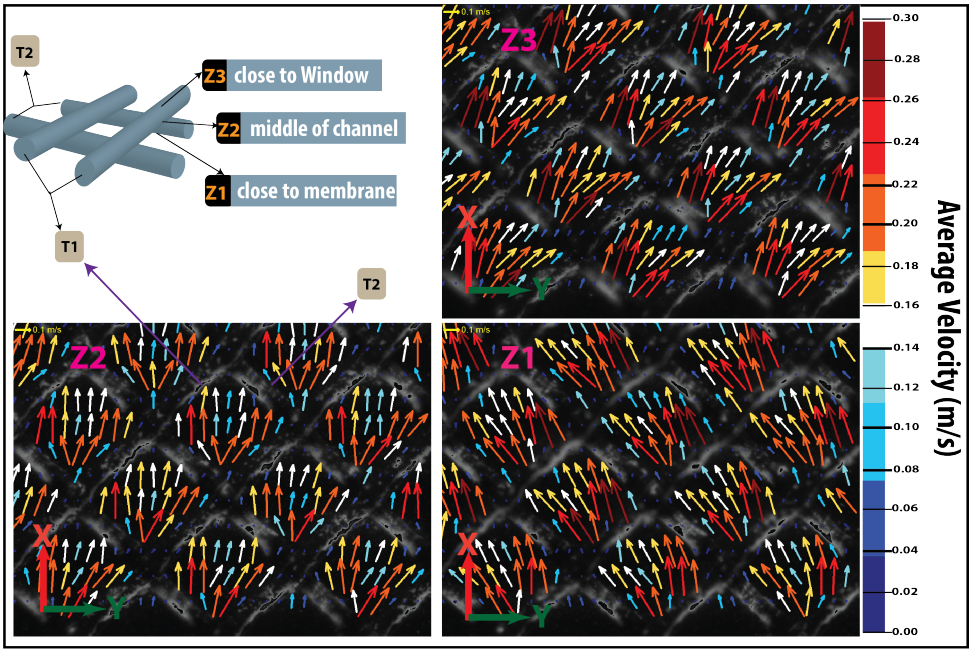

Figure 5.2: spatial variations of the velocity averaged over time for the spacer-filled channel at different levels; close to the membrane (Z1), at the middle of the channel (Z2) and close to the observation window (Z3). The inlet velocity used here was 0.17 m/s.

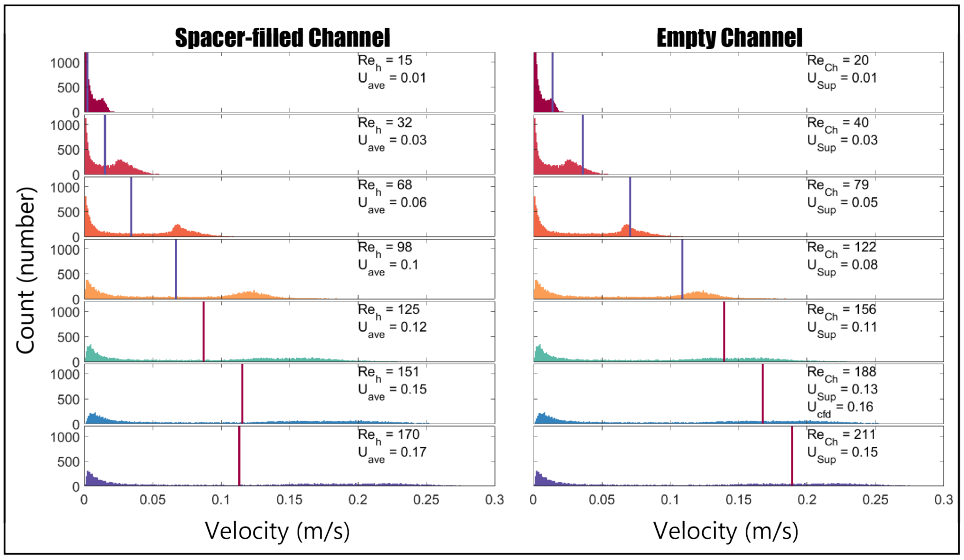

Figure 5.3: Development of velocity inside the empty channel and the spacer-filled channel. The vertical line indicates the median of the data. The measured velocity is shown on the x-axis and the number of corresponded particles on the y-axis. By the increase of flow, the average velocity increases but the velocity patterns remain the same.

particularly at Z1 and Z3 planes. In these low flow conditions, the flow pattern was not aligned in the direction of the filaments anymore but in the direction of the flow from the inlet to outlet in a straight line albeit with some deviations close to the filaments.

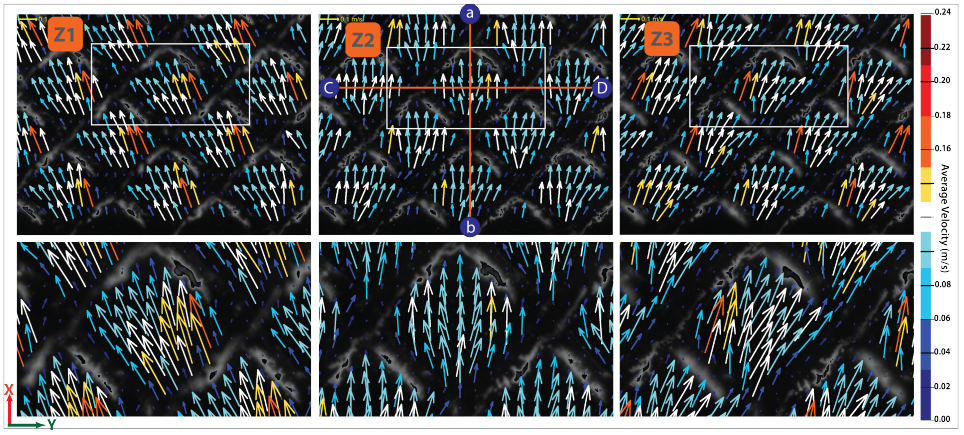

Figure 5.4: The pictures on the left show total field of view for three levels (Z1, Z2 and Z3) and the pictures on the right-side illustrate the zooming panel for one mesh. The velocity patterns shown here are for an average velocity of 0.1 m/s ($Re = \pm 100$). The velocity profiles along lines $a-b$ and $C-D$ are shown in figure 5.5.

As expected, the flow in the empty channel was in the straight line from the inlet to the outlet (the results are not shown here). In the conditions with an average velocity lower than 0.04 m/s, however, the flow was slightly deviated from the straight line patterns especially at the Z1 and Z3 planes. The average velocity in empty and spacer-filled channel was deviated from the measured velocity. This difference is the results of measuring the fully developed flow velocity at the middle of the channel, while introducing the inlet velocity as the average velocity by the Equation 3.10. The fully developed velocity has a parabolic shape in the Z direction with the lowest velocity at Z1 and Z3 and the highest velocity at Z2. The entrance length, which is defined as the length of the channel that the flow becomes fully developed, is about 2.17 cm for a rectangular channel with an aspect ratio of 1/50 (H/W) [175].

Figure 5.4 illustrates the velocity pattern with an average inlet velocity of 0.1 m/s for the field of view (left) and a magnification of a mesh (right). The results show that when the camera is focused on Z1-plane, the highest velocity occurs when the fluid passes over a filament, enter the mesh and passes under the filament at shortest distance to exit the mesh. When the camera is focused on the Z3-plane, the highest velocity occurs when the fluid passes under a filament, enter the mesh and passes over a filament at the shortest distance to exit the mesh. The lowest velocity can be observed at the upstream corner of each mesh (figure 5.4). The pattern described here is in agreement with the velocity

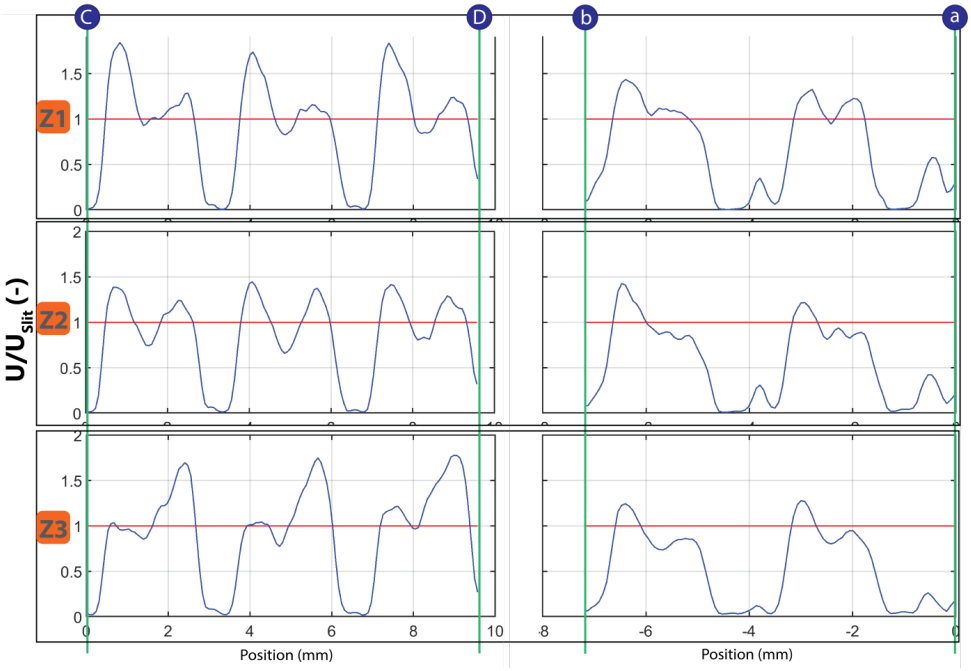

Figure 5.5: Normalized velocity variation along a line in direction of the flow (line a-b) and perpendicular to the direction of the flow (line C-D) between two nodes of a spacer for planes Z1-Z3. $U_{ave} = 0.1\ m/s$ ($Re = \pm 100$)

map shown by Bucs et al. [230] (fig. 03C; in their work). The velocity pattern can be directly related to the fouling. For instance, the places with highest fouling potential can be identified by knowing the lowest velocity regions. An example of such relation can be observed by comparing of the velocity patterns showed in figure 5.4 with the deposition patterns of the particles which are observed by Radu et al. [215]. The locations of lowest velocity pattern in our study were in agreement with the deposition locations of microsphere particles when Radu et al. [215] used the same orientation as in our study. Figure 5.5 shows the normalized velocity profile (U/U_{Slit}) over the section a-b (parallel to flow) and C-D (perpendicular to flow) at the three different levels. The velocity pattern at Z1 mirrors the pattern of Z3 along the line C-D. The velocity pattern along the C-D line at Z2 (middle of the channel) is such as the mixed pattern of Z1 and Z3.
The velocity along the line a-b has the same patterns in all three levels indicating that the flow patterns between two nodes along the flow remain the same irrespective to the height of the measurement. It is obvious that a slight shifting of these lines results in another velocity pattern. For instance at a distance of about 25% from each node toward the middle of a mesh, the velocity pattern along a-b in Z1 mirrors the velocity pattern of Z3 while the velocity pattern along C-D remains the same as the patterns of figure 5.5 (graphs are not shown here).

TEMPORAL VELOCITY PATTERN

The results from former section consider the effect of average inlet velocity on pressure drop and the variation of the velocity in place. In this section, we study the effect of time on the velocity in some specific points. Generally, a high velocity variation is preferred at a point, specifically a variation with a value above the specific average velocity. A high variation of velocity implies a local pulsation at a point and generation of unsteady flow. This unsteadiness contributes to fouling reduction, because the amplitude shear oscillation is better than shear alone in minimization of fouling specially concentration polarization [231]. Figure 5.6 provides an overview of the temporal velocity variation for five points inside a mesh at three different heights (Z1, Z2 and Z3). The time interval between each measurement was in the range of milliseconds (figure 4.6). The results shown here correspond to the average velocity values of 0.17 m/s (equation 3.10). Each box represents 50 measurements. The median, average and outliers are shown respectively with a straight line, empty circle inside the box and filled circles. Figure 5.6 shows an unsteady characteristic of the flow in which the velocity varies over time at a particular point. The highest unsteadiness is observed in the middle of the mesh (E) and the lowest at downstream angle of the mesh (A) in all three levels. Also, the temporal velocity of where the water enters a mesh under a filament (point D) is higher compare to other points. In most cases, the unsteadiness at the membrane sides (Z1 and Z3) is slightly higher than the middle of the channel.

5.4. DISCUSSION

Many computation models are validated with experimental methods of much lower resolutions than the computational calculations itself. As shown in this work, PIV can provide detailed velocity profiles in empty and spacer-filled channels. Hence, such experimental information can be used as the input values for validation of computa-

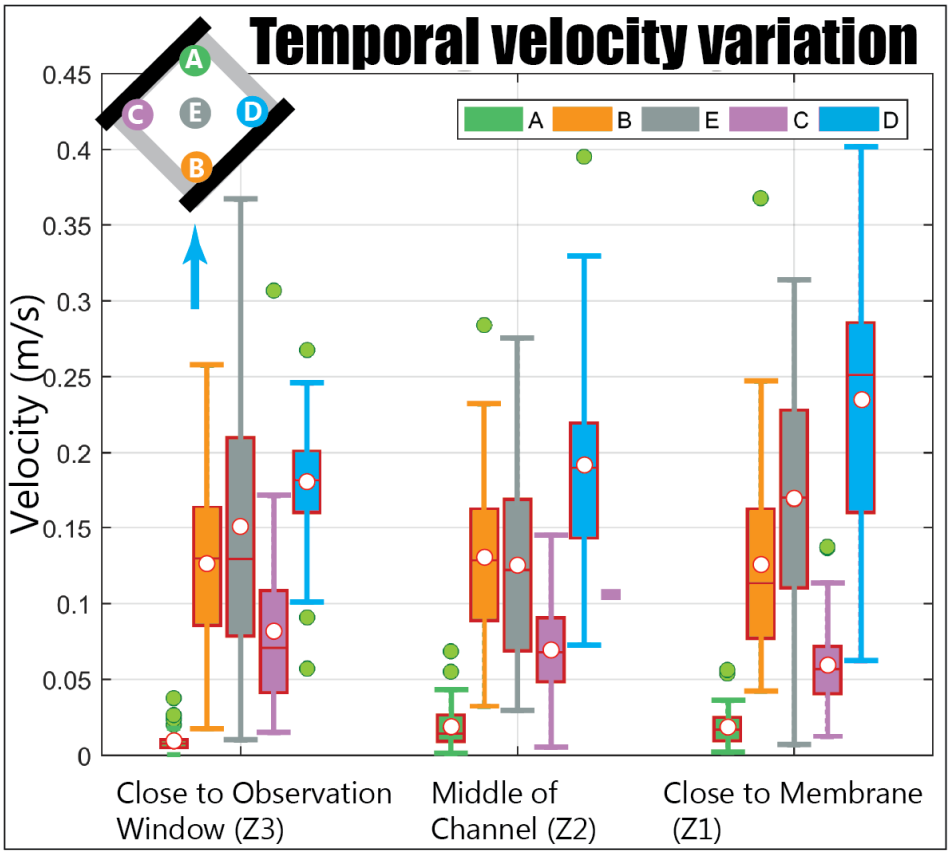

Figure 5.6: Variation of temporal velocity for five points inside the spacer-filled channel for an verge velocity of 0.17 m/s ($Re = \pm 265$).

tional models. Relating of the velocity pattern with the fouling can be used as a tool for a better understanding of the fouling phenomena and improvement in the feed spacer design in the future. For instance, the temporal and spatial velocity patterns in this study show that downstream of nodes (location such as point A in figure 5.6) have high fouling potentials compare to the other places. The practical results show that such locations are places that particulate fouling occurs more intensively [215] than other places and the biofouling starts at such points. The initiation and development of biofouling at the nodes of the spacers is shown by different researchers [142, 232].

This study has also illustrated the difference between the flow patterns in the empty and spacer-filled channel. The velocity has a shape of a unimodal and a bimodal normal distribution statistically respectively in the empty and the spacer-filled channel (figure 5.3). By the increase of the inlet velocity as the results of increasing of the flow, the standard deviation of the velocity increases, which indicates a better mixing of the flow in xy-plane. A higher velocity at XY-plane is desirable for postponing of the fouling. How-

ever, this will be achieved by application of higher flow and consequently higher energy consumption. In this case, the pressure drop increases linearly in the empty channel and with a velocity power of about 1.74 for a spacer with the same geometry as described in this chapter.

5.5. CONCLUSIONS

The temporal and the spatial velocity are investigated in the flat empty and the spacer-filled channel with the height of 0.76 mm, which is a very common channel height in Spiral Wound Membrane (SWM) modules of reverse osmosis (RO). The particle image velocimetry technique is used to obtain high-resolution velocity maps and coated particles were used in combination with a cutoff filter to improve the quality of these vector maps. This chapter gives information on the velocity pattern in the XY-plane and pressure drop over the length of the channel. The results achieved in this study showed agreement with previous numerical and experimental studies. Measurement of the velocity showed that there are low- and high-velocity zones inside each mesh. Some of these low-velocity zones, which also have low temporal velocity variations, are the places that deceleration of the particles happens and (bio)fouling initiates. The results from this study can provide information to validate computational studies. The PIV-measurement for other configurations of the feed spacers reveals the effect of the spacers' geometry on the velocity pattern and the fouling potential of the feed spacers. Combining such measurement with the measurement of pressure drop and the results from the computational studies will lead to a better understanding of the hydraulic conditions in the spacer-filled channel and consequently, the design of the perfect spacer.

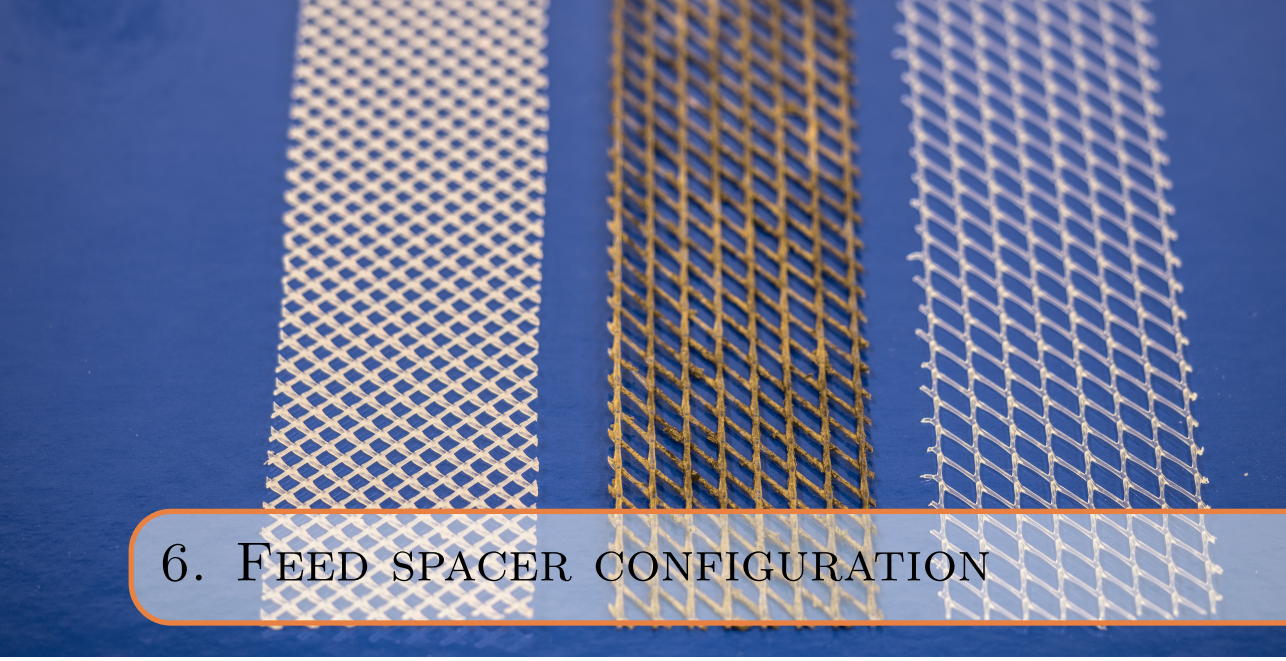

6. Feed spacer configuration

Summary

Making improvements to the feed spacer of spiral-wound membrane (SWM) modules of reverse osmosis (RO) systems is a necessary step towards a wider application of these modules. This study sets out to evaluate the performance of six commercial feed spacers by comparing their actual velocity profiles and their pressure drop. Velocity profiles are obtained from particle image velocimetry (PIV). Comparing images from PIV with the corresponding friction losses revealed that the transition from steady to unsteady flow occurs at the moment when the incline of the friction factor changes from steep to slight. From the two types of spacers used, the zigzag spacers showed a better distribution of flow than the cavity spacers did, but at the cost of higher pressure drop. The flow was in a straight line from inlet to outlet with zigzag spacers only at low Reynolds numbers and with cavity spacers for the entire studied range of Reynolds numbers. Additionally, results showed that hydraulic conditions in channels with cavity spacers are mainly affected by geometric characteristics of transverse filaments. The results from this chapter can be used to understand the effects of spacer geometry on the hydraulic conditions inside the feed channel and as a validation tool for computational modeling.

Parts of this chapter have been submitted to Journal of Membrane Science

6.1. INTRODUCTION

Safe and clean water is in short supply in many corners of the globe. Reverse osmosis (RO) is a popular desalination technique, which has been employed to satisfy the ever-growing demand for water for municipal and industrial consumption. Aside from desalination, there is likely to be a growing trend towards the use of RO for purification of fresh water from rivers, canals, and faucets, because RO can provide an excellent barrier against micro- and nano-contaminants. Dealing with emerging micro- and nano-pollutants remains a continuing challenge for treatment plants, because these pollutants are often dangerous even at low concentrations and cannot (easily) be removed from the feed water with conventional techniques [233]. For instance, Wong et al. [234] have reported that certain species are in danger of extinction in almost half of European and North American rivers and lakes because of the pollution of these ecosystems [233].

A wider application of RO is possible by bringing down the unit costs of water production in these membranes. Considering the worldwide water production by RO (74.4 million m^3 in 2015) [54], high energy costs, and the fact that spiral-wound membrane (SWM) modules are the most popular commercial configuration of RO [235], the costs of RO systems can be significantly reduced even by small improvements in the efficiency of these modules. Improvements in SWM modules can be achieved by modification of important pieces of a membrane module such as the number and size of envelopes [58, 236], the physical and chemical properties of membrane material and adapting the spacers' configuration. Spacers are inexpensive parts in an SWM module, which are used to prevent membrane surfaces from touching each other; they thereby provide permeate and feed flow paths (channels). The feed spacer also facilitates mixing between the bulk of fluid and the fluid adjacent to the membrane surface [14]; it thereby minimizes the effects of concentration polarization. The latter has been considered to be the primary function of feed spacers, since feed spacers in RO were historically designed to prevent concentration polarization in seawater modules.

A slight increase in feed spacer thickness (from 28 to 34 $mils$) is one of the few changes that feed spacers of RO have undergone. A proper design of a feed spacer for new applications would be possible through the investigation of hydraulic conditions in SWM modules. The hydraulic conditions of SWM modules can be investigated through performing numerical and experimental studies on the pressure drop and velocity development inside spacer-filled channels. For instance, effects of the ratio of filament length to channel height (l_m/H_{CH}), flow attack angle α, and hydrodynamic angle β have been subjects of many numerical and experimental studies related to spacer performance [15, 61, 167, 170, 189, 197, 205, 228, 237, 238].

Numerical studies have made a great contribution to a better understanding of spacer performance. In this context, Schwinge et al. [13] and Fimbres and Wiley [180] contributed comprehensive overviews. While in many numerical calculations spacers with a simplified filament cross-section are used, the experimental data with commercial feed spacers [12, 58, 152, 157] have shown that detailed characteristics of filaments are essential for determining flow conditions in spacer-filled channels. For instance, Neal et al.

[12] showed that the precipitation of particles is influenced by the shape of filaments in commercial spacers. They [12] observed that particle deposition mostly occurs around the point where the attached filaments bulge outward. In this light, some researchers [215, 239] have started to use spacers with closer geometrical similarities to those of commercial spacers for the numerical studies. Additionally, while numerical studies are able to provide detailed information on velocity profiles, they are usually validated with low-resolution experimental studies because of a limited number of direct experimental studies on the detailed velocity profiles [141, 180].

Particle image velocimetry (PIV) is a non-invasive technique for measurement and visualization of the flow with high resolution. Results of PIV are instantaneous velocity maps, which can be averaged over time. The velocity maps can be used to determine the state of flow, identify the low and high velocity areas and dead zones, determine the flow distribution, etc. However, to the authors' knowledge, there are only limited studies done with PIV in the field of membrane technology. Gaucher et al. [200] made use of PIV for visualization of the flow in ultrafiltration flow cells without a spacer. The flow in their experiment [200] was from inlet to outlet in a straight line with small deviations around the inlet and outlet. They [200] found a lower average velocity with PIV than the expected average velocity. Gimmelshtein and Semiat [203] and Willems et al. [141] used the PIV technique to visualize the flow inside spacer-filled channels. Gimmelshtein and Semiat [203] reported that the flow was from the inlet to the outlet in a straight line while Willems et al. [141] indicated that flow was along the attached filaments at the corresponding channel heights. The difference between the results of these two studies was the consequence of using different setups. Gimmelshtein and Semiat [203] used a spacer thinner than the channel height [141] and due to this, a space was created above the spacer in which the flow was in a straight line. Willems et al. [141] used spacers with thicknesses the same as channel heights. In a previous study [28], we compared the flow inside an empty channel with that of a spacer-filled channel by using the PIV technique. The results showed that the flow was in a straight line from inlet to outlet in the empty channel, thus in agreement with the results of Gaucher et al. [200], and it was along the filament at the corresponding height in the spacer-filled channel, thus in agreement with the results of Willems et al. [141]. This indicates that the camera in the study done by Gimmelshtein and Semiat [203] was probably focused on the empty part of the feed channel.

The purpose of this chapter is to compare commercial spacers of different configuration by using PIV and measuring the pressure drop along their flow channel. In this context, velocity profiles with high resolution will be provided without any simplification to geometric characteristics of spacers. First, the setup and the measurement method are explained. Then, pressure losses and friction factors are illustrated for examined spacers. Next, variations in simultaneous velocity profiles are revealed for particular points from the field of view. After that, the averaged spatial velocity map is discussed for a specific flow and then for the entire range of flows. Finally, PIV results at which the friction factor shows extreme changes are illustrated for one of the spacers.

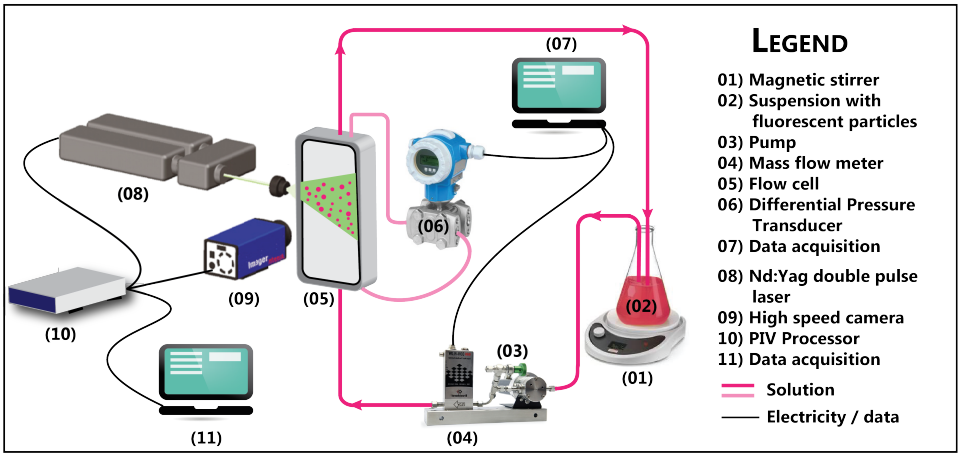

Figure 6.1: The experimental setup that was used for measurement of the pressure losses over the flow cell and for visualization of the temporal and spatial velocity inside the spacer-filled channel [153]

6.2. EXPERIMENTAL

Figure 6.1 illustrates a schematic view of the experimental setup used in this study. A solution (02) containing fluorescent particles is circulated through a mass flow meter (04) and then a flow cell (05) by means of a pump (03) to the feed tank. The pressure drop over the flow cell is measured by means of a differential pressure transducer (06). Values from the pressure transmitter are used to calculate the friction losses. Simultaneously, velocities are measured when a laser (08) emits two light pulses and a high-speed camera

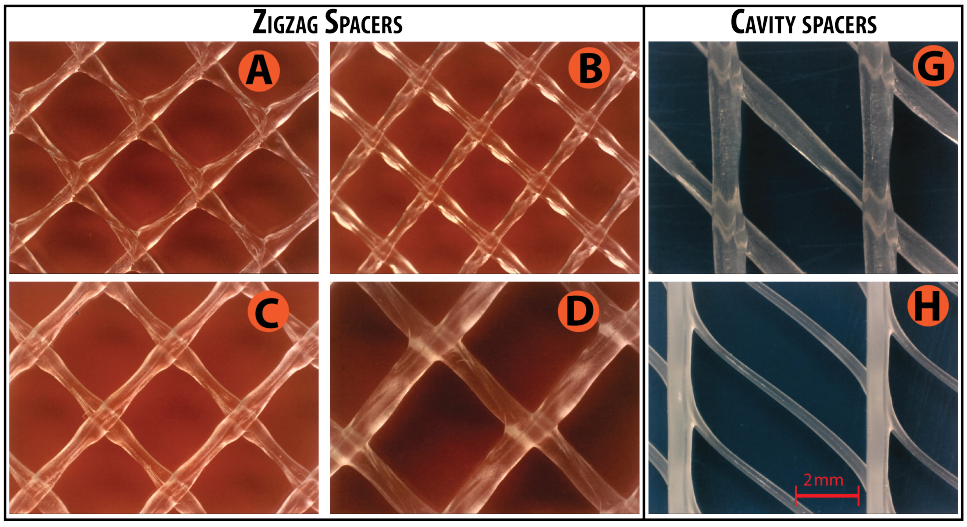

Figure 6.2: The feed spacers are categorized into two configurations: zigzag spacers and cavity spacers.

(09) takes two images (11) within a short time interval. The captured images are used to determine the temporal and spatial velocity maps using a commercial software application called Davis 7.2. A detailed description of instruments and the setup can be found in chapter 4. Measurements were taken inside the flow channel ($L = 200\ mm$ and $W = 40\ mm$) embedded in a flat flow cell ($L = 260\ mm$, $W = 85\ mm$, $H = 55\ mm$). The flat flow cell may be used in these types of experiments because feed channels in SWM modules are small enough to ignore the curvature effects of these modules on the flow [61, 189].Together with spacers, a membrane coupon (Trisep-AMC1) was placed inside the embedded flow channel. Plastic shims were used to adjust the channel height according to the spacer thickness in such a way that the channel's height was equal to the spacer's thickness. The experiments were conducted without the permeate production, because the ratio of permeate is small compared to the cross-flow velocity in RO. The non-woven commercial feed spacers (DelStar Technologies, INC.) were made of polypropylene without any further modifications. The studied spacers are shown in figure 6.2, and their geometric specifications are given in table 6.1.

Table 6.1 shows that the ratio of filament thickness to the channel height (relative height) is higher than 0.5 in all cases of zigzag spacers. That is in contradictory with most numerical studies that assume a relative height of 0.5. Each filament thickness mentioned in table 6.1 is an average of 10 measurement points over the length of a filament in a mesh. The two required frames for determining a velocity field are captured at a known distance (100 mm) from inlet and from channel edges (15 mm) to limit effects of boundaries (entrance, edges and exit) on the flow and to ensure a fully developed flow. The time interval between the two frames was adjusted to the particle displacement in order to reduce the number of pairing losses [153]. The fluorescent particles (tracers) had a mean diameter of 10 μm and a density of 1.19 g/cm^3. The Stokes number for these particles was around 5×10^{-3} for the thinnest spacer used (spacer A), and thus tracing accuracy errors were below 1% [240] in all experiments. The quality of vector maps was improved by using a combination of coated particles with Rhodamine-B, green light laser (wavelength = 545 nm) and an optical filter. PIV measurements are taken at three different heights in the feed channel separately: close to the camera (Z3), at the middle of the channel (Z2) and far from the camera or close to the membrane sheet at the bot-

Table 6.1: Structure properties of feed spacers used in this study. The spacers are categorized into the zigzag spacers (A-D) and the cavity spacers (G and H).

Description	Nomenclature	Unit	Zigzag Spacers				Cavity Spacers	
			A	B	C	D	G	H
Spacer/Channel height	$h_{SP} = H_{CH}$	$10^{-3}m$	0.71	0.76	0.86	1.22	1.15	1.25
Filament diameter parallel to flow	$d_{f_{CP}} = d_{f1}$	$10^{-3}m$	0.39	0.45	0.49	0.80	0.65 × 0.92	1.01 × 0.58
Filament diameter perpendicular to flow	$d_{f_{CT}} = d_{f2}$	$10^{-3}m$	0.39	0.45	0.49	0.80	0.50 × 0.81	0.24 × 0.33
Filament length parallel to flow	lm_{CP}	$10^{-3}m$	2.85	2.45	3.20	4.41	4.87	3.08
Filament length perpendicular to flow	lm_{CT}	$10^{-3}m$	2.85	2.45	3.20	4.41	4.87	6.36
Hydrodynamic angle	β	∘	89.5	89.0	89.2	89.8	45.0	45.0
Flow attack angle	α	∘	45.5	46.0	45.8	45.2	135.0	135.0
Aspect Ratio	lm_{CP}/H_{CH}	-	4.01	3.21	3.72	3.62	4.23	2.47
Ratio of filament's distance to thickness	$lm_{CP}/d_{f_{CT}}$	-	7.33	5.44	6.53	5.51	6.0-7.5	9.3-12.3
Relative height	df_{CT}/H_{CH}	-	0.55	0.59	0.56	0.66	0.44-0.70	0.19-0.26
Porosity	ϵ	%	88	83	88	81	80	82
Hydraulic diameter	dh	$10^{-3}m$	0.88	0.8	1.08	1.26	1.1	1.21

tom of the feed channel (Z1) (figure 6.3). The thickness of laser sheet light (2 mm) was greater than the feed channel height (0.71 – 1.62 mm), and therefore, the entire depth of the channel was illuminated. That is a common situation in μPIV [141] and can be solved by fixing the focus of the camera at a specific distance from the lens and moving the flow cell [141, 222]. In this study, the camera was displaced using a translation stage because moving the flow cell was not possible. The camera was initially arranged in such a way that only particles in the plane close to the camera (Z3 in figure 6.3) were in focus and particles at the middle of the channel (Z2 in figure 6.3) and close to the membrane (Z1 in figure 6.3) were barely in focus. The camera was then moved in steps of 50 μm to the subsequent positions (Z1 and Z2) using the translation stage. The camera's depth of field was about 0.14 mm. At each depth, 50 pairs of images (100 frames) were taken for a specific flow rate. An instantaneous (momentary) velocity map is calculated from each pair of successive frames. These 50 instantaneous velocity maps are used to analyze variations of velocity in time (temporal velocity). An average velocity map (averaged spatial velocity profile) is calculated from the 50 momentary velocity profiles and is used to study the spatial velocity inside the feed channel [153].

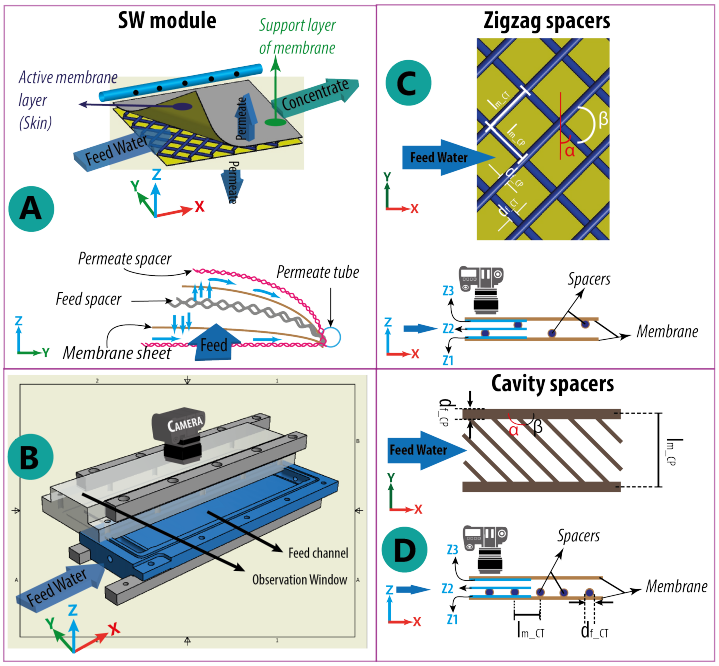

Figure 6.3: Each envelope in SWM modules is formed by gluing two flat sheets along their three edges at the non-active side (support layer). In this way, the active layers (skins) of the membrane's sheets face the feed spacer and the support parts of the sheets face the permeate spacer (*A*). The feed spacer is relatively thicker and more porous than the permeate spacer (*A*). The schematic view of the flow cell, location of the feed channel, and position of the camera is shown (*B*). The top and side views of a zigzag spacer (*C*) and a cavity spacer (*D*) are shown. The camera is focused at three heights: Z1 (rear part of the channel and close to the membrane coupon), Z2 (middle part of the channel) and Z3 (front part of the channel and close to the observation window) (*C*, *D*).

6.3. RESULTS

6.3.1. PRESSURE DROP AND FRICTION FACTOR

Figure 6.4 illustrates variations of pressure drop against the increasing flow rate (A) and the variation of friction losses against Reynolds number in the normal (B) and logarithmic (C) view. Each line in figure 6.4 demonstrates a spacer wherein each point is the average of at least 450 measurements, which are performed parallel to the PIV measurements. Pressure drop and friction losses are important in the design of a spacer because they are related to the additional energy cost in SWM modules. Figure 6.4-A shows that the pressure drop increases by increasing the flow rate in each spacer and by the decrease in the channel height for a particular flow. Additionally, figure 6.4-A shows that discrepancies in the pressure drop of different spacers are greater at a higher flow rate. The pressure drop in zigzag spacers (spacers *A*, *B*, *C* and *D* with an approximate $\beta = 90°$) was higher than the cavity spacers (spacer *G* and *H* with an approximate $\beta = 45°$) even when the channel height of the zigzag spacer (spacer *D*) was approximately the same as with cavity spacers. That is due to the size of transverse filaments, their distance from each other and the specific orientation of these filaments in cavity spacers. Da Costa et

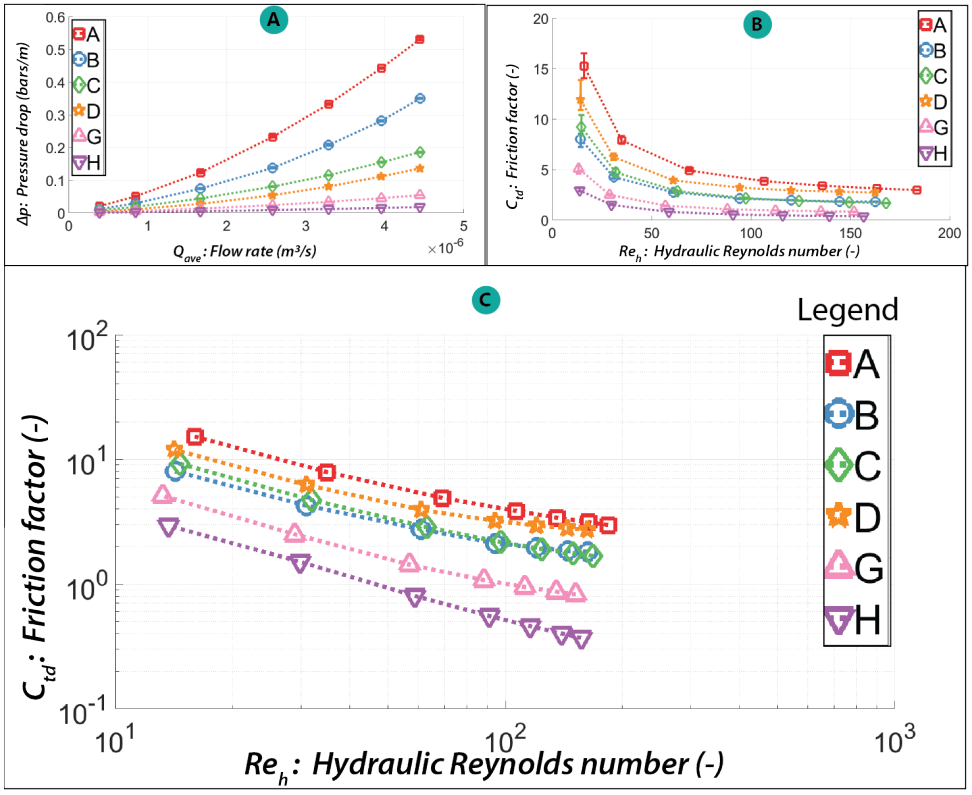

Figure 6.4: Development of pressure drop against increasing flow rate (A) and variation of friction factor for increasing hydraulic Reynolds number in a normal view (B) in logarithmic view (C).

al. [152] showed that there is a relation between the pressure drop and the aspect ratio (l_{mCT}/H_{CH}). The result from this chapter indicates that the pressure drop increase was consistent with the decrease of the aspect ratio (l_{mCT}/H_{CH}) in cavity spacers but not in the zigzag spacers. Spacer *C* is the exception in our experiment, which has a smaller ratio of l_{mCT}/H_{CH} than spacer *D* but also a lower pressure drop.
Figure 6.4-B shows that the friction factor is remarkably lower in the cavity spacers than in the zigzag spacers. In a numerical simulation, Koutsou et al. [167] investigated the effects of spacer geometry on the pressure drop. They used dimensionless pressure drop, which was related to a friction coefficient. They [167] found that the pressure drop in zigzag spacers increased at a smaller ratio of the filament's distance to the filament's diameter (l_m/d_f) independently of the hydrodynamic angle. Their result was in agreement with similar previous studies [58, 61, 157, 170, 219, 220]. The results from our study showed that decrease of the friction factor was inconsistent in spacer *C* with respect to the increase of the l_m/d_f ratio. This inconsistency arose because commercial spacers are different in more characteristics than just the l_m/d_f ratio. For instance, Koutsou et al. [167] mentioned that there were exceptions when the ratio of l_m/d_f is combined with the hydrodynamic angle of spacer (β), which is also the case in our experiment (table 6.1). In addition, filaments in commercial spacers are not perfectly circular in shape, and their diameters are not uniform and equal over the filaments' length, as is usually assumed in numerical studies. Therefore, it is difficult to draw a general conclusion based only on the presented data.
Figure 6.4-B shows that friction factor curves against the Reynolds number have the shape of a decreasing power equation, as was expected according to equation 3.5: $C_{td} = A'/Re^n$. Former studies [157, 167, 220] have illustrated decreasing linear lines, which are in agreement with the tail part of the curves in this study ($Re_h > 100$). The changing pattern of the friction factor from descent with steep incline to descent with slight incline in these curves ($30 < Re_h < 90$) is the moment that mixing of flow was extremely enhanced and might be the moment that flow conditions change from steady to unsteady flow. This issue will be discussed in more detail and with consideration of the PIV images in section section 6.3.2 using PIV images. Figure 6.4-C represents the logarithmic view of figure 6.4-B. Except spacer *H*, other spacers have a breakpoint in the friction factor lines at a Reynolds number close to 90, i.e. the lines at $Re_h > 90$, except spacer *H*, become less steep indicating a higher unsteadiness with these spacers. These results are based only on the friction factor calculation and measurement of the pressure drop. More visual evidence will be provided by the PIV images at section 6.3.2.

6.3.2. ACTUAL VELOCITY MEASUREMENTS WITH PIV

This section includes velocity maps obtained from PIV. The camera's field of view (approximately $H = 7.5\ mm \times W = 9.5\ mm$) is the same in all velocity maps presented in the next sections.

TEMPORAL VELOCITY PROFILES

In PIV, a momentary velocity map is shaped by determining the shifting distance of particles between two frames at a particular time interval (figure 6.5). Fifty momentary velocity profiles are made for a particular flow of a spacer at each channel height. Figure 6.6

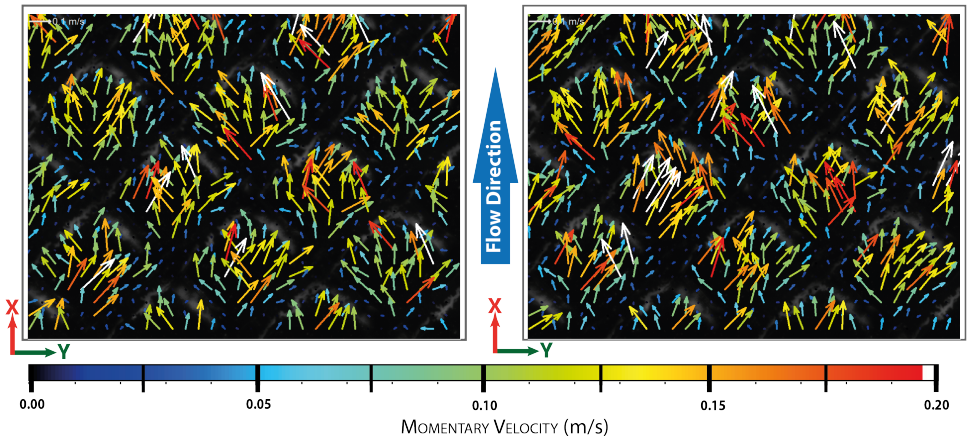

Figure 6.5: Two momentary velocity profiles of spacer B at the middle of the channel (Z2 in figure 6.3) for an average velocity of about 0.1 m/s (Re = 95).

illustrates variations of normalized velocity ($U_{meaured-in-E}/U_{ave}$) along the 50 instantaneous velocity profiles for point E, which is located in the middle of one of the meshes in the field of view; i.e., point E has the same XY-coordinates but different Z-coordinates

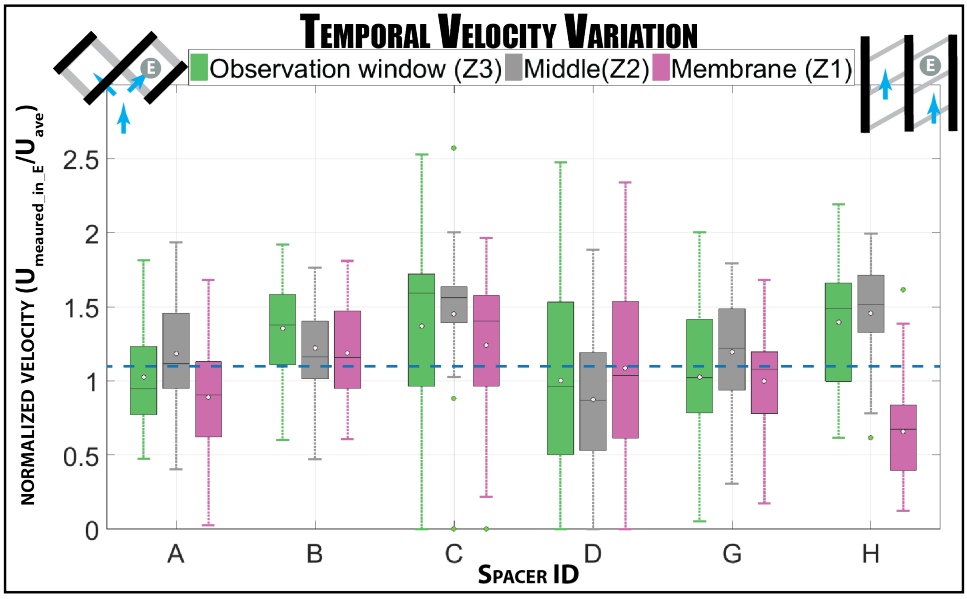

Figure 6.6: Variations of normalized velocity ($U_{meaured-in-E}/U_{ave}$) in time inside the feed channels at three levels: middle of the channel (Z2), next to the window of the flow cell (Z1) and close to the membrane (Z3). Circles inside the box represent the average of data and continuous horizontal lines the median. The filled circles outside the box represent the outliers.

(Z1, Z2 and Z3 in figure 6.3). The circles and horizontal lines inside each box denote the mean and median of the data respectively and the filled circles outside the boxes represent the outliers. A normalized velocity is used because the magnitude of velocity was not the same in all spacers. The position of the mean and the median with respect to each other describes the behavior of flow at the studied point. For instance, when the mean is smaller than the median, the data symbolize a left-skewed normal distribution in which momentary velocities with a higher magnitude occur more frequently at the studied point, and therefore, a higher shear applied more frequently at point E for a specific spacer. According to this, higher shear occurs more frequently in the middle of the meshes of spacer *C* and *H* at all three channel heights (figure 6.6). However, spacer *H* has a considerably lower velocity than expected at the membrane side where transverse filaments touch the membrane coupon. In most studied spacers (figure 6.6), the normalized velocity shows a value around one or higher. This indicates that the measured average velocity is about the same as or higher than the average velocity at point E. Spacers *B*, *C* and *G* show a normalized velocity greater than one in all three channel heights at point E. figure 6.6 shows that there is probably a relation between the spacer thickness (channel height) and velocity variations in a channel. A greater channel height will probably result in a stronger vortex shedding at point E. Velocity variation in time could be related to the fouling and concentration polarization. In zigzag spacers, the velocity variation increases by the increase of the channel height at the observation window and the membrane side. At the middle of the channel, however, it decreases with increase of channel height until spacer *C* and then increases in spacer *D*. The velocity variation in cavity spacers is almost the same in both spacers because they have approximately the same channel heights. The latter indicates that the velocity variation depends on the channel height rather than the transverse filaments' thickness. Spacer *C* has the highest relative discrepancy between the variation of velocity at the middle of the channel (Z2) and membrane sides (Z1 and Z3). It is desirable to have velocity with low variations in the middle of the channel and velocity with high variations at the membrane sides when designing a feed spacer, because this situation can reduce the chance of fouling formation with the lowest possible energy losses. In cavity spacers, the average velocity is lower on the channel side that the transverse filaments are attached to (Z1) than the side without transverse filaments (Z3). The average velocity of spacer *H* at Z1 is notably lower than other spacers. The transverse filaments in spacer H are thinner than longitudinal filaments, and the ratio of lm_{CP}/H_{CH} is smaller in this spacer than in other spacers.

AVERAGED SPATIAL VELOCITY PROFILES AT $U_{ave} = 0.1\ m/s$

The results from the previous section discussed only one point of velocity maps. To investigate how velocity changes spatially, the 50 momentary velocity fields were averaged into one velocity map at each channel height and for a particular flow (figure 6.7).
In the zigzag spacers, the flow direction at Z1 is perpendicular to Z3 and along the filaments at the corresponding heights. The velocity profiles at the middle of the channel (Z2) are the mix of the velocity profiles at Z1 and Z3. These results are in agreement with results obtained by Willems et al. [141].

As shown in figure 6.7, the location of the highest and lowest velocity differs in each spacer at the specific channel height. In the zigzag spacers, the highest velocity occurs

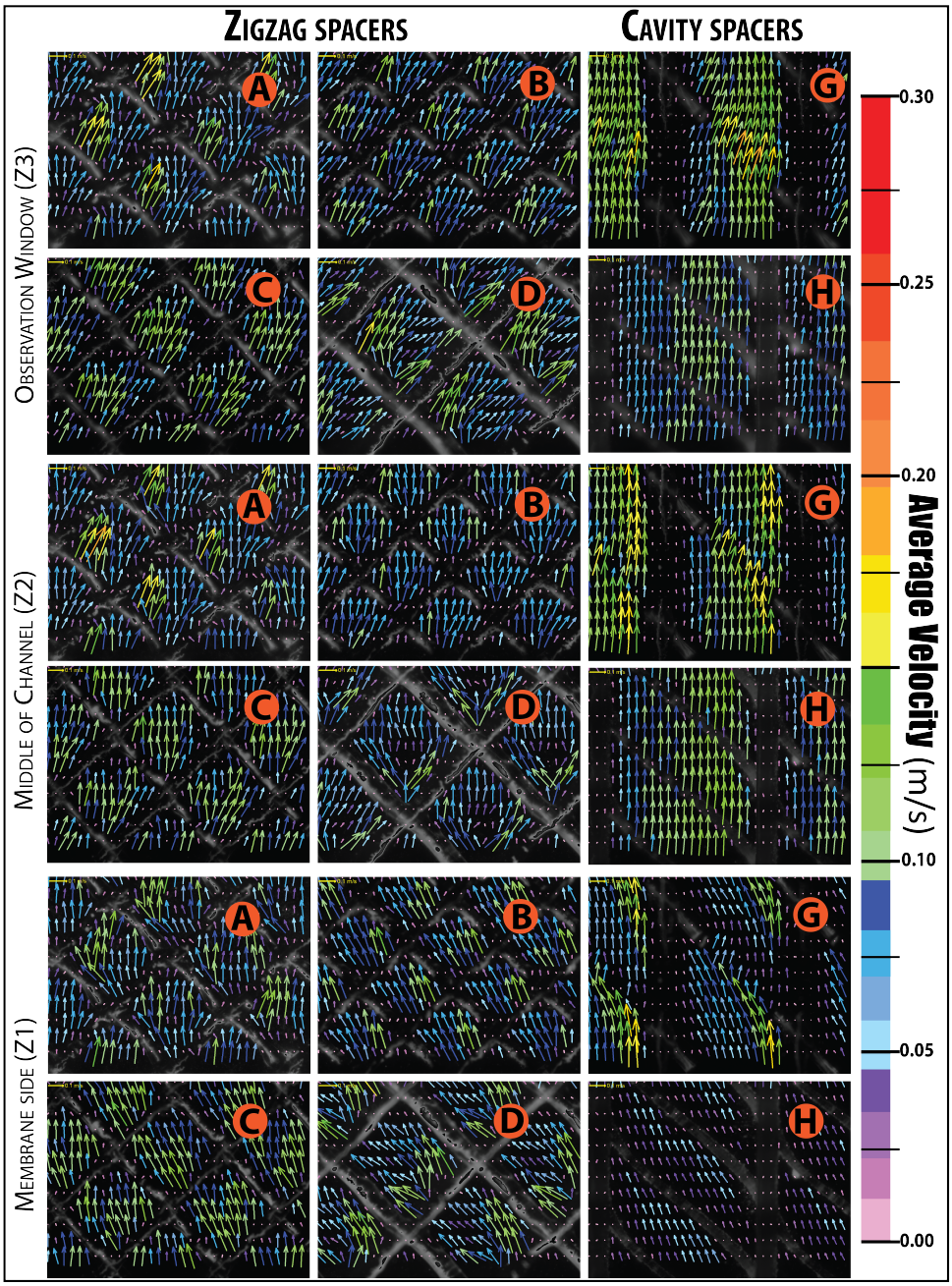

Figure 6.7: Time-averaged velocity fields for spacers at three channel heights: Z1, Z2 and Z3 for an average velocity of approximately 0.1 m/s

near the mesh entrance where water passes over or under a filament, i.e. the areas with high-velocity values at Z1 and Z3. More specifically, the highest velocity occurs when water passes over a filament at the entrance of a mesh and under the adjacent outlet filament (shortest route). The lowest velocity in a mesh occurs close to the inner angle of the downstream node.
Figure 6.7 also illustrates that the flow is in an almost straight line from the inlet to the outlet and parallel to longitudinal filaments in the cavity spacers. In addition, the velocity magnitude is much lower at the side of a mesh where transverse filaments are attached to the membrane. The flow disruption is greater in spacer *G* than spacer *H*, because transverse filaments are larger in spacer *G*. Additionally, figure 6.7 shows that the highest velocity occurs over the transverse filaments with spacer *G* and at a short distance behind transverse filaments, with a low-velocity zone in between with spacer *H*.

AVERAGED SPATIAL VELOCITY AT INCREASING FLOW RATE

Figure 6.8 shows the development of averaged spatial velocity for the entire range of flow rates at the middle of the channel. Each plotted box corresponds to a particular flow rate in a spacer. As expected, the variation and the averaged value of measured velocity (figure 6.8) increased by increasing of the flow rate with each spacer. Additionally, the average velocity and the velocity variation decrease with an increase in channel height at a particular flow in both types of spacers. Notably, in all spacers there are velocities very close to zero for the whole range of flow rate, indicating the existence of dead zones in all spacers and for all applied flows. In all cases, the lower whisker is smaller than the upper whisker, indicating a greater variation in higher velocity ranges. In most cases, except for spacer *B* at $Q = 16\ l/h$, the position of first quartile becomes higher with the increase of flow, indicating the shift of main flow to higher velocity values. The exception in spacer B might be due to the low ratio of lm_{CP}/H_{CH} in this spacer and the creation of more dead zones at higher flow rates. The latter indicates that there is an optimal flow rate for each spacer. However, more experiments are required to confirm this. In zigzag spacers, interestingly, the greatest difference between boxes occurs at the flow transition from $Q = 6\ l/h$ to $9\ l/h$. This is the area in which the incline in friction factor curves changes from descent steep to descent slight ($30 < Re_h < 95$ in figure 6.8-B). Figure 6.9 visualizes the development of the flow pattern for spacer *B* at $30 < Re_h < 95$ at the three heights of the channel when the incline of the friction factor curve changes suddenly in this spacer. At $Re_h = 30$, the velocity is in a straight line from the inlet to the outlet at all three heights. By increasing the Re_h to 60, the flow direction at the top and the bottom of the channel changes along the filament's direction, but the flow in the middle of the channel remains in a straight line from inlet to outlet. By further increasing the Re_h to 95, the flow at the middle of the channel starts to show the mixing pattern as discussed in the previous studies [141] and in the previous sections of this study (figure 6.7).

The phenomenon described above was also observed in other studied zigzag spacers (figure 6.10). This indicates that a notable flow mixing in zigzag spacers occurs at Reynolds numbers around $60 - 100$. Figure 6.10 illustrates the variation of velocity in time with an increasing Reynolds number for point *E*, the middle of the mesh. The low variation of velocity at low Reynolds numbers ($Re_h < 30$) indicates the existence of steady flow in

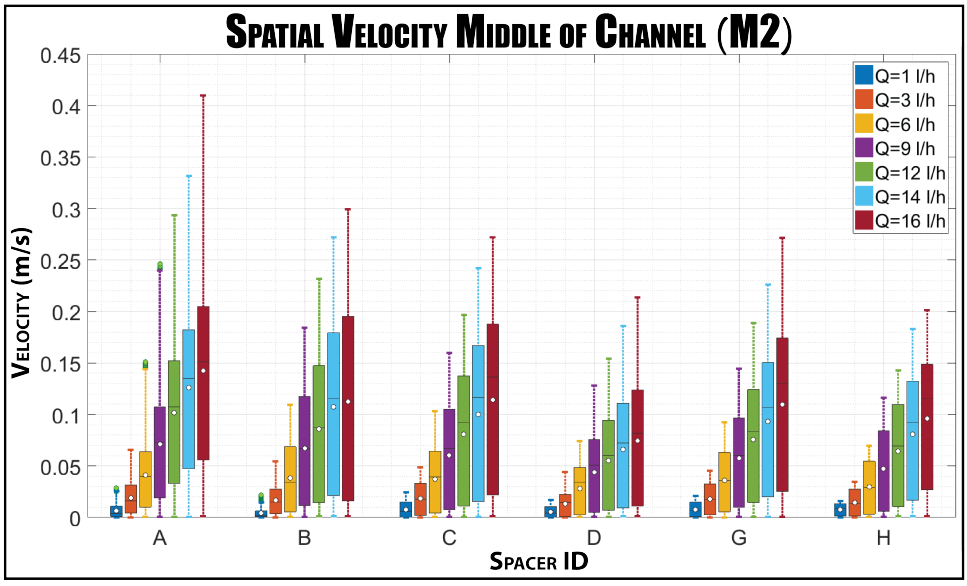

Figure 6.8: Development of averaged spatial velocity for the whole field of view at the middle of channel. Each plotted box corresponds to the measured velocity at a specific flow rate.

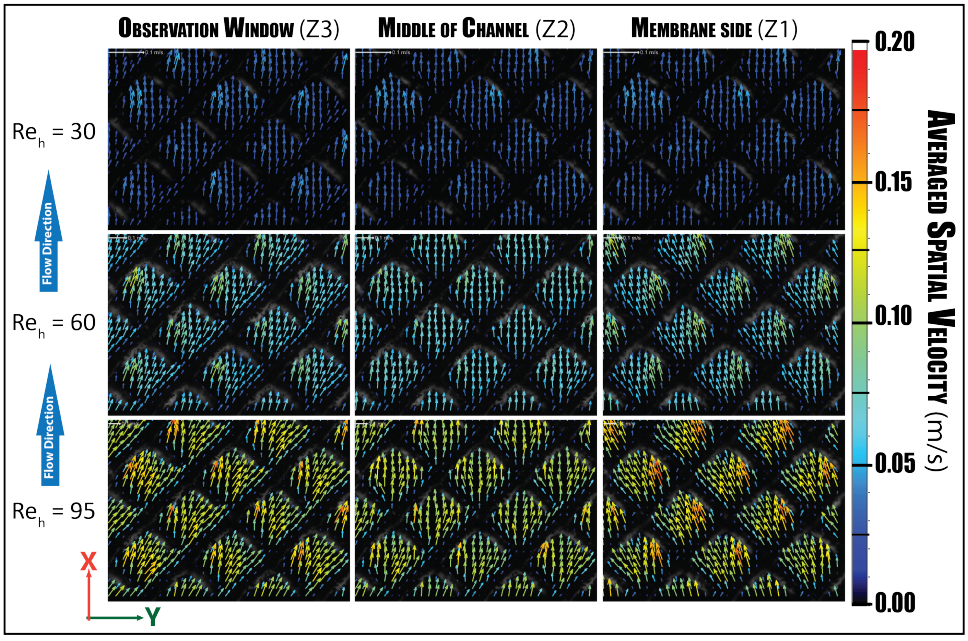

Figure 6.9: Development of flow pattern with spacer *B* for Reynolds number of 30, 60 and 95 at three channel heights. The corresponding friction factor curve has a break point in $30 < Re < 95$ from descend steep incline to descend slight incline.

these conditions and starting the unsteadiness at $Re_h > 30$. The obtained for the zigzag spacers are in agreement with the common belief that spacers induce flow instabilities at low Reynolds number and with results from previous studies [167]. Koutsou et al. [167] found that a transition to unsteady flow occurs at relatively low Reynolds numbers ($Re = 35 - 45$). Additionally, there is a significant variation of velocity at $Re_h > 90$, which indicates a significant improvement of flow instabilities in the channels. This is agreement with practical situations in which the reverse osmosis membranes are operated at $100 < Re_h < 300$.
Variation of velocities from the mean becomes significant at Reynolds numbers around 90. The difference between the velocity at the membrane side (Z1) with the velocity at the middle of the channel (Z2) and the observation window (Z3) at $30 < Re_h < 65$ might be due to the existence of preferential flow at one side of the membrane at this range of Reynolds number in the zigzag spacers.
In cavity spacers, the difference in velocity between two measured sequential Reynolds numbers can be noticed more easily by considering the velocity at the membrane side (Z1), on which transverse filaments are placed. This difference starts at $Re_h = 60$.

In conclusion, the flow with spacers and conditions used in this study can be characterized as a laminar-steady flow for $Re_h < 30$ and laminar-unsteady for $Re_h > 90$. The flow is laminar because Reynolds numbers are much lower than the values for turbulent flow conditions ($Re_h > 4000$) and even transition conditions ($2000 < Re_h < 4000$). The flow becomes unsteady at $Re_h > 90$ because the velocity variation in time become significantly higher than the temporal velocity variation at $Re_h < 90$.

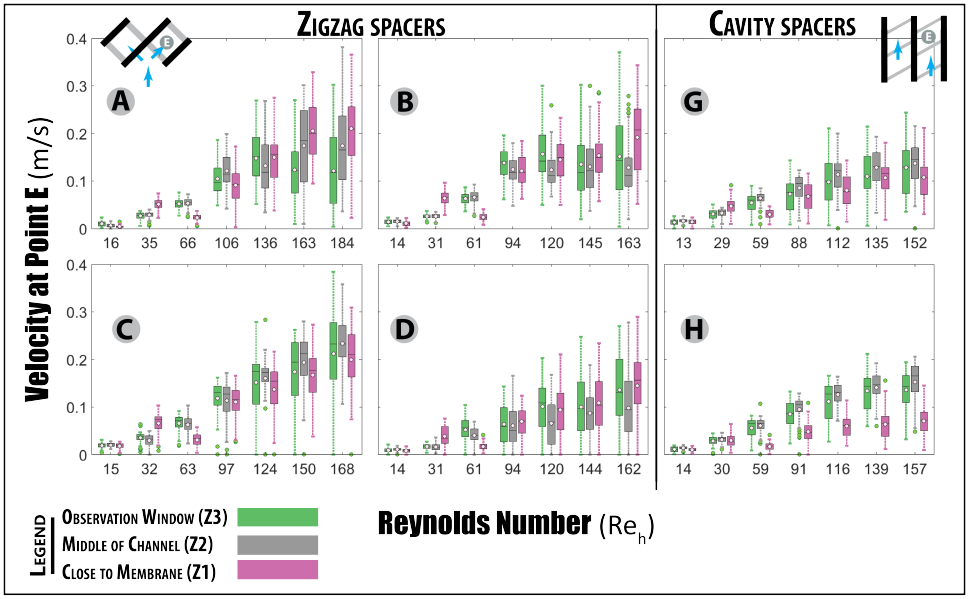

Figure 6.10: Variation of velocity in time for point E in the middle of the mesh.

6.4. CONCLUSION

In this chapter, we experimentally evaluated the performance of spacers with different configurations by determining their pressure drop, flow conditions and local velocity profiles. The pressure drop increased by increasing the Reynolds number for a constant geometry of spacer and feed channel. The pressure drop increased by decreasing the channel height in zigzag spacers and by increasing the thickness of transverse filaments in cavity spacers. The results from particle image velocimetry (PIV) showed that the variation of velocity increases by the increase in the channel height in the zigzag spacers and the increase of the transverse filament's thickness in the cavity spacers.
As expected, the averaged value of measured velocity, the variation of velocity and the pressure drop increased by increasing the flow rate with each spacer.
Curves of the friction factor against the Reynolds number had the shape of a decreasing power function. The transition region from steady to unsteady flow was the moment that the incline of friction factor changed from steep to slight, i.e. at Reynolds number greater than 30. The flow in zigzag spacers was in a straight line from inlet to outlet at $Re_h < 30$, but it was along filaments at each depth at higher Reynolds numbers. At $30 < Re_h < 90$, the flow in zigzag spacers was along the spacers' filaments at the membrane sides (Z1, Z3) but in a straight line from the inlet to outlet in the middle of the channel. At $Re_h > 90$, the flow pattern in the middle of the channel (Z2) was the same as it is described by Willems et al. [141], i.e. the flow was a mixture of flow patterns at the top part of flow channel (Z3) and the rear part of the flow channel (Z1).
The velocity variation over time, which indicates the degree of unsteadiness, was very subtle at $Re_h < 30$ and considerable at $Re_h > 90$. These values are in agreement with respectively the common belief that spacers induce flow instability and the practical operation of reverse osmosis membrane. It must be emphasized that such a clear demonstration of flow instability was not found in previous studies related to spacer-filled channel. These results can be used to evaluate configurations and geometries of feed spacers. The high-resolution velocity profiles in our study could be exploited as a testing tool for numerical studies. While our results provide a reasonable estimation of the velocity maps at the X- and Y-direction of the flow asynchronously at three different heights (Z1, Z2 and Z3) of a channel, further experimental investigations would be required to quantify the effect of velocity in the Z-direction simultaneously with that of the XY-plane.

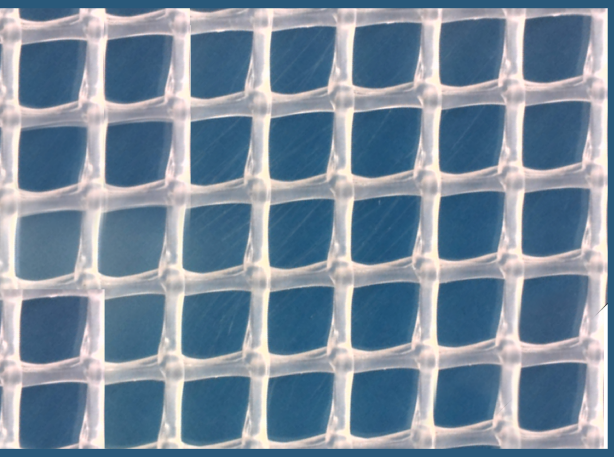

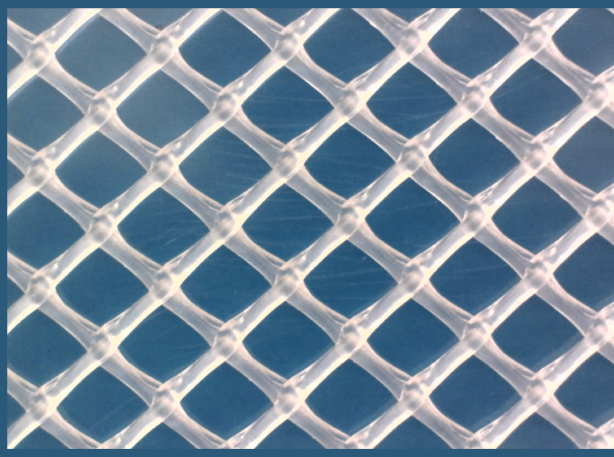

7. Feed spacer orientation

Summary

Feed spacer orientation affects the velocity pattern and pressure drop of spacer-filled channels such as those encountered in Spiral-wound Membrane (SWM) modules of reverse osmosis (RO). However, there are only limited numbers of experimental studies on this topic. This study sets out to reveal more detailed information on the pressure drop and velocity patterns of spacer-filled channels. Particle image velocimetry (PIV) is used to provide high-resolution velocity maps for three commercial feed spacers of different thicknesses at a flow attack angle of 45° and 90°. The pressure drop is measured for the applied operational conditions ($Re < 250$). Results showed higher pressure losses, a better mixing of flow, a lower variation of temporal velocity, and a smaller variation of velocity over the channel height in the orientation with a flow attack angle of 45° compared to 90°. The results presented here can be used to validate numerical studies, determine the fouling-sensitive regions in a spacer-filled channel and consequently, design the optimal spacer with respect to its orientation and thickness.

Parts of this chapter have been submitted to Journal of Membrane Science

7.1. INTRODUCTION

Reverse osmosis (RO) has become a popular technology around the world for production of highly purified water. The coming decades are likely to witness an even greater use of RO for purification of fresh surface water as a consequence of the emergence of new types of micropollutants such as drug residues in fresh water, which cannot be removed with conventional treatment plants. For instance, Wong et al. [234] reported that certain species are in danger of extinction in almost half of European and North American rivers and lakes because of the pollution of these ecosystems [241].
The Spiral-Wound Membrane (SWM) configuration is the most common configuration applied in Nanofiltration (NF) and RO because it offers a good balance between ease of operation, fouling control, permeation rate and packing density [12–15]. However, a wider and more efficient application of SWM configuration requires further improvements of the module's components such as the feed spacer [62, 148]. The feed spacer works as a supporting net and keeps two adjacent envelopes apart [1, 60]; it thereby provides a passing channel for feed water to move tangentially over the active layer of membrane sheets [61]. In addition, the feed spacer determines the hydraulic conditions of the feed channel such as the pressure drop and the time and location of initiation of the fouling. Thus, any alteration in geometrical characteristics of the feed spacer results in the changing of hydraulic conditions of the SWM module. A slight increase in the thickness of the feed spacer (from 28 to 34 $mils$) is one of the few changes that feed spacers have undergone since the first design of SWM modules of RO. This improvement led to the manufacturing of low-pressure RO modules. At a constant production rate, low-pressure modules have a lower fouling tendency and pressure drop [64] and consequently consume less energy compared to modules composed of 28 $mils$ (0.7 mm) spacers. Such improvements are particularly attractive when fresh water is used as the feed for SWM modules of RO because of a higher ratio of pressure losses to applied pressure in fresh water. This higher ratio can be explained by the fact that the applied pressure in fresh water is lower than brackish water and seawater due to its lower osmotic pressure, but the pressure drop along a (clean) SWM module is the same for all types of water due to constant geometrical characteristics of the feed spacer and feed channel in commercial modules.
Considering the amount of water produced by RO plants worldwide and high energy costs, even a small improvement in the efficiency of the feed spacer can be translated into large savings or increased water output [235]. Therefore, it is crucial to understand the effects of geometric modification of the feed spacer on hydraulic conditions of the feed channel, such as the pressure drop and the velocity pattern. While many studies have investigated the effect of feed spacer geometry on the energy losses and the hydrodynamics inside the feed channel, only a few have addressed the effects of orientation. The orientation of a feed spacer is determined by the flow attack angle α, which is defined as the angle between the flow and hydrodynamic angle β of the spacer (figure 7.1). The hydrodynamic angle is the interior angle, relative to feed flow, at the intersection of longitudinal and transverse filaments. Zimmere and Kottke [61] studied effects of the flow attack angle (α) and the ratio of filaments length to channel height (lm/H_{CH}) on the pressure drop, mass transfer and mixing behavior of flow by physiochemical principles using ammonia. In addition, they used a tracer of ammonia for visualization of the

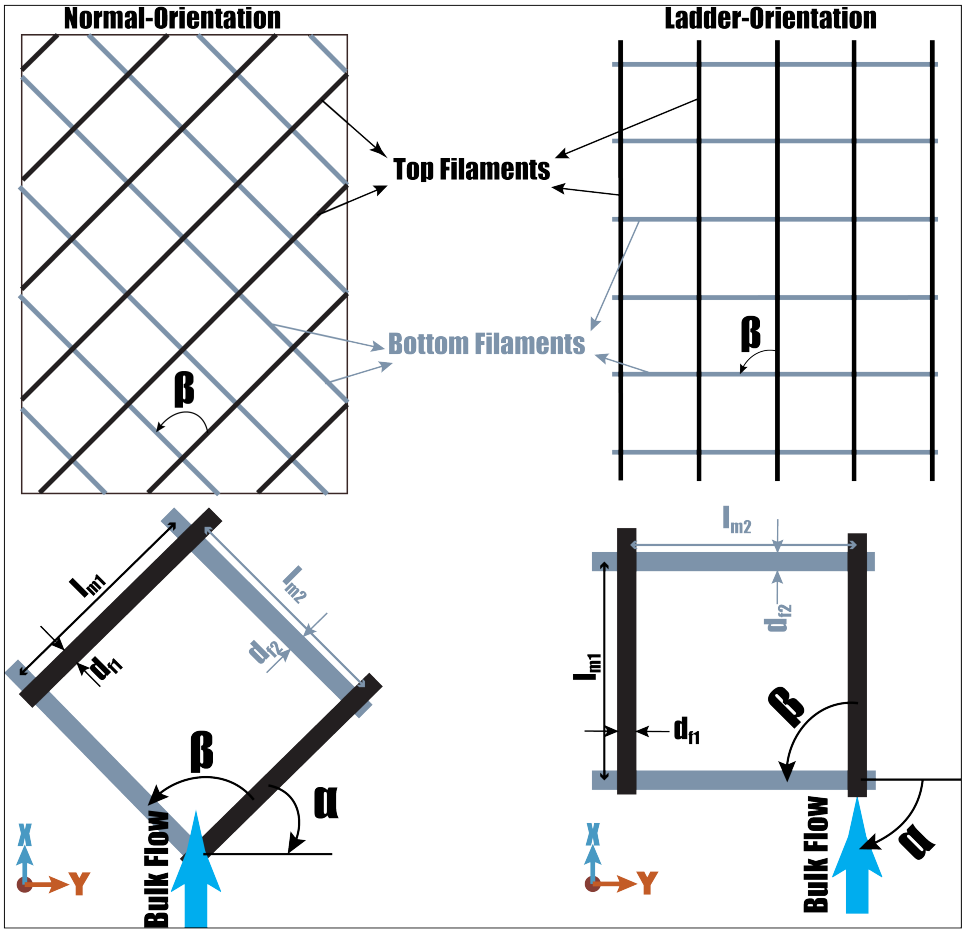

Figure 7.1: Schematic view of spacers with flow attack angle of 45° (normal orientation) and 90° (ladder orientation). The flow attack angle is denoted with α and the hydrodynamic angle with β. The relative distance between axes of two consecutive spacer filaments is defined as the ratio of filament length ($l_m = l_{m1} = l_{m2}$) to the channel height (H_{CH}). Spacers used in this chapter have the same filament mesh in flow direction (l_{m1}) and perpendicular to the flow (l_{m2}). The XY-plane is defined as the 2D space that represents the direction of flow in X- and Y-direction. X denotes the main direction of the flow (x-component of flow) and Y denotes the flow direction perpendicular to the main flow and perpendicular to the channel height (Z).

flow and of the mass transfer inhomogeneity in the feed channel. They concluded that a proper choice of the lm/H_{CH} ratio and the flow attack angle (orientation) of the feed spacer results in overlapping of two basic flow types (channel flow and corkscrew flow) and creation of mixing by which a homogeneous mass transfer combined with a good residence time behavior at acceptable energy costs could be achieved. Geraldes et al. [177] investigated the effect of lm/H_{CH} ratio in a ladder type feed spacer and found that the value of the Reynolds number at which the flow becomes unstable decreases due to the increase of inter-filament distance between two transverse filaments. Santos et

al. [189] used experimental and numerical studies to determine the shear stress and the mass transfer at the membrane wall for ladder-oriented spacers. They [189] introduced a modified friction factor and found that it is linearly related to the Sherwood number. Based on this linear relation, they [189] suggested that the modified friction factor may be used for selecting the best spacers in terms of mass transfer efficiency. Additionally, they showed that the flow structure is mainly affected by transverse filaments and that effects of longitudinal filaments are marginal. Li et al. [228] used a computational fluid dynamics (CFD) simulation to calculate the mass transfer and power consumption of non-woven spacers at different lm/H_{CH} ratio, flow attack angle and hydrodynamic angle. They concluded that there should be an optimum value for the lm/H_{CH} ratio, the hydrodynamic angle and the flow attack angle. Koutsou et al. [242] performed experimental and numerical simulation at a typical Reynolds number for RO ($50 < Re < 200$). They investigated the effect of both Reynolds (Re) and Schmidt (Sc) numbers on the Sherwood (Sh) number in spacer-filled channels by changing the lm/H_{CH} ratio, the flow attack angle and the hydrodynamic angle of spacers. They demonstrated that the local mass transfer was lower in sparser spacer geometries, but increased by increasing the hydrodynamic angle. Additionally, they showed that the distribution of average mass transfer was similar to the corresponding distribution of shear stress at the channel walls. While the previously mentioned researchers used spacers with a simplified cross-section for numerical simulations, more recent numerical studies, e.g. studies done by Bucs et al. [230] and Radu et al. [215], have started to use spacers with closer geometrical similarities to those of commercial ones. However, it remains a challenge in numerical methods to use spacers with a geometry that exactly matches the geometry of commercial spacers, and therefore, the use of feed spacers with detailed geometry, such as the commercial feed spacers, remains limited to experimental methods. Schock and Miquel [58] used various commercial spacers to measure the mass transfer and pressure drop. They showed that spacer-filled channels have higher mass transfer compared to empty channels over the same range of Reynolds numbers, albeit at the increased pressure drop. Da Costa et al. [157] studied the effect of spacer filament orientation on the flux enhancement in ultrafiltration membranes. They found a maximum flux for a flow attack angle of $40-45^{\circ}$. In another study [152], they used dye injection and microbubbles to visualize the effects of the spacer's configuration on the flow pattern of spacer-filled channels. They showed that in spacers with a smaller flow attack angle, the flow is more widely spread in the XY-plane (figure 7.1). Neal et al. [12] investigated the orientation effects of commercial feed spacers on particle deposition. They used a spacer with a geometry similar to the standard 28 mil feed spacer used in most SWM modules of RO, albeit in combination with a microfiltration membrane. They [12] linked the deposition patterns of particles to the orientation of feed spacer and the non-uniform shape of the filaments in commercial spacers.

While numerical studies enhance our understanding of hydraulic conditions of spacer-filled channels at relatively low costs and risks compared to experimental methods, they may be associated with challenges such as matching the geometry of the modeled feed spacer with commercial ones and an accurate verification and validation of numerical modules. As a result, it is recommended [141, 180] to use direct, non-invasive, high-resolution experimental methods such as particle image velocimetry (PIV). Gimmelshtein

and Semiat [203] used PIV for investigation of the liquid flow in the spacer-filled channel in the velocity ranges from 0.06 to 1.3 m/s. They showed that the bulk of fluid flows in a straight line from inlet to outlet with only small deviations near the filaments. Willems et al. [141] investigated the fluid velocity profiles of water and water-air mixture in spacer-filled channels. They found that liquid flows mainly parallel to the spacers' filaments and therefore, the direction of flow changed 90° over the height of the channel. The disagreement of their results with results of Gimmelshtein and Semiat [203] was due to the fact that the latter researchers used a spacer which was 20% thinner than the channel height and thus created an empty space in the channel height. Additionally, the PIV results obtained by Gimmelshtein and Semiat [203] indicate that they may have measured the velocity only in the empty part of the channel. Haidari et al. [153] compared the flow pattern of an empty channel with a spacer filled-channel using PIV. They showed that the flow in the empty channel was in a straight line from inlet to outlet and in the spacer-filled channel, which was in agreement with the results of Willems et al. [141]. In addition, they showed that the low-velocity regions were in agreement with the fouling sites detected by other researchers.
The purpose of experiments in this chapter is to determine the effects of orientation of commercial feed spacers on the fluid flow and the pressure drop. Three different spacers were considered, each at two orientations: normal orientation and ladder orientation (figure 7.1). The effect of orientation on the pressure drop of the same spacers was investigated. A short description of the PIV technique is given in the experimental part of this chapter. The detailed description of the technique is provided by Adrian et al. [202]. The effect of the spacers' orientation on the spatial and temporal velocity was studied at three heights of the feed channel. Finally, the flow patterns were compared with fouling sites mentioned by previous studies with the objective of linking the flow pattern with the fouling.

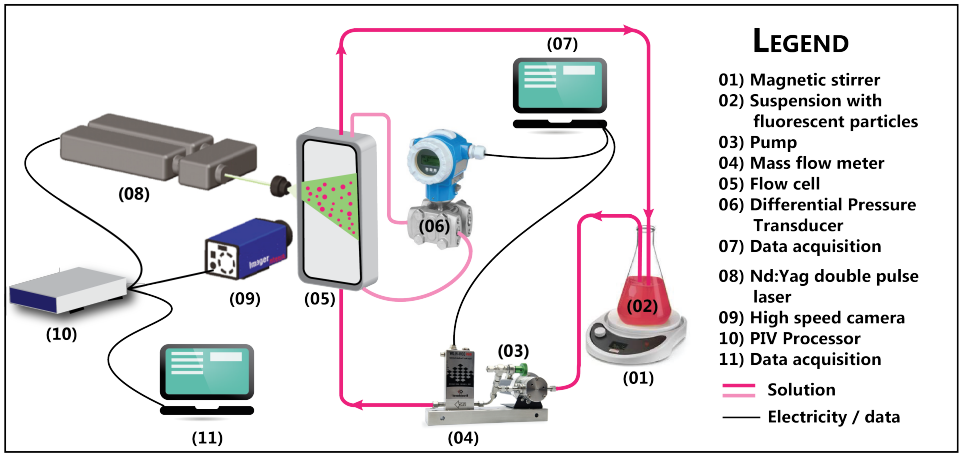

Figure 7.2: The experimental setup that was used for measurement of the pressure losses over the flow cell and for visualization of the temporal and spatial velocity inside the spacer-filled channel [153].

7.2. EXPERIMENTAL

The experimental setup is shown in figure 7.2. A suspension with fluorescent particles (02) flows through a pump (03) and a mass flow meter (04) to the flow cells (05). The pressure drop over the flow cell is measured by means of a differential pressure transducer (06). The values from the pressure transmitter and from the mass flow meter are used to determine the friction factor. Simultaneously, velocities are measured as the laser (08) emits two light pulses that illuminate a well-defined plane and have a short time interval, synchronized with a high-speed camera (09) that takes two images (11). The captured frames are used to determine the temporal and spatial velocity maps inside the channel using commercial software (Davis 7.2). A detailed description of the setup can be found in a previous chapters. The curvature effects of SWM modules on the flow can be neglected because of the small channel height in these modules [177, 189] in comparison with the radius. Therefore, it is a common practice to use flat flow cells to study hydraulic conditions of thin spacer-filled channels such as those of SWM modules of RO. The flow cell used in this study ($L = 260mm$, $W = 85mm$, $H = 55mm$) included an embedded flow channel ($L = 200\ mm$ and $W = 40\ mm$) for the membrane coupon and a spacer. The height of the flow channel is changed according to the spacer thickness by using plastic shims.
The experiments were conducted without the permeate production as the ratio of permeate in RO is small compared to the cross-flow velocity. The nonwoven commercial feed spacers ($DelStarTechnologies, INC.$) in this chapter were made of polypropylene without any further modifications. The geometric specifications of these spacers are given in table 7.1. The same spacer is used at two different orientations: the orientation with the flow attack angle of 45°, which is common in SWM modules of RO and here referred to as the normal orientation and the orientation with the flow attack angle of 90°, which is not usual in SWM modules of RO and will be referred to as the ladder orientation.

Experiments are done at constant temperature (< 1% errors from the average temperature (°C)) and different flow rates. Different flow rates were required to determine the dependency of friction factor (C_{td}) to hydraulic Reynolds number (equation 3.5: $C_{td} = A'/Re^n$). The dependency of the friction factor on the Reynolds number can be used to determine the flow conditions of the channel. Determining the power n

Table 7.1: Geometric characterizations of the commercial spacers used in this study. Each spacer was used in two orientations: normal orientation with a flow attack angle 45° and ladder orientation with a flow attack angle of 90°.

Description	Nomenclature		Ladder orientation			Normal orientation		
	Symbol	Unit	A1	B1	C1	A2	B2	C2
Spacer/Channel Height	$h_{SP} = H_{CH}$	$10^{-3}m$	0.71	1.22	1.63	0.71	1.22	1.63
Filament diameter parallel/perpendicular to flow	$d_f = d_{f1} = d_{f2}$	$10^{-3}m$	0.39	0.72	0.84	0.39	0.72	0.84
Mesh length parallel/perpendicular to flow	$l_m = l_{m1} = l_{m2}$	$10^{-3}m$	2.85	3.8	3.63	2.85	3.8	3.63
Hydrodynamic angel	β	°	90	90	90	90	90	90
Flow attack angle	α	°	45	45	45	90	90	90
Aspect ratio	l_m/H_{CH}	-	4.01	3.11	2.23	4.01	3.11	2.23
Relative height	d_f/H_{CH}	-	0.55	0.59	0.52	0.55	0.59	0.52
Porosity	ϵ	%	88	82	81	88	82	81
Hydraulic diameter	d_h	$10^{-3}m$	0.88	1.26	1.53	0.88	1.26	1.53

of the Reynolds number in the definition of the friction factor, in equation 3.5, gives a better understanding of the flow conditions in the feed channel. A lower value of n indicates a higher state of flow disturbance in the channel. Da Costa et al. [152] achieved n-values between $0.16 - 0.34$ for different spacers at velocities that varied between $0.27 - 2.91$ m/s. A' is a constant which is determined by geometry of the spacer and the channel. The definition used for the Reynolds number here is equivalent to the one used by Schock and Miquel [58] and Fimbres-Weihs and Wiley [180, 217] (equation 3.6: $Re_h = U_{ave} \times d_h \times \rho/\mu$). Other typical definitions for the Reynolds number used in the literature are the channel Reynolds number [96] and the cylinder Reynolds number [15]. The channel and cylinder Reynolds number make use of the average velocity in the empty channel (U_{sup} in equation 3.11: $U_{ave} = U_{sup}/\epsilon$) respectively in combination with channel height and filament diameter. The calculation of average velocity (equation 3.11) is done with a single average filament thickness value, while the thickness of a manufactured filament in commercial spacers varies over its length. The velocity in the PIV experiments is determined by capturing two frames that are taken at about 100 mm from the inlet and 15 mm from each edge of the cell in order to limit the effects of boundaries (entrance, edges and exit) on the flow and to ensure a fully developed flow. The flow along the channel is traced by using fluorescent particles with a mean diameter of 10 μm and a density of 1.19 g/cm^3. The calculated Stokes number of particles was around 5×10^{-3} for the thinnest spacer used (28 mil spacer: 0.71 mm spacer), and thus tracing accuracy errors were below 1% [240]. Fluorescence was used in combination with an optical filter to improve the quality of images. The time interval between two pulses (two frames) was adjusted to the particles displacement in order to reduce loss of particle images within the interrogation window from the first frame to the second frame [153]. An interrogation window or a sub-window is an area smaller than the area of a captured frame, here 7.4×7.4 μm^2, from which information is obtained related to the most probable displacement of the particle pattern in a short time interval.
The PIV measurements were performed at three different heights in the feed channel separately: close to the camera (Z3), in the middle of the channel (Z2) and far from the camera or close to the membrane sheet at the bottom of the feed channel (Z1). The

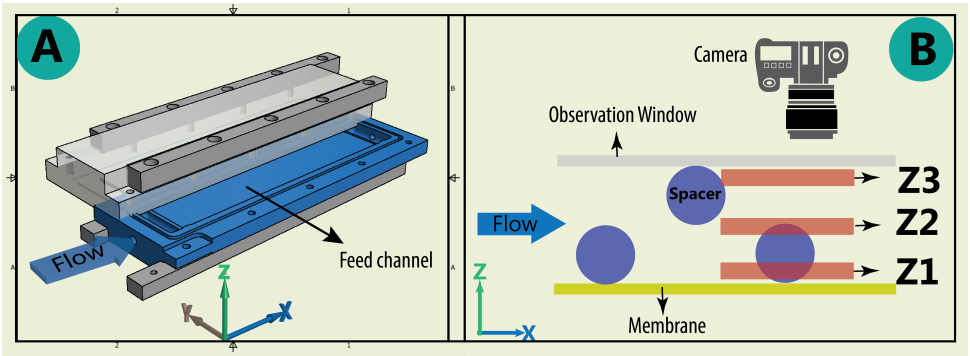

Figure 7.3: The flow cell used in this study (A) and the cross-section of the flow channel (B) with locations at which PIV measurements are done: Z1 (far from the camera and close to the membrane coupon), Z2 (middle of the channel) and Z3 (close to the camera and observation window).

whole depth of the channel was illuminated because the thickness of the laser sheet light (2 mm) was greater than the thickness of the feed channel (0.7 mm). That is a common situation in μPIV [141] and can be solved by fixing the focus of the camera at a specific distance from the lens and moving the object [141, 222]. In this study, moving the flow cell was not an option and therefore, the camera was moved on a translation stage (50 μm in each step). The camera was initially placed such that particles in the middle of the channel and close to the membrane were barely in focus (Z3 in figure 7.3). Then the camera was moved to the subsequent positions (Z1, Z2 in figure 7.3) with a translating stage. The camera's depth of field in this setup was about 0.14 mm. At each depth, 50 pairs of images (100 frames) were taken for a specific flow. A momentary velocity map is calculated for each pair of frames. These 50 momentary velocity maps are used to compare the velocities inside the feed channels over time (temporal velocity). An average is calculated from these 50 momentary velocity maps (averaged spatial velocity profile) and is used to study the spatial variation of the velocity inside the feed channel [153].

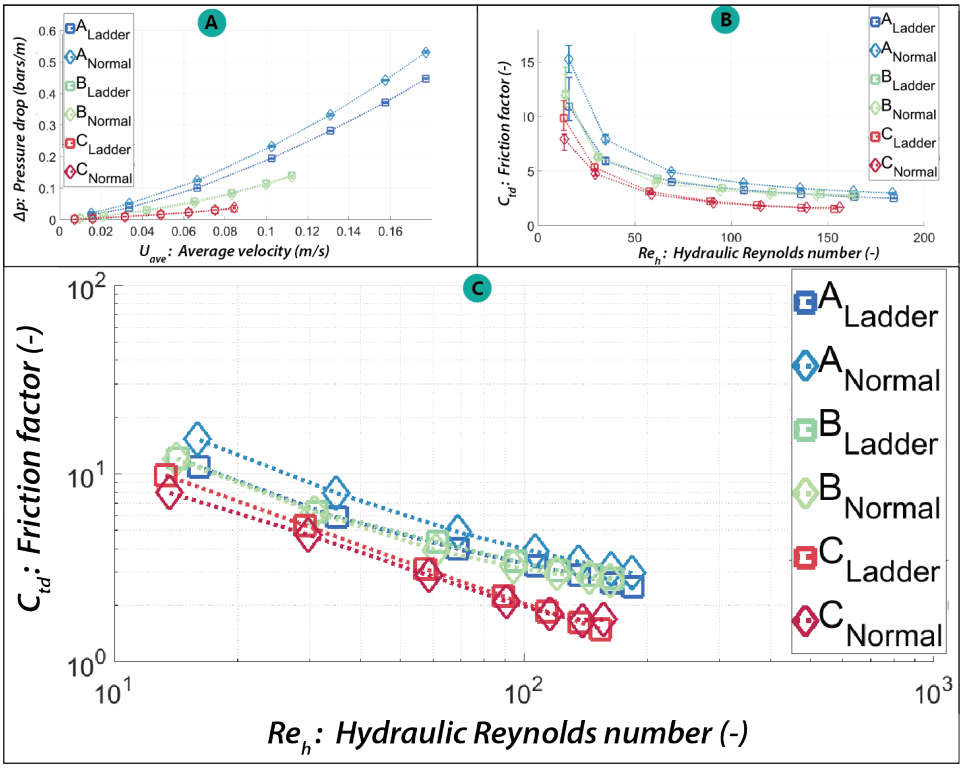

Figure 7.4: The variation of pressure drop with the hydraulic Reynolds number (A) and the variation of the friction factor with hydraulic Reynolds number (B). The diamond-shape lines represent the normal orientation, and the squared-shape graphs symbolize the ladder-orientation.

7.3. RESULTS AND DISCUSSION

7.3.1. PRESSURE DROP AND FRICTION LOSSES

Figure 7.4 illustrates the dependency of pressure drop (Δp) on average velocity (U_{ave}) and dependency of friction factor (equation 3.5: $C_{td} = A'/Re_h$) on hydraulic Reynolds number (Re_h). In parallel to PIV measurements, each point in figure 7.4 represents an average of at least 450 measurements. The same feed flow range ($1.4 - 16.0\ l/h$) was applied to the spacers, and therefore, each feed spacer is operated at a slightly different average velocity range. The range of average velocity in spacers *C* was slightly lower than values commonly used in experimental studies for RO. However, these values are interesting for low salinity water purification in which water permeation could be relatively significant.
Figure 7.4-A shows that for these experimental conditions, the pressure drop differs notably only in two orientations of the spacer A and, as expected, the pressure drop is lower with the ladder orientation. Additionally, figure 7.4-A shows that apparently the pressure drop decreases with increasing spacer thickness. However, it is difficult to draw such a conclusion based only on the presented data because the spacers do not change merely in thickness but also in geometric characterizations such as mesh length, hydraulic diameter and porosity. The best fitted values for dependency of the velocity on pressure drop are illustrated in table 7.2.

Table 7.2: Constants in the total drag dependency on Re-number (A' and n), and the exponent in pressure drop dependency on velocity (K and m) for the feed spacers used in this study.

Description	Nomenclature		Ladder orientation			Normal orientation		
	Symbol	Unit	A1	B1	C1	A2	B2	C2
Numerator power equation	A'	–	63	68	73	82	71	52
Re power in denominator power equation	n	–	0.64	0.65	0.78	0.64	0.68	0.71
Constant pressure drop dependency on velocity	K	$depends$	6.1	3.6	0.76	6.0	3.7	0.70
Exponent pressure drop dependency on velocity	$depends$	–	1.51	1.49	1.25	1.56	1.53	1.29

Considering only the m-values, the flow is more similar to a Stokes flow in the ladder orientation than in the normal orientation. In addition, the flow with spacer *C* is more similar to a Stokes flow than other spacers. The n-values, which are obtained from the best fitted data of figure 7.4-B, do not match the flow conditions between the two orientations as mentioned earlier. However, the n-values confirm the fact that the flow with spacer *C* appears more Stokesian than with the two other spacers.

7.3.2. THE ACTUAL VELOCITY FIELDS DETERMINED BY PIV

This section presents the spatial and temporal velocity maps obtained by PIV. In contrast to the average velocity (equation 3.11: $U_{ave} = Q_{ave}/W \times H_{CH} \times \epsilon$), which is normally expressed as a single value, the PIV results are shown in the form of velocity fields or velocity maps. PIV provides information about the velocity development at a particular point in time (temporal velocity). A momentary spatial velocity profile is created by measuring the velocity of all the points in the camera's field of view at a particular time step. Averaging all momentary spatial velocity profiles results in the averaged spatial velocity profile. Following the line of former studies, the term "average velocity" refers to

the theoretically inferred velocity at the feed channel inlet (equation 3.11) and without considering whether the value is fully developed. The flow becomes fully developed at some distance downstream of the inlet, which is called the entrance length. The entrance length in empty rectangular channels depends on the aspect ratio, defined as the ratio of the channel height to the channel width [175] and is rather small for the setup used in this study (about 2.17 mm). It is, however, challenging to calculate the entrance length in spacer-filled channels. PIV measurements are performed at some distance from the inlet to avoid effects of the entrance length. Figures 7.5, 7.6 and 7.7 illustrate averaged spatial velocity patterns of the ladder and normal orientation in the middle of the channel for an average velocity of 0.1 m/s with spacers A and B and 0.08 m/s with spacer C. Figure 7.8 illustrates momentary variations of the velocity at a particular point inside a mesh.

SPATIAL VELOCITY PATTERNS

Velocity at the middle of channel height: Figure 7.5 shows averaged spatial velocity profiles for two examined orientations of each spacer at the middle of the channel (Z2 in Figure 3). The zones with velocity close to zero above the filaments can be used as an indication that the images are taken at the middle part of the channel. However, there is a slightly different scenario in C1 and C2 (respectively the ladder orientation and normal orientation of spacer C). Long arrows, which indicate high velocity regions, appear on top of the filaments mainly close to the nodes of the spacer on the right side of the meshes. This is the result of the non-uniform shape of filaments over their length in the commercial feed spacer, which is slightly thinner at the places with higher velocity than other parts. At the thinner part, the filament is slightly out of the camera's focus and therefore does not measure the velocity exactly on the filament's surface. This shows that the enhanced geometric characterizations introduced to the numerical studies done by Bucs et al. [230] and Radu et al. [215] is very close to the actual flow behavior as it occurs in a feed channel filled with commercial feed spacers.

Additionally, figure 7.5 shows that the flow in the ladder orientation (type 1) is in a straight line from the inlet to the outlet, while in the normal orientation the bulk flows along the filaments close to it. Local averaged spatial velocities change from very low values up to more than two times the average velocity in some areas. The difference between the low- and high-velocity regions is greater in the ladder orientation than in the normal orientation, comparing different spacers. Velocity values with spacer B1 are highest, reaching almost 0.26 m/s in some places.

In the ladder orientation, a low velocity region is formed downstream of the filaments. This region differs slightly from the particle deposition area, interpreted as a region with low velocity, described by Neal et al. [12], but it was in close agreement with the results of particle deposition achieved by Radu et al. [215] (Fig. 08 in their work). Neal et al. [12] used a spacer with the same geometric characteristics as spacer A, and observed that particles were deposited on the microfiltration membrane at some distance from the filaments and not directly at the downstream area. This no-deposition area directly downstream of the filaments is explained by the work of Cao et al. [191] who showed that relatively strong eddy currents are present in this area. The difference regarding the presence of the no-deposition zone directly behind the transverse filament between the results from this chapter and the study done by Neal et al. [12] could be explained by the

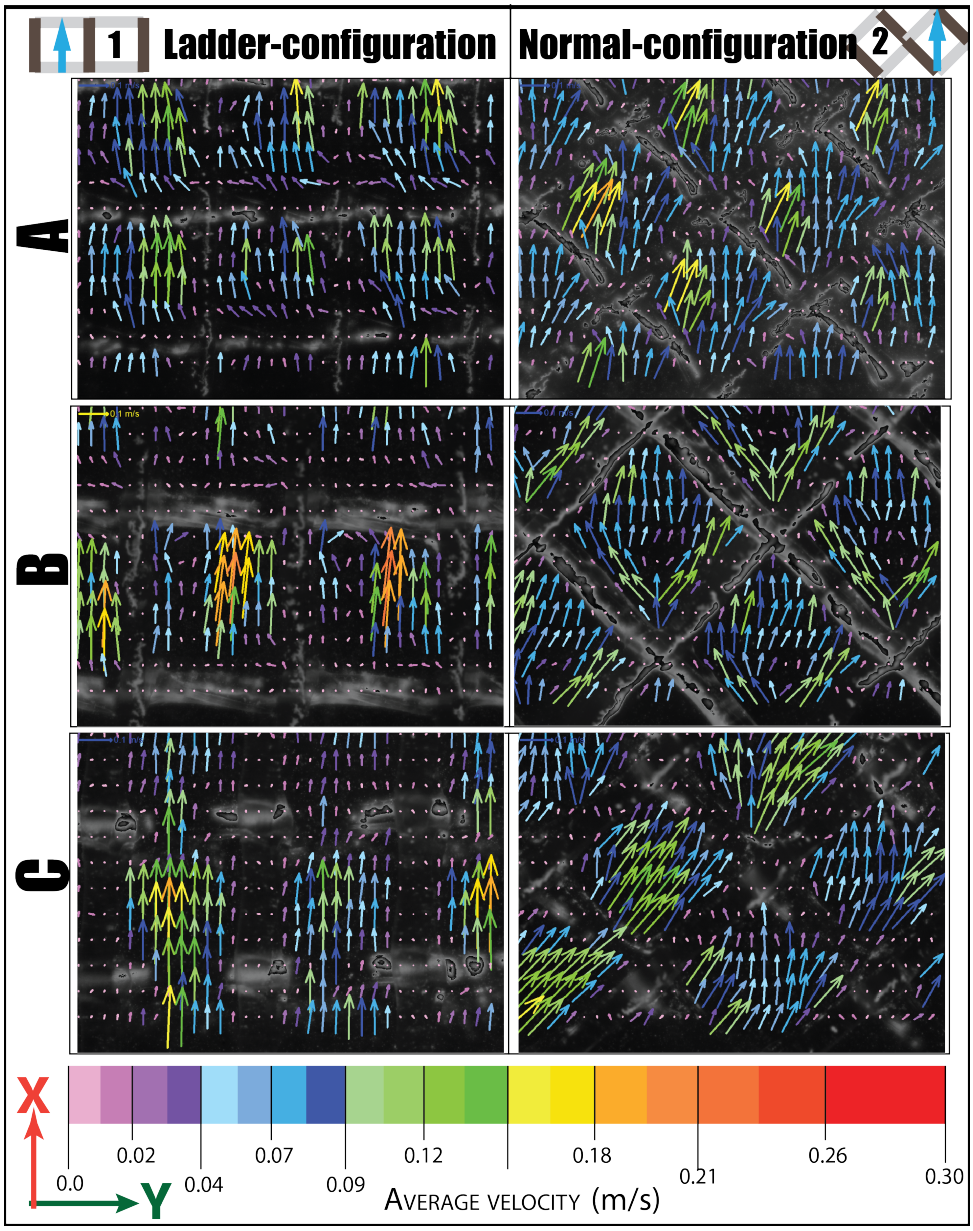

Figure 7.5: The averaged spatial velocity patterns at the middle of the feed channel (Z2) for the ladder orientation (1) and for the normal orientation (2). The average velocity in spacer C ($U_{ave} = 0.085\ m/s$) is lower than the velocity in spacers A and B ($U_{ave} = 0.1\ m/s$)

fact that they used higher flow rates ($Re < 400$) than in this study ($Re < 200$).
Notably, the velocity magnitude downstream of filaments with the ladder orientation is not uniform along the entire filament's length, which is probably the consequence of the

filament's cross-sectional shape. The highest velocity downstream of a filament is observed at locations where filaments bulge toward the flow. The acceleration effect was more apparent over the swelled part of transverse filaments in thicker spacers than thinner spacers.
In the normal orientation, water passes over the filaments attached to the membrane and under the filaments attached to the observation window and is mixed in the following mesh; this is repeated for every mesh. This complex mixing behavior of the flow together with the particular geometry of each spacer (thickness and porosity) and filaments makes it difficult to give a general prediction of the lowest and highest velocity areas. For instance, in the channel with spacer *A*, the lowest velocity region is observed in that half of the mesh where the water passes over a filament to enter the mesh and under the adjacent filament to leave the mesh (right half of the meshes in figure 7.5), and the highest velocity is at the other half of the mesh where water passes under a filament to enter the mesh and over a filament to leave the mesh. With spacer *B*, the highest velocity occurs directly downstream of the filaments at the entering parts of the mesh and the lowest at the confluence of these streams. With spacer *C*, the lowest velocity occurs in the diagonal part of the mesh. The upstream node of the mesh, where both flows exit the mesh, is the only point in all spacers with a similar low-velocity region.

Velocity pattern at different channel heights: The velocity patterns as described in the previous section (figure 7.5) are only valid for the situation in which the camera is focused on the middle part of the channel (Z2 in figure 7.3). Figure 7.6 shows averaged spatial velocity patterns at the membrane side (Z1 in figure 7.3) on which the transverse filaments are placed. The operational conditions were the same as the operational conditions at the middle of the channel. Velocity magnitudes of the ladder orientation are significantly lower over the membrane side than the middle part of the channel. In addition, the velocity decrease in ladder orientation over the membrane compared to the middle of the channel is greater with thicker spacers. In the normal orientation, the velocity close to the membrane is approximately the same as in the middle of the channel. The flow direction, on the other hand, differs clearly from the flow direction at the middle of the channel in both orientations. In the normal orientation, the flow is along the direction of attached filaments. In the ladder orientation, the flow direction close to the membrane side is a function of the spacer thickness. For instance, the flow direction with spacer *A* is approximately the same as in the middle of the channel from the inlet to the outlet with the largest deviation downstream of the filaments. These areas are referred to as the particle deposition area by Neal et al. [12]. The magnitude of the velocity is respectively 44% and 57% lower for spacer *B* and *C* compared to spacer *A*. Figure 7.7 includes the statistical representation of figure 7.5, figure 7.6 and averaged spatial velocity profile at the front part of the channel (Z1 in figure 7.3), i.e., each box shows the velocity variations over the total field of view at a specific height (Z1, Z2 and Z3 from figure 7.3). The median, average, and outliers are shown respectively with a straight line, empty circle inside the box and filled circles. Figure 7.7 shows that the averaged spatial velocity is higher at the side of the channel without the transverse filaments (Z3) than in the middle of the channel (Z2) in the ladder orientation for the same conditions.
The velocity magnitude at the observation window (Z3) was on average higher, from

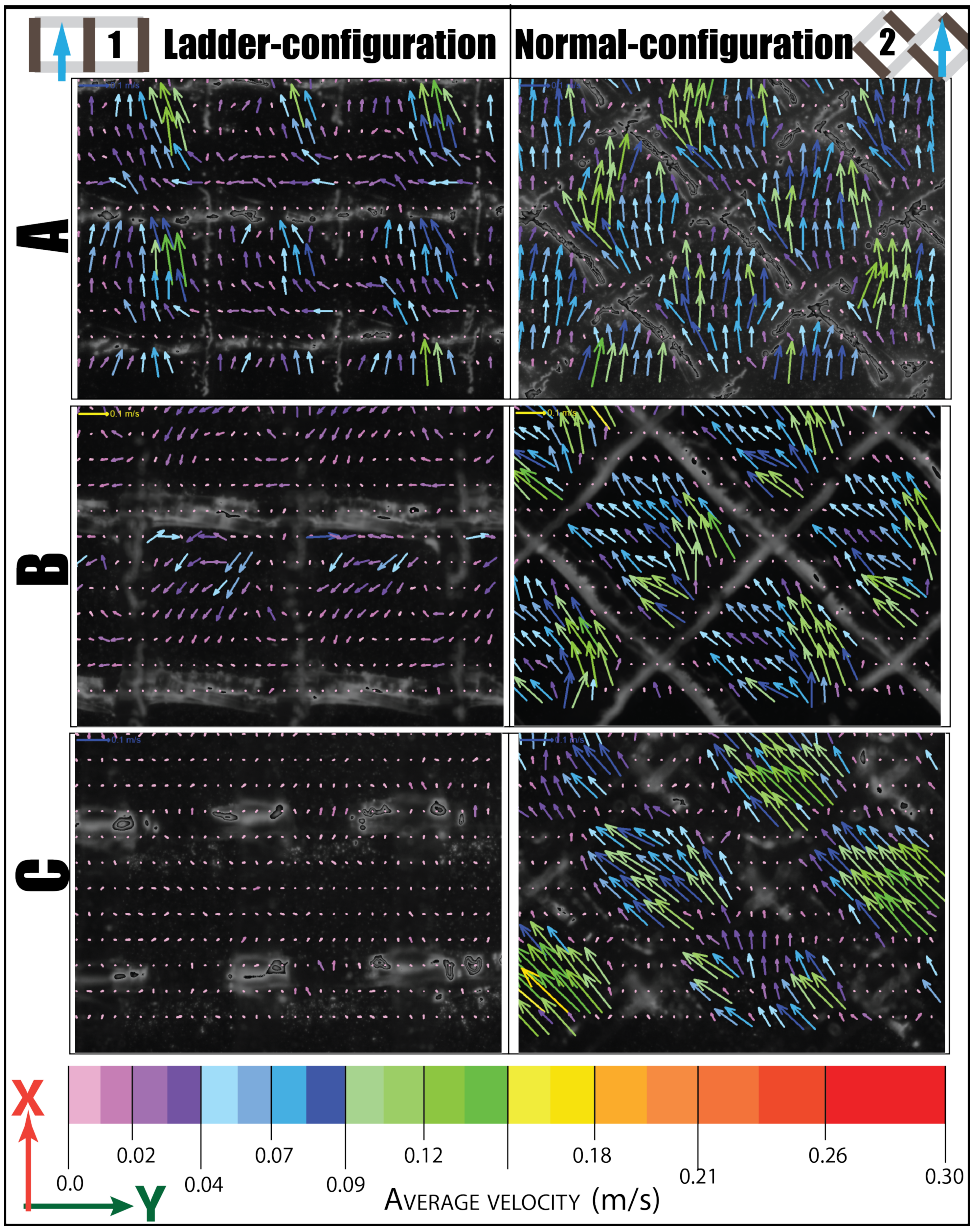

Figure 7.6: The averaged velocity pattern close to the membrane side over which the transverse filaments are placed (Z3) for the ladder orientation (1) and for the normal orientation (2). The average velocity in spacer$C$ ($U_{ave} = 0.085\ m/s$) is lower than the inlet velocity in spacer A and B ($U_{ave} = 0.1\ m/s$)

3.6% in spacer A to 54% in spacer B, in ladder orientation than in normal orientation. The velocity magnitude at the membrane side (Z1) was lower, from 28% in spacer A to 68% in spacer C, in ladder orientation compared to normal orientation. At the middle

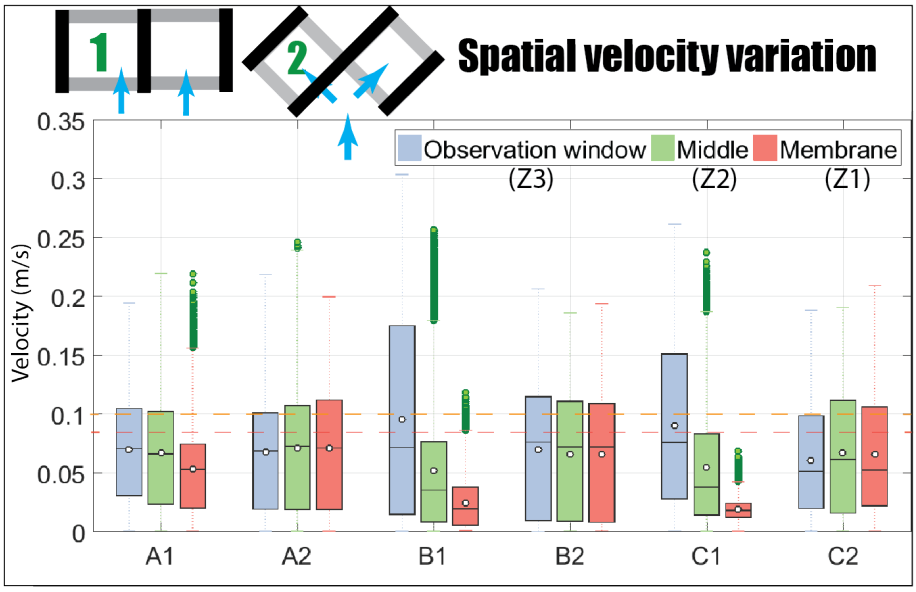

Figure 7.7: Spatial variations of averaged spatial velocity profiles at three channel heights for the ladder (1) and normal orientation (2). The average velocity is about 0.1 m/s for spacers A and B and 0.08 m/s for spacer C. The membrane side (Z1) indicates the channel side far from the camera where the transverse filaments are placed in ladder orientation and the observation window (Z3) indicates the channel side close to the camera without transverse filaments in ladder orientation.

7

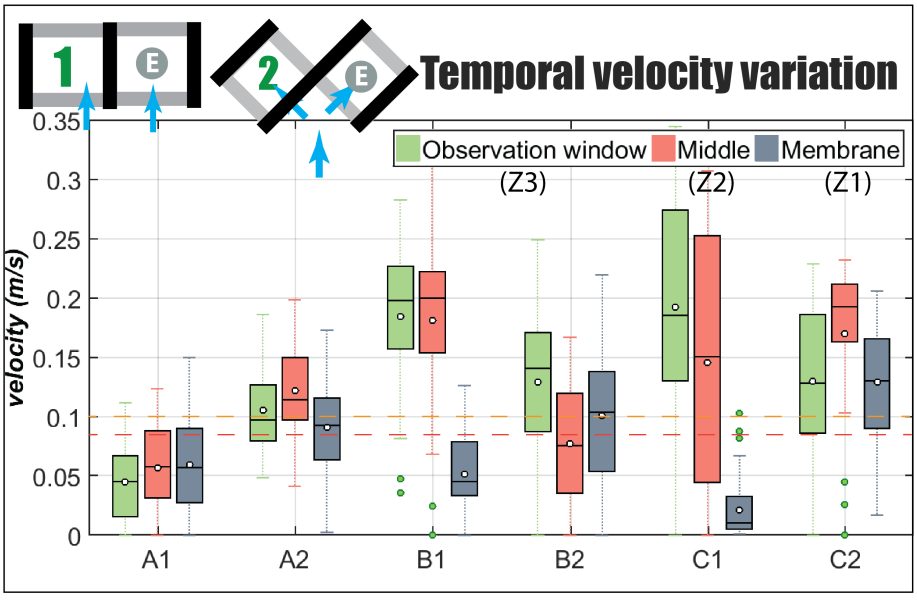

Figure 7.8: Variation of temporal velocity at a point in the middle of a mesh (point E) for an average velocity of 0.1 m/s (spacer A and B) and 0.08 m/s (spacer C)

of the channel (Z2), the velocity magnitude was lower, from 5% in spacer *A* to 27% in spacer *C*, in ladder orientation than in the normal orientation.
The lower velocity at the membrane side of the ladder orientation can be explained by considering the role of transverse filaments. Transverse filaments accelerate the flow at the opposite half of the channel as they are narrowing the flow path. In the normal orientation, both filament layers contribute to flow acceleration, i.e. there are accelerated flows at the top and bottom of the membrane. Because the flow attack angle is 45°, top and bottom flows cross each other and a proper mixing of flow occurs in the feed channel. In the ladder orientation, where the flow attack angle is 90°, only transverse filaments contribute to flow acceleration, i.e. there is no acceleration due to filaments parallel to the flow on the side that transverse filaments are attached to; therefore, the flow becomes more isolated between two successive filaments, and low-velocity areas are formed.

TEMPORAL VELOCITY VARIATION

Figure 7.8 shows variations of the velocity in time for the point *E* in the center of a mesh for three channel heights. The median, average, and outliers are shown respectively with a straight line, empty circle inside the box and filled circles. In general, the velocity variations for the normal orientation are less than with the ladder orientation, which resembles the averaged spatial profiles as shown in figure 7.7. As expected, the variation in time is greater than in space since the spatial variations are based on time-averaged velocities.
Figure 7.8 illustrates that the magnitude and variation of the temporal velocity is clearly lower in ladder orientation compared to the normal orientation, particularly in spacers *B* and *C*. Remarkably, with the ladder orientation, the variation of velocity is higher (particularly with spacer *B* and *C*) in the middle of the channel (Z2), compared to the observation window (Z3) and at the membrane side (Z1). This is probably the result of a clear separation in the flow magnitude at the top (high velocity) and bottom (low velocity) parts of the flow channel. The high-velocity variations could be the result of vortex shedding in the lee side of filaments or due to the existence of unsteadiness as the consequence of acceleration and deceleration of flow when moving from one mesh to the other one. In either case, high-velocity variation in time is considered beneficial with respect to fouling prevention and concentration polarization destabilization. However, the high-velocity variations observed with the ladder orientation occur in the middle of the channel, while fouling and concentration polarization tend to happen on the membrane sides; the benefit could therefore be minimal in this case. In the normal orientation, the velocity has the same magnitude at the top and bottom parts of the channel because both layers of filaments contribute to the flow acceleration in the channel.

7.4. CONCLUSION

In this chapter, the impacts of two orientations of three spacers with different thicknesses are experimentally assessed with regards to the pressure drop and velocity patterns at three heights in the channel: close to the membrane (Z1 in figure 7.3), close to the observation window (Z3 in figure 7.3) and in the middle of the channel (Z2 in figure 7.3).

The results reveal higher benefits for the ladder orientation compared to the normal orientation only for the case of the thinner spacer. The pressure drop with the ladder orientation was 10% and 17% lower compared to the normal orientation respectively for the thickest (*C*) and thinnest (*A*) spacer. The velocity maps in this chapter, obtained using particle image velocimetry (PIV), were in agreement with the particle deposition patterns described by Neal et al. [12] and Radu et al. [215].

In general, there was a distinct difference in velocity magnitude for the ladder orientation at three heights in the feed channel, but minor differences with the normal orientation. Moreover, the difference was less evident with the ladder orientation of spacer A than spacers B and C. In addition, the velocity magnitude was enhanced for spacer A in the ladder orientation over the channel height compared to the normal orientation. The same is reported by Neal et al. [12], which is likely because they used a spacer with a similar geometry as spacer *A*.

In the ladder orientation of spacer *B* and *C*, the lowest velocity was observed at the membrane side with attached transverse filaments and the highest at the membrane side without transverse filaments. In addition, the velocity magnitude at the membrane side is decreased with the increase in spacer thickness. Low-velocity regions created at the membrane side with transverse filaments could have a high fouling potential because of low shear stresses in these areas. On the other hand, the high velocity at the membrane side without transverse filaments might not be beneficial, because there is an optimal shear required to prevent fouling, and values above this value will cause increased pressure drop without a significant effect on the fouling remediation. In conclusion, the advantage of ladder orientation is obtained when applied with thinner feed spacers rather than thicker ones.

While our results provide a reasonable estimation of the velocity maps, asynchronously at three different heights (Z1, Z2 and Z3) inside the feed channel, further experimental investigations would be required to quantify the effect of velocity in the Z-direction and associated shear stresses simultaneously with velocity in the X- and Y-direction. It would probably be possible to reconstruct 3D maps of mean velocities from the measured 2D values in this chapter. However, the reconstructed images would not always be relevant, as they have been captured at different time steps. The findings from this study can be exploited as a validation tool for numerical studies, because of their high resolution. In addition, they can be used to design an optimum feed spacer for SWM modules of RO.

8. Summary, conclusions and outlook

The Moving Finger writes; and, having writ,
Moves on: nor all thy Piety nor Wit
Shall lure it back to cancel half a Line,
Nor all thy Tears wash out a Word of it.

Khayyam

The work presented in this thesis investigated the friction losses and variation of actual fluid velocity in time and place for narrow spacer-filled channels. The spatial and temporal velocity profiles are determined with particle image velocimetry (PIV) and the friction losses are determined by measuring the pressure drop. Analyzing relationships between fluid flow, pressure drop and actual velocity profiles in the feed channels provided insights into the hydraulic conditions occurring inside spiral-wound membrane (SWM) modules. These knowledge can be used to develop strategies to improve the design of filaments and meshes in feed spacers for a specific type of water, and it can thereby reduce the operational cost of SWM modules. In additions, the obtained velocity profiles can be used to validate computational fluid dynamics (CFD) models.

PIV provides a flexible and practical way for measuring and visualizing the velocity variation in flow channels representing the SWM modules at different flow rates and different geometric characteristics. Flow data from PIV can be represented in any position inside the field of view and at any moment during the measurement. In PIV, the real conditions inside the feed channel is determined instead of simulated situations. For instance, with PIV, commercial feed spacers or printed ones could be used and fouling could be take into considerations. These make the PIV a more attractive technique compared to mathematical models because reproducing feed spacers with all their details, to be used in mathematical models, is a difficult and time-consuming job. Additionally, the CFD models becomes more challenging when fouling is involved in an investigation. Ultimately, because the numerical models are just simpler copies of reality and use the known theories (equations), several assumptions are made when solving them. PIV, on the other hand, enables us to measure velocities in an actual way (real time) without any assumption.

The PIV technique is an indirect method in a sense that it does not measure the velocity in SWM modules but in flat test-cells and that it measures the movements of the tracers rather than the fluid. Therefore, the tracers used in PIV should be as small as possible to follow the motion of the fluid. However, the accuracy of the measurement also depends on the scattered light from the seeds, which is a function of particles size. Bigger particles have a higher scattering cross-section, defined as the ratio of the total scattered power to the laser intensity incident on the particle.
Unlike CFD studies, PIV is hardly ever used to determine the hydraulic conditions of spacer-filled channels. There are not any investigations related to the hydraulic conditions of spacer-filled channels with 3D-PIV. To the authors' knowledge, also, the 2D-PIV is rarely used for this purpose. The only two known 2D-PIV investigations [141, 203] could elucidate a part of the complex flow mechanism of the spacer-filled channel. This thesis made an attempt to provide additional insight into hydraulic conditions of the spacer-filled channel by using 2D-PIV.

One of the objectives of this thesis was to compare the hydraulic conditions inside an empty channel with those inside a spacer-filled channel. To this aim, a common commercial feed spacer (30 mil) is inserted into the feed channel and the pressure drop and velocity profile of the spacer-filled channel is compared to those of the empty channel.

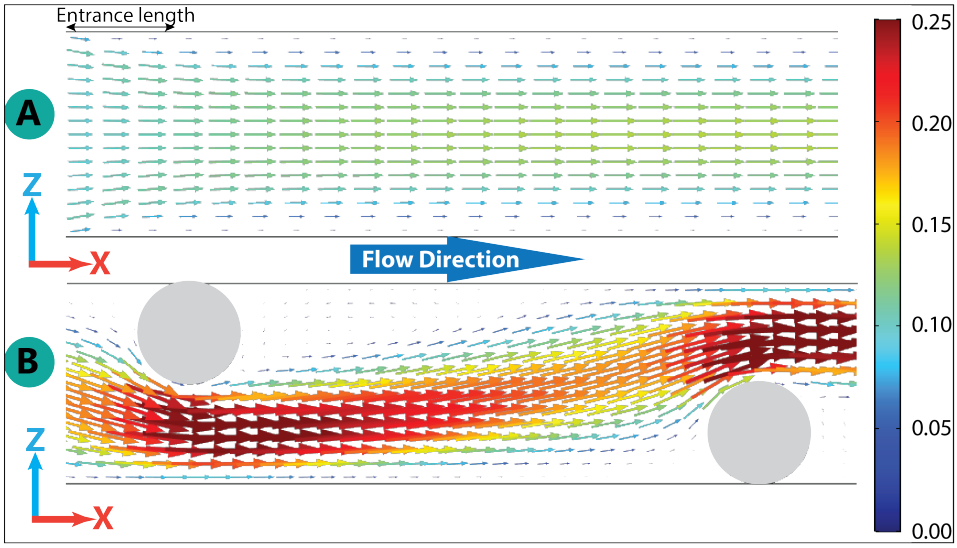

Figure 8.1: The velocity profiles in the empty (A) and spacer-filled channel (B). The profiles are made using a numerical method. The flow is applied in the x-direction in a way that the theoretically average velocity was about 0.1 m/s. The velocity is not limited to one value, neither in spacer-filled nor in the empty channel. At the entrance length in the empty channel, the velocity is lower than the part that flow is fully developed. At the first part of the entrance length, the velocity is almost the same over the channel height. That is the value called the average velocity in literature.

The achieved relation between the pressure drop and the velocity along the flow direction (equation 3.12 :$dp \propto K \times U_{ave}^{m}$) showed that in contrast to the empty channel, the flow in the spacer-filled channel could be considered as transitional. This conclusion was based on the obtained value for m, the exponent in the equation of velocity dependency on the pressure drop, the logarithmic view of friction losses against Reynolds number and definitions from former studies. In previous studies [152, 173], the laminar flow has been defined by an m-value equal to 1, the fully developed turbulent flow by an m-value equal to 1.75 and higher and the transitional flow would be all the $m-$exponents in between. In contrast to this conclusion, it was also found [154, 179–181, 243] that referring to the flow, which encounters in SWM modules of RO, as turbulent is a common misunderstanding. That is because the turbulent flow should assign only to flows with high Reynolds numbers (i.e. $Re > 4000$) at which turbulence can be assumed to be isotropic and fully developed [179–181, 243], while SWM modules of RO usually operate at much lower Reynolds numbers (i.e. $Re < 500$) and the flow conditions in these modules are laminar in nature [162, 244]. Finally, to be consistent with the most literature, this thesis concluded that the flow conditions encountered in SWM modules of RO are laminar.

The velocity used to determine the m-exponent was the applied inlet velocity or the average velocity, which was determined theoretically. The experimental velocity values were obtained by using PIV. The average velocity is normally expressed as one value in the literature while it changed over the channel height as well as channel length (figure

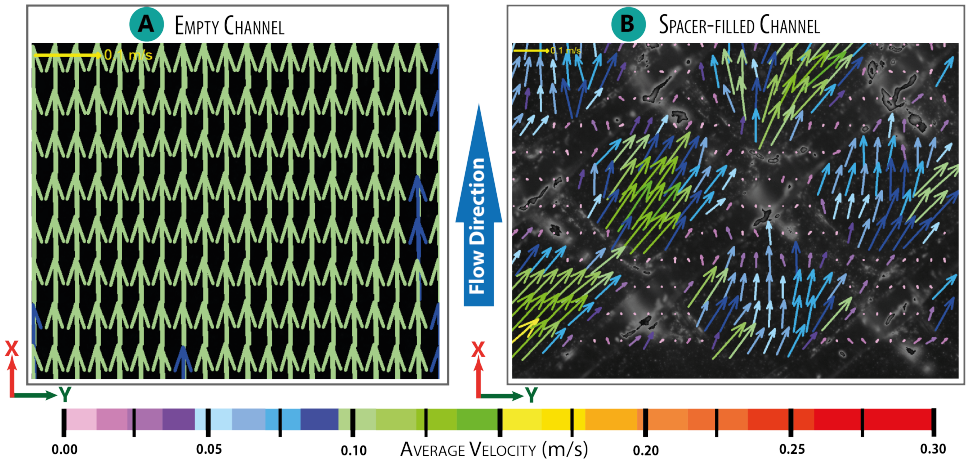

Figure 8.2: Flow in the empty (A) and spacer-filled channel (B). The velocity fields are determined with PIV at the middle of the channel.

8.1). The calculated average velocity in literature is the value at the channel inlet and not when the flow is fully developed. The flow becomes fully developed in some distance downstream of channel inlet; called the entrance length. The entrance length in empty rectangular channels depends on the ratio of the channel height to the channel width [175]. However, it is difficult to calculate the entrance length in spacer-filled channels. Numerical and experimental studies are able to illustrate variations of the velocity in an empty or in a spacer-filled channel (figure 8.1 and figure 8.2) at locations that flow is fully developed or not. While numerical studies enhance our understanding of hydraulic conditions of spacer-filled channels at relatively lower costs and risks compared to experimental methods, they may be associated with challenges such as matching the geometry of modeled feed spacers with commercial ones and an accurate verification and validation. As the results, it is recommended [141, 180] to use direct, non-invasive, high-resolution experimental methods such as PIV. Therefore, after determining friction losses with average velocity, the actual velocity profiles are determined experimentally by using PIV. With the PIV setup used in this study, images with a resolution as high as $7.4 \times 7.4 \mu m^2$ were captured.

PIV-results showed that when compared to the average velocity, the local velocity was higher at the middle of the empty channel and lower close to the membrane side and observation window. In fact, the flow in the empty channel had a semi-parabolic shape as it is known from literature and the flow direction was in a straight line from inlet to outlet (figure 8.2 A). The flow was steady compared to the spacer-filled channel (figure 8.2 B) and the steadiness decreased by the increase of the flow rate.
Introducing a spacer into the empty channel caused an increase in the unsteadiness of the flow. The velocity variation in the spacer-filled channel, at the maintained inlet velocity of 0.1 m/s, was about -100% to $+75\%$ of the empty channel depending on locations that measurements are done.

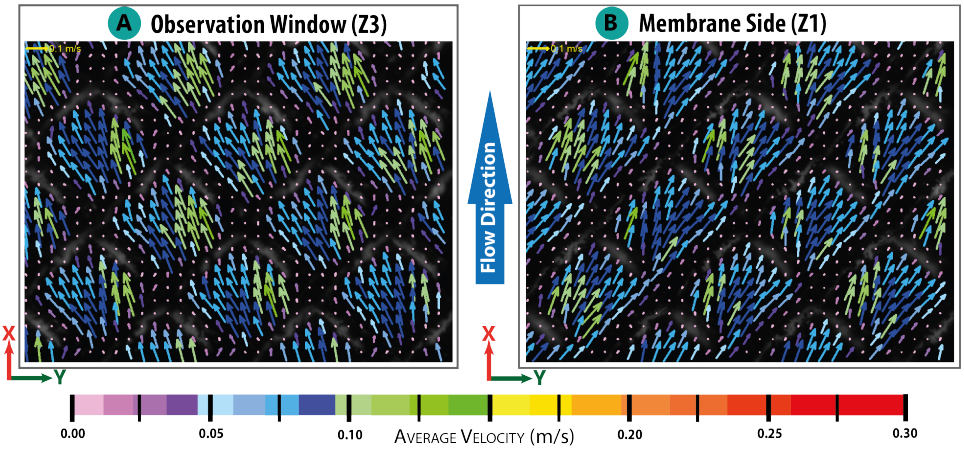

Figure 8.3: Water at each height of the channel flows along the attached filaments at that height.

The averaged spatial velocity profiles of spacer-filled channel showed a bimodal shape for flow pattens. The bimodal shape indicates the presence of low and high flow regimes. The low-velocity regimes occurred at regions close to the filaments and high-velocity regimes occurred at narrowed parts of the channel or directly after these narrowed parts. The increase in flow generates a greater distance between two distinct local maxima of the bimodal curve indicating generation of higher velocity at some locations, which is consistent with results from previous studies. The flow increase causes the increase in velocity magnitude and generation of a higher shear. However, this higher shear is not necessarily beneficial for the spacer-filled channel because the optimal flux as the results of destabilization of the concentration polarization layer is limited to a specific velocity and further increase of the velocity magnitude has an only marginal effect on the permeate flow increase.

The flow in the spacer-filled channels was along filaments of the spacer at a particular height (figure 8.3). For instance, the flow was in the direction of filaments from right to the left in front part of the channel (figure 8.3 A) and from left to the right at the rear part (figure 8.3 B) of the channel. Because the filaments at the top and bottom of channel make a 90° angle, the flow at the top was perpendicular to the flow at the bottom (figure 8.3). The flow at the middle of the channel had a pattern such as the mixture of the flow at the front (Z3) and rear part (Z1) of the channel.

Understanding the effect of spacer's geometry on flow and consequently on mass transfer, was another objective of this study, which was achieved by comparing several commercial feed spacers of different configurations. Six spacers with two different configurations, zigzag and cavity (figure 8.4), were used. In the zigzag spacers, top and bottom filaments had the same thickness and thus the channel height was twice the filament's thickness. In the cavity spacers, the filaments parallel to flow were thicker than transverse filaments. The channel height was respectively about 0.71, 0.76, 0.86, 1.22, 1.14, 1.24 mm in spacer A, B, C, D, G and H.

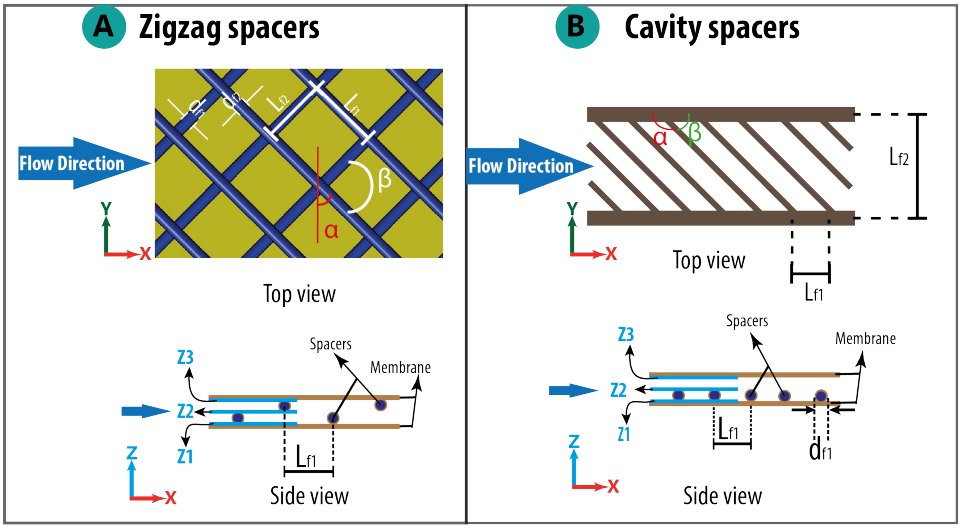

Figure 8.4: The top and the side view of zigzag (A) and cavity (B) spacers.

In general, the flow was more distributed toward both membranes in channels with zigzag spacers than cavity spacers. In channels with cavity spacers, the velocity was higher along the membrane side without transverse filaments (Z3) and the flow was in a straight line from inlet to outlet (figure 8.5 A). The flow at the membrane side with attached transverse filaments (Z1) was much lower in magnitude and variation because of the order of sequential transverse filaments (figure 8.5 B). In spacers, the flow accelerates due to the presence of transverse filaments. In channels with cavity spacers, transverse

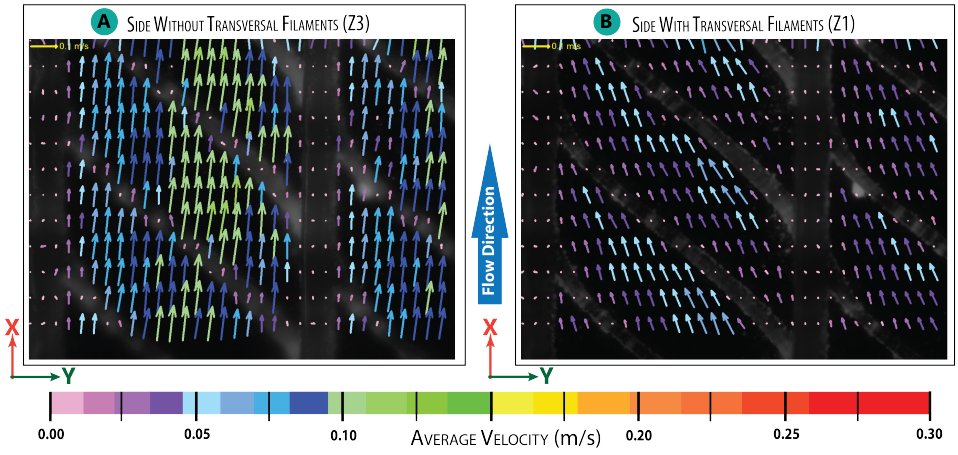

Figure 8.5: The velocity profile at the membrane side without transverse filaments (A) and with transverse filaments (B)

filaments are attached to one side of the channel and therefore, the acceleration happens without changing in the flow direction at the side without transverse filaments, which results in a major flow difference at the channel side with and without the transverse filaments. Less variation of the flow direction resulted in a lower flow mixing and a lower pressure drop in the channels with cavity spacers than zigzag spacers. Among the cavity spacers, the one with smaller transverse filaments and smaller inter-filament distance had lower velocity.

The exponent in the power or friction losses equation (equation 3.5: $C_{td} = \frac{A'}{Re^n}$) was clearly higher in the cavity spacers than zigzag spacers indicating lower mixing conditions with these spacers. The mixing condition is related to the relative height of a spacer defined as the ratio of transverse filament height to the channel height. The increase of relative height is directly related to the increase of friction losses, i.e. the increase of A'-value and decrease of n-value. A lower n-value occurs mainly at a higher relative height, which means greater mixing and consequently, a higher friction factor. For instance, among the cavity spacers, the one with the smallest relative height and the largest n-value has a lower mixing ability than other spacers. The thin transverse filaments of this spacer cause small wakes and small friction losses around these filaments, which are not big enough to generate large flow disturbances and eddies. Flow patterns at the channel side without transverse filaments and at middle, which were straight lines from inlet to outlet without disturbances, were indication of not big enough mixing in this channel.

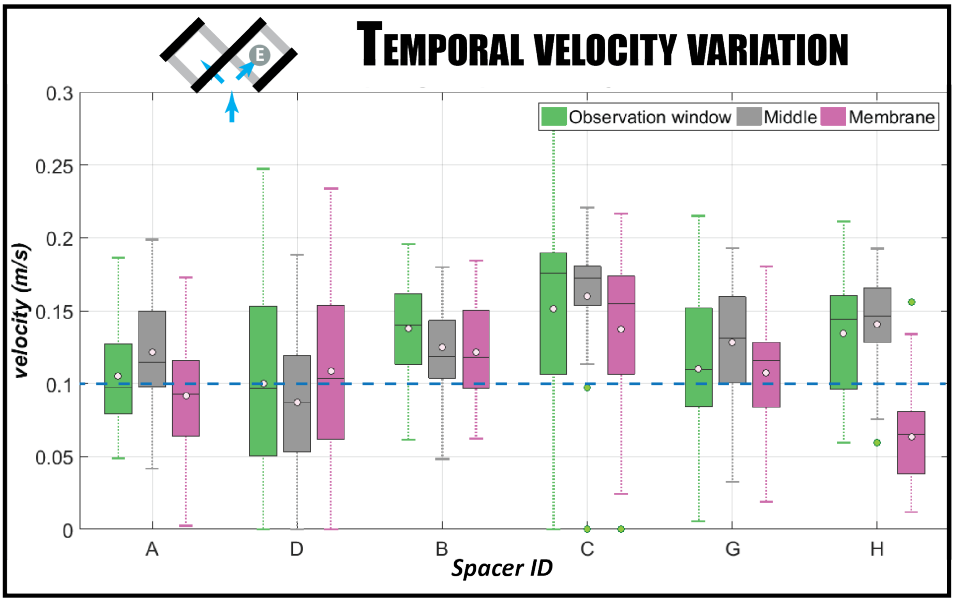

Figure 8.6: Temporal velocity at of examined spacers at three channel heights; in from of channel (Z3), in the middle of the channel (Z2) and at the rate part of the channel (Z3). The flow arranged in a way to generate an average velocity of $0.1 m/s$ in feed channels.

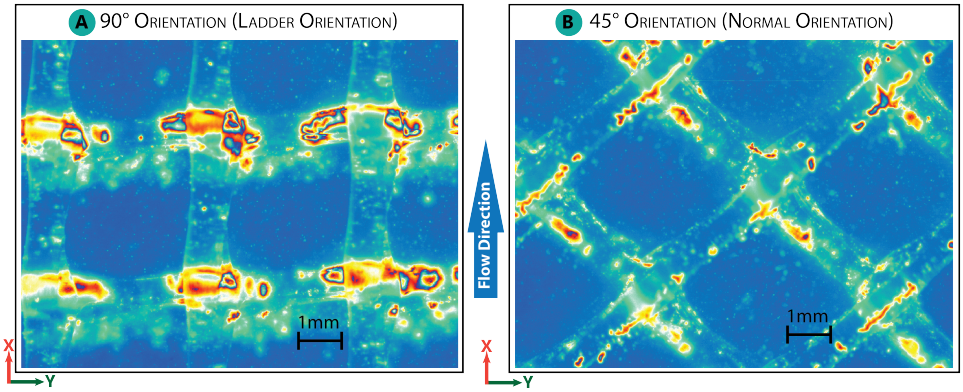

Figure 8.7: The orientation in which transverse filaments make an angle of 90° with flow called ladder orientation and the orientation where transverse filaments make an angle of 45° is called normal orientation.

The velocity in a specific grid (point) changed over time (unsteady flow). Only at limited locations inside a mesh, the averaged value of temporal velocity was in the range of the average velocity known from theoretical calculations, i.e. that only limited locations inside a mesh have a model behavior according to our expectation with regard to fouling and energy losses. The range of velocity variation was greater in spacers with bigger transverse filaments in both types (cavity and zigzag) of spacers (figure 8.6). A higher variation of the instantaneous velocity results in higher flow unsteadiness and lower particle deposition potential.

The orientation of feed spacers is determined by the way that hydrodynamic angle faces the flow. This study considered two orientations for each feed spacer, the 45° orientation (normal orientation) and the 90° orientation (ladder type orientation) (figure 8.7). Hydraulic conditions of three spacers of different thickness are examined at these two orientations. The filaments' thickness at the top and bottom layers was on average the same for each spacer.
In general, the pressure drop was lower in ladder orientation than normal orientation. In the applied conditions ($Re < 200$), the effect of the pressure drop was only significant for the thinnest spacer. It was also found that the mixing ability of the normal orientation is better than ladder orientation because zigzag spacers had a higher m-value (equation 3.12 : $dp \propto K \times U_{ave}^{m}$).

The flow was in a straight line from inlet to outlet in channels with spacers at ladder orientation and it was along the filaments in channels with spacers at normal orientation (figure 8.8). The flow in channels with spacers at normal orientation was more complex than ladder orientation. In channels with spacers at the normal orientation, water passes over the filaments attached to the membrane and under the filaments attached to the observation window and mixed in the following mesh. This pattern repeats in every mesh. This complex mixing behavior of the flow together with the particular geometry of each spacer (thickness and porosity) make it difficult to give a general prediction about the areas with lowest and heights velocity.

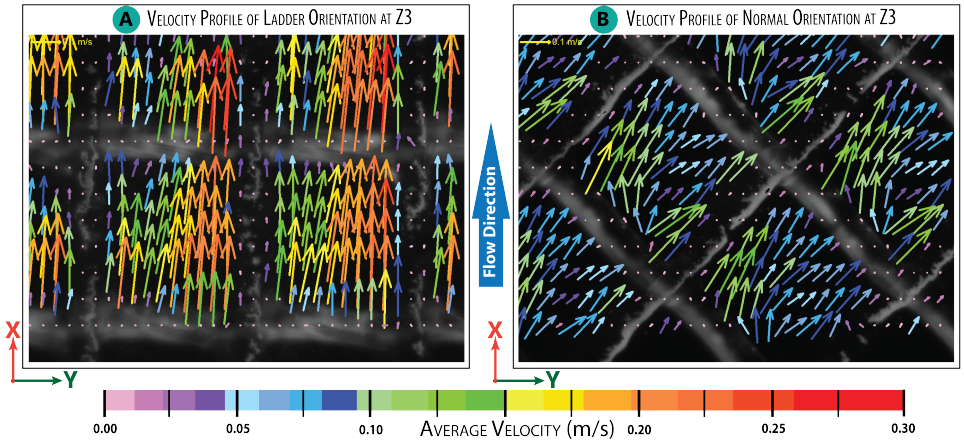

Figure 8.8: The velocity profile for ladder orientation (A) and normal orientation (B). The conditions are adjusted in a way to achieve an average velocity of $0.1 m/s$. These profiles are measured at the front part of the channel (Z3).

When points with a different channel height were compared, a greater difference in spatial velocity was obtained in channels with spacer at the ladder orientation. Considering only the middle part of a channel, a low-velocity region was formed directly at downstream of transverse filaments. The non-uniform shape of filament's cross-sectional caused a non-uniform velocity pattern at downstream of filament in channels with spacers at ladder orientation. The highest downstream velocity was observed at locations where the filaments bulge toward the flow. The acceleration effect along a filament was more apparent over the swelled part of the transverse filaments in thicker spacers than thinner spacers.

In channels with spacers at normal orientation, the lowest velocity region was the inner angle at the upstream node of meshes, where both flows exit the mesh. Compared to the velocity at the middle of the channel, the velocity in channels with the ladder orientation was significantly lower over the membrane side with transverse filaments but higher over the membrane side without transverse filaments.
As mentioned earlier, transverse filaments accelerate the flow in the opposite half of the channel they are placed on by narrowing the flow path. In channel with spacers at the normal orientation, both filament layers contribute to flow acceleration and because the flow attack angle is 45°, top and bottom flow cross each other and a proper mixing of flow occurs in the feed channel. In the ladder orientation where the flow attack angle 90° is, only one side of channel contributes to flow acceleration, i.e. there is no acceleration at the side of channel where transverse filaments are attached, and therefore, the flow becomes isolated between two successive filaments and low-velocity areas are formed.

It was found that temporal velocity variations in channels with spacer at normal orientation were less than ladder-orientation. Additionally, temporal velocity variations at the middle of the channel were higher in the channels with spacers at ladder orientation compared to the normal orientation, which is probably the result of an interface in the

flow magnitude at the top (high velocity) and bottom (low velocity) of the channel.

Knowledge about friction losses and the regions with low and high velocity are important when designing a new spacer. Therefore, chapters 5, 6 and 7 of this thesis investiagted the pressure drop and variation of velocity pattern in narrowed feed channels. Higher velocity results in increased wall shear, which is of particular importance for high Schmidt number. An enhanced mass transfer is the consequence of a thinner boundary layer and lower membrane fouling and can be obtained by an effective increase of the shear at the membrane surface and thus an effective increase of velocity. However, due to energy losses, there is an optimum velocity for controlling the fouling and concentration polarization. The increase of velocity above this optimum could be translated into a higher ratio of energy losses to the production rate, i.e. applying velocities higher than optimum velocity results in the increase of energy consumption without having additional effect in minimizing the concentration polarization layer and reducing of fouling. A proper design of a feed spacer also incorporates the ability of the spacer to generate velocity variations in time because high variations could be the indication of vortex shedding in the lee side of filaments or the existence of pulsating flow, which is beneficial for fouling prevention and destabilizing of concentration polarization layer.
The benefits of higher velocity magnitude and frequency depend on the channel height. It is desirable to have higher velocity values close to the membrane walls rather than middle of the channel because increasing the velocity in the middle of the channel results in the increase of friction losses without significant effect on the fouling. The high-velocity variation in channels with spacers at ladder orientation occurs at the middle of the channel, while fouling and concentration polarization happen on the membrane sides and therefore, it is not beneficial for fouling prevention. In channels with spacer at normal orientation, the velocity has the same magnitude at top and bottom parts of the channel because both layers of filaments contribute to flow acceleration in the channel.

Because experiments in this thesis are preformed at a low range of Reynolds numbers ($Re < 200$), there is no guarantee that the geometries and orientations which resulted in the lowest dynamic power losses under these circumstances will also act in a similar way with a different set of conditions, such as a complex matrix of water or when permeate is produced. However, according to the presented data, in general, the hydrodynamic power losses are lower in channels with cavity spacers and at ladder orientation than in channels with zigzag spacers and at normal orientation. Economic analysis is not performed because the experiments were carried out without the permeate production. However, the effects of capital costs are considered by a short discussion.

The cost of produced permeate by membrane is the sum of capital and operational costs. For a determined operation time and flux, the capital cost depends on the materials costs, feed water characteristics and amortization factor. The membrane cost is usually a major part of material costs in RO. For a determined feed water quality and at a constant pump efficiency and energy cost, the operational cost depends on the channel height and the pressure drop per unit length of the membrane.

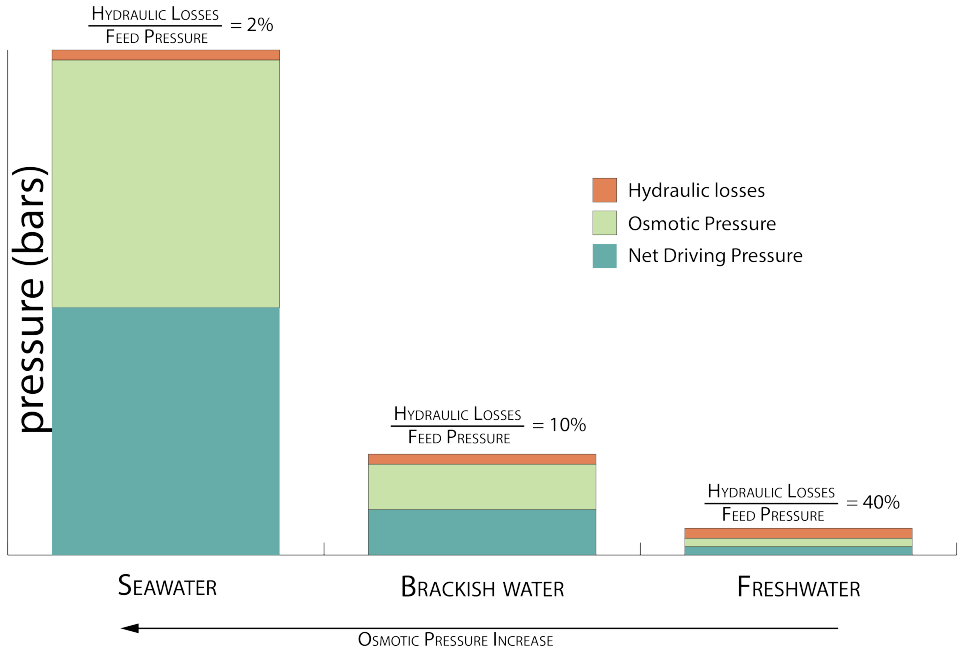

Figure 8.9: The ratio of hydraulic losses to feed pressure increases by decreasing of the water salinity.

Current trends indicate that capital membrane costs are decreasing and energy costs are increasing. This emphasizes the need to reduce membrane operations costs by improving the design of treatment plants and membrane modules to reduce the energy losses and to control the fouling efficiently. In this context, the feed spacer has major effects on the membrane material usage, by determining the channel height and hydraulic conditions. The impact of spacers on the packing density of SWM modules wanes due to the gradual shifting toward automated manufacturing techniques for enlargement of the membrane active area such as the use of robotics for precise placement of glue lines. In addition, production costs of current feed spacers are significantly lower than those of the membrane sheets. Therefore, it is of great interest to find an optimal spacer design that reduces the membrane operating costs.

It is beneficial to define the optimal design of a feed spacer for the specific circumstances wherein a membrane module operates. Thus, it is improbable that single spacer geometry is suitable for all types of feed water. As mentioned, the optimal design of a feed spacer is a function of several factors such the production costs of the feed spacer, type of feed water and the operating conditions. Design of a totally new type of spacer, e.g. a spacer with three or more layers of filaments, would require a major adaption of manufacturing facilities, which is costly and time-consuming and will result in an increase of the membrane element capital costs. Therefore, it would be more advantageous to adapt the current configuration of feed spacers to the type of water and operating conditions.

The fresh groundwater is the most common source for drinking water production in most parts around the world. However, the use of other sources such as the fresh surface water, brackish groundwater and seawater as an alternative to fresh groundwater is increasing by the day due to the increasing rise in shortage of fresh groundwater as the result of overdraft, salinization and fouling of this resource. Consequently, the application of techniques such RO, to purify the saline water and to provide a barrier against a rapid and continuous increase of new contaminants in water resources, increases. The mentioned emerging contaminates could be dangerous even in very low concentrations and usually they could not be removed with conventional water treatment processes. Despite this and the important role of feed spacers in determining hydraulic conditions of SWM modules, the configuration of feed spacers is hardly changed since its first design. Feed spacers of RO were, historically, designed to minimize the effect of concentration polarization in brackish water and seawater desalination. Therefore, the modification of a feed spacer according to the type of feed water is a critical step to a wider application of SWM modules of RO.

In light of the data presented in this thesis, it can be expected that ladder spacers with some modifications could be a more proper choice for purification of fresh surface water because ladder spacers cause a lower pressure drop increase in the feed channel. Additionally, ladder spacers could be cleaned more effectively with mechanical cleaning methods such as air-water cleaning.
The necessity of generation of extreme mixing to reduce the concentration polarization is not essential in freshwater because of low salt concentration, when these systems operate at the same flux range as systems with saline feed water. However, the formation of stagnant zones should be avoided because of a high biofouling potential of fresh surface water. Therefore, required modifications should consider changing the location of transverse filaments in the channel height in order to enhance the flow distribution toward both membrane sides (figure 8.10). This will probably cause a slight increase in the pressure drop inside the feed channel compared to unmodified spacers.

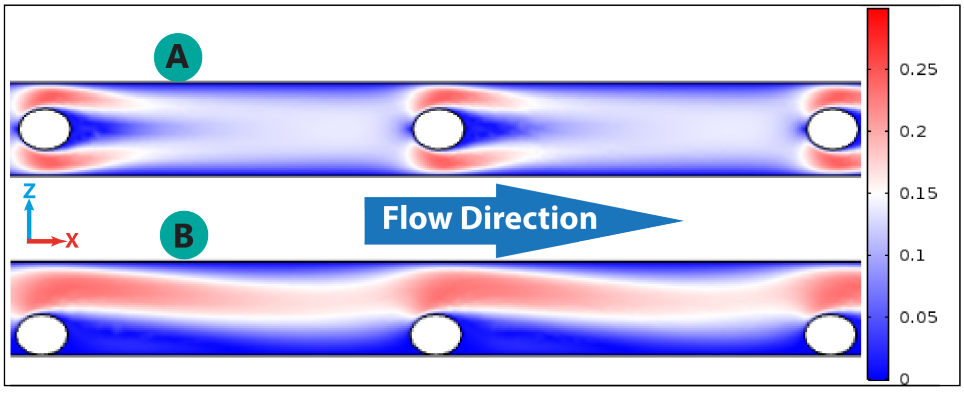

Figure 8.10: A simple numerical demonstration of effects of changing the place of transverse filaments in cavity spacers on the velocity profiles. A higher flow is directed to membrane sides in situation A instead of the middle of the channel situation B.

It has been shown that the pretreatment cost is a major cost element in seawater desalination and fresh surface water purification by RO. Although, the RO can reject almost all kinds of contaminates, pretreatment is applied to elongate the lifespan of RO. Limiting the pretreatment to only mechanical processes will reduce the membrane operation costs, the load of chemical discharges to the environment and the increase of membrane lifespan. However, limiting the chemical cleaning in the pretreatment requires more effective and more frequent application of the mechanical cleaning methods, such as application of higher flow or air-water cleaning. In air-water cleaning method, modified ladder spacers, e.g. ladder spacers with transverse filaments at the middle of parallel filaments, may be preferred over zigzag spacers because they create fewer stagnant areas. However, this is not proven in this thesis.

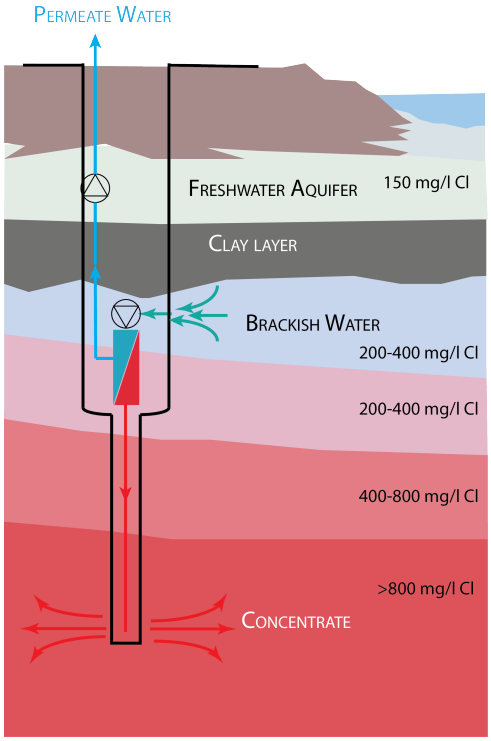

Figure 8.11: The PURO concept. The vertically located membrane use the brackish groundwater as feed and dispose the concentrate into the lower part of ground with approximately the same concentration as the concentrate stream. The installation makes use of the available hydrostatic pressure and requires 40% less energy compared a conventional installation of the same capacity and recovery.

PURO and fresh keeper are examples of the application of RO without any chemical pretreatment on the brackish water, in which the effect of concentration polarization is more pronounced than biofouling. Chapter 2 described the PURO concept (figure 8.11), which make use of the available free energy in nature for driving the RO without any chemical pretreatment.

Additionally, the obtained results from this study can be used to validate numerical studies. Validation with experimental studies of proper resolution is one of the main challenges that most numerical studies within the field of membrane science face. Although no numerical studies were conducted in this thesis, the obtained results were successfully compared with the previous studies and a good agreement was found with published data.

In conclusion, PIV has proven to be a valuable tool for the performance analysis of feed spacers and can provide detailed information for validation of numerical studies. The novelty of PIV is that it measures directly the actual velocity without having problems with the geometric complexity of commercial spacers or the presence of fouling inside the feed channel. Once the setup is made, various experiments with spacers of different configuration and orientation could be performed. With PIV, the actual temporal

and spatial velocity can be determined by changing the important geometric characterizations of feed spacers such as filament's thickness, spacer orientation and transverse filaments distance, which play primary roles in mixing the flow, distribution of the flow toward the membrane side, varying of flow in a particular point and determining the pressure losses.
The method used in this study can provide starting points for experimental validation of mathematical models related to spacers and a new way for designing the optimal spacer for each type of feed water. Future studies following the line of work presented in this thesis should mainly focus on the use of artificial feed spacers, in which the relative height and relative length can be changed systematically. This should be done parallel with the numerical studies to get a better insight into the processes occur inside the feed channel.
The experiments described in this thesis were performed with a clean membrane and clean feed spacer and without permeate production. Therefore, permeation and fouling phenomena should be incorporated in future studies to get a better understanding of the performance of each spacer. The method can be used in parallel to the mass transfer coefficient of the membrane and the variation of electrical conductivity of the feed and concentrate to determine the initiation of preferential paths.
The thesis also includes measurements of the spatial and temporal velocity at three different levels to get a better insight into hydraulic conditions at these three levels. That is done asynchronously, i.e. that the focus of the camera is changed for each height. More advanced methods that provide a better understanding of the hydraulic conditions inside a spacer-filled channel are 2D2C-PIV, volumetric PIV, or shake the box method wherein more than one camera is used. The main difference between the volumetric PIV and shake the box method with 2D2C camera is that using of the former methods will results in a 3D illustration of the flow. By 2D2C, the Z-velocity component (the velocity in the direction of the channel height) can be measured.

Designing a proper feed spacer for each type of feed water and eliminating the chemical pretreatment of RO possibly opens a whole new world for designing of the RO-based treatment plant. For instance, there could be a shift toward designing of decentralize treatment plants to overcome the two main challenges regarding the future drinking water production; the increasing number of emerging pollutants in water resources and a sustainable distribution network. The current centralized water distribution network requires significant investments for maintenance to deliver an acceptable water quality. Decentralized treatment plants reduce the construction costs of water pipes and reduce the risk of the outbreak of (particular) contaminant. In additions, each particular plant can use locally available resources to alleviate the environmental load on a specific water resource and to deliver the water according to the requirements of individual consumers.

Bibliography

[1] J.C. Crittenden et al. “Membrane Filtration”. In: *MWH’s Water Treatment: Principles and Design, Third Edition*. John Wiley & Sons, Inc., 2012, pages 819–902.

[2] T. Oki and S. Kanae. “Global Hydrological Cycles and World Water Resources”. In: *Science* 313.5790 (2006), pages 1068–1072.

[3] I.A. Shiklomanov. “World water resources”. In: *Water in Crisis.New York, Oxford* (1993).

[4] A. Shrivastava, S. Kumar, and E.L. Cussler. “Predicting the effect of membrane spacers on mass transfer”. In: *Journal of Membrane Science* 323.2 (2008), pages 247–256.

[5] G. Grakist et al. “Keeping our wells fresh”. In: *Proceedings of SWIM - 17.Delft University of Technology, Delft* (2002), pages 337–340.

[6] K. Jena. “Water Stress”. In: *Obituary* (2013), page 12.

[7] L.F. Greenlee et al. “Reverse osmosis desalination: Water sources, technology and today’s challenges”. In: *Water Research* 43.9 (2009), pages 2317–2348.

[8] M. Uchymiak et al. “Brackish water reverse osmosis (BWRO) operation in feed flow reversal mode using an ex situ scale observation detector (EXSOD)”. In: *Journal of Membrane Science* 341.1-2 (2009), pages 60–66.

[9] S. Belfer et al. “Surface modification of commercial composite polyamide reverse osmosis membranes”. In: *Journal of Membrane Science* 139.2 (1998), pages 175–181.

[10] S. Belfer, Y. Purinson, and O. Kedem. “Surface modification of commercial polyamide reverse osmosis membranes by radical grafting: An ATR-FTIR study”. In: *Acta Polymerica* 49.10-11 (1998), pages 574–582.

[11] W. Byrne. *Reverse Osmosis: A Practical Guide for Industrial Users*. Tall Oaks Pub., 1995.

[12] P.R. Neal et al. “The effect of filament orientation on critical flux and particle deposition in spacer-filled channels”. In: *Journal of Membrane Science* 214.2 (2003), pages 165–178.

[13] J. Schwinge et al. “Spiral wound modules and spacers: Review and analysis”. In: *Journal of Membrane Science* 242.1–2 (2004), pages 129–153.

[14] A.R. Da Costa and A.G. Fane. “Net-Type Spacers: Effect of Configuration on Fluid Flow Path and Ultrafiltration Flux”. In: *Industrial & Engineering Chemistry Research* 33.7 (1994), pages 1845–1851.

[15] C.P. Koutsou, S.G. Yiantsios, and A.J. Karabelas. “Numerical simulation of the flow in a plane-channel containing a periodic array of cylindrical turbulence promoters”. In: *Journal of Membrane Science* 231.1-2 (2004), pages 81–90.

[16] W. Kaminski and J. Stawczyk. “An effect of vortex flow on fluxes in ultrafiltration plate-frame modules”. In: *Journal of Membrane Science* 123.2 (1997), pages 157–164.

[17] J.A. Howell. *The Membrane Alternative: Energy Implications for Industry: Watt Committee Report Number 21*. Taylor & Francis, 1990.

[18] A.H. Haidari et al. “PURO: A unique RO-design for brackish groundwater treatment”. In: *Desalination* 403 (2017). Desalination Using Membrane Technology, pages 208–216.

[19] G.M. von Medeazza and V. Moreau. “Modelling of water–energy systems. The case of desalination”. In: *Energy* 32.6 (2007). Third Dubrovnik Conference on Sustainable Development of Energy, Water and Environment Systems, pages 1024–1031.

[20] J.J. McCarthy. *Climate change 2001: impacts, adaptation and vulnerability: contribution of Working Group II to the third assessment report of the Intergovernmental Panel on Climate Change*. Cambridge University Press, 2001.

[21] N. Voutchkov. “Overview of seawater concentrate disposal alternatives”. In: *Desalination* 273.1 (2011), pages 205–219.

[22] L.C. Rietveld et al. “Possibilities for reuse of treated domestic wastewater in The Netherlands”. In: *Water Science & Technology* 64.7 (2011).

[23] N. Wolthek et al. “Desalination of brackish groundwater and concentrate disposal by deep well injection”. In: *Desalination and Water Treatment* 51.4-6 (2012), pages 1131–1136.

[24] P. Stuyfzand and K. Raat. “Benefits and hurdles of using brackish groundwater as a drinking water source in the Netherlands”. In: *Hydrogeology Journal, Springer-Verlag* (2010), pages 117–130.

[25] T.N. Olsthoorn. “Brackish groundwater as a new resource for drinking water; specific consequences of density dependent flow and positive environmental consequences”. In: *Salt water Intrusion Meeting*. 2008, pages 174–177.

[26] V.E.A. Post. “Groundwater salinization processes in the coastal area of the Netherlands due to transgressions during the Holocene”. In: (2006).

[27] J.W. Kooiman et al. “Pumping Brackish Groundwater to Prepare Drinking Water and Keep Salinizing Wells Fresh: A Feasibility Study”. In: *18th Salt Water Intrusion Meeting (SWIM)*, pages 625–635.

[28] J.M. Beltran and S. Koo-Oshima. “Water desalination for agricultural applications”. In: *FAO Land and water discussion paper* 5 (2006), page 48.

[29] U. Yermiyahu et al. “Rethinking Desalinated Water Quality and Agriculture”. In: *Science* 318.5852 (2007), pages 920–921.

[30] A. Perez-Gonzalez et al. “State of the art and review on the treatment technologies of water reverse osmosis concentrates”. In: *Water Research* 46.2 (2012), pages 267–283.

[31] K. Raat et al. “Dutch Fresh-keepr worldwide applicable (in Dutch: Nederlandse ’Zoethouder’ Wereldwijd Toepasbaar)”. In: *H2O (Water matters)* (2015), pages 43–46.

[32] K. Raat. *Counteracting Salinisation of Well Fields: Freshkeeper in Florida*. type. KWR-water, 2013.

[33] B. Scheffers and N. Robat. “The future of drinking water: A pilot study is testing a new system for producing fresh drinking water from brackish groundwater”. In: *GeoDrilling International* (2013).

[34] C. Fritzmann et al. “State-of-the-art of reverse osmosis desalination”. In: *Desalination* 216.1-3 (2007), pages 1–76.

[35] I.C. Watson, O.J. Morin, and Henthorne L. *DESALTING HANDBOOK FOR PLANNERS*. Report. Bureau of Reclamation, July 2003.

[36] C. Bartels, M. Hirose, and H. Fujioka. “Performance advancement in the spiral wound RO/NF element design”. In: *Desalination European Desalination Society and Center for Research and Technology Hellas (CERTH), Sani Resort 22-25 April 2007*. 2007, pages 207–214.

[37] H.Y. Ng and S.L. Ong. “A Novel 400-mm RO System for Water Reuse and Desalination”. In: *JOURNAL OF ENVIRONMENTAL ENGINEERING AND MANAGEMENT* 17.2 (2007), page 113.

[38] K.J. Raat et al. *Water quality changes following deep well injection of BWRO concentrate. Results from the BWRO pilots Noardburgum and Zevenbergen*. Report. KWR Watercycle Research Institute, Nieuwegein, the Netherlands, 2011.

[39] H.M. Ettouney et al. “Evaluating the economics of desalination”. In: *Chemical Engineering Progress* 98.12 (2002), pages 32–40.

[40] *The Purchase Advantage*. 2014. URL: http://www.thepurchaseadvantage.com/page/TPA/CTGY/codeline_side_entry_ro_pressure_vessels.

[41] *Grundfos Pumps*. 2014. URL: http://www.lenntech.com/grundfos/CRN64/96123816/CRN-64-8-2-A-F-G-V-HQQV.html.

[42] MyTub Ltd. “Grundfos Pump”. In: (2014), Mytub.co.uk.

[43] C. Garcia, F. Molina, and D. Zarzo. “7 year operation of a BWRO plant with raw water from a coastal aquifer for agricultural irrigation”. In: *Desalination and Water Treatment* 31.1-3 (2011), pages 331–338.

[44] I.C. Karagiannis and P.G. Soldatos. “Current status of water desalination in the Aegean Islands”. In: *Desalination* 203.1–3 (2007), pages 56–61.

[45] I.C. Karagiannis and P.G. Soldatos. “Water desalination cost literature: review and assessment”. In: *Desalination European Desalination Society and Center for Research and Technology Hellas (CERTH), Sani Resort 22-25 April 2007*. Edited by editor. 2007, pages 448–456.

[46] Y. Al-Wazzan et al. “Desalting of subsurface water using spiral-wound reverse osmosis (RO) system: technical and economic assessment”. In: *Desalination* 143.1 (2002), pages 21–28.

[47] I.S. Jaber and M.R. Ahmed. “Technical and economic evaluation of brackish groundwater desalination by reverse osmosis (RO) process”. In: *Desalination* 165.0 (2004), pages 209–213.

[48] D. Sambrailo, J. Ivic, and A. Krstulovic. “Economic evaluation of the first desalination plant in Croatia”. In: *Desalination* 179.1–3 (2005), pages 339–344.

[49] Vewin: Vereniging van waterbedrijven in Nederland. *Kerngegevens Drinkwater 2014*. Report. Vewin: Vereniging van waterbedrijven in Nederland, 2014.

[50] M. Wilf. “Fundamentals of RO–NF technology”. In: *International Conference on Desalination Costing, Limassol*.

[51] J.P. MacHarg and S.A. McClellan. “Pressure Exchanger Helps Reduce Energy Costs”. In: *JOURNAL AWWA* (2004), page 45.

[52] W.G.J. van der Meer et al. “Optiflux®: from innovation to realisation”. In: *Desalination* (2003). Desalination and the Environment: Fresh Water for all, pages 159–165.

[53] J.A.M. van Paassen, W.G.J. van der Meer, and Post J. “Optiflux®: from innovation to realisation”. In: *Desalination* (2005). Membranes in Drinking and Industrial Water Production, pages 325–331.

[54] DesalData. *DesalData 2015*. 2015. URL: https://www.desaldata.com.

[55] M.A. Eltawil, Z. Zhengming, and L. Yuan. “A review of renewable energy technologies integrated with desalination systems”. In: *Renewable and Sustainable Energy Reviews* 13.9 (2009), pages 2245–2262.

[56] J. Kucera. “Membranes”. In: *Reverse Osmosis*. John Wiley & Sons, Inc., 2015, pages 49–93.

[57] L.A. Lien. “Spiral-wound membrane with improved permeate carrier”. 4802982. 1989.

[58] G. Schock and A. Miquel. “Mass transfer and pressure loss in spiral wound modules”. In: *Desalination* 64.0 (1987), pages 339–352.

[59] C.P. Koutsou, A.J. Karabelas, and M. Kostoglou. “Membrane desalination under constant water recovery – The effect of module design parameters on system performance”. In: *Separation and Purification Technology* 147 (2015), pages 90–113.

[60] W.G.J. van der Meer. *Mathematical Modelling of NF and RO Membrane Filtration Plants and Modules*. 2003.

[61] C.C. Zimmerer and V. Kottke. “Effects of spacer geometry on pressure drop, mass transfer, mixing behavior and residence time distribution”. In: *Desalination* 104.1-2 (1996), pages 129–134.

[62] J. Johnson and M. Busch. “Engineering Aspects of Reverse Osmosis Module Design”. In: *Desalination and Water Treatment* 15.1-3 (2010), pages 236–248.

[63] J.S. Vrouwenvelder, M.C.M. van Loosdrecht, and J.C. Kruithof. “A novel scenario for biofouling control of spiral wound membrane systems”. In: *Water Research* 45.13 (2011), pages 3890–3898.

[64] R. Franks, C. Bartels, and A. Anit. *Demonstrating improved RO system performance with new Low Differential (LD) technology*. Report. Hydranautics, Oceanside, CA., 2010.

[65] M. Busch and W. E. Mickols. “Reducing energy consumption in seawater desalination”. In: *Desalination* 165 (2004), pages 299–312.

[66] V.G. Molina, M. Busch, and P. Sehn. “Cost savings by novel seawater reverse osmosis elements and design concepts”. In: *Desalination and Water Treatment* 7.1-3 (2009), pages 160–177.

[67] K.P. Lee, T.C. Arnot, and D. Mattia. “A review of reverse osmosis membrane materials for desalination—Development to date and future potential”. In: *Journal of Membrane Science* 370.1–2 (2011), pages 1–22.

[68] J.T. Arena et al. “Surface modification of thin film composite membrane support layers with polydopamine: Enabling use of reverse osmosis membranes in pressure retarded osmosis”. In: *Journal of Membrane Science* 375.1–2 (2011), pages 55–62.

[69] J. Gilron et al. “Effects of surface modification on antifouling and performance properties of reverse osmosis membranes”. In: *Desalination* 140.2 (2001), pages 167–179.

[70] G. Kang et al. “A novel method of surface modification on thin-film composite reverse osmosis membrane by grafting poly(ethylene glycol)”. In: *Polymer* 48.5 (2007), pages 1165–1170.

[71] Q. Li, Z. Xu, and I. Pinnau. “Fouling of reverse osmosis membranes by biopolymers in wastewater secondary effluent: Role of membrane surface properties and initial permeate flux”. In: *Journal of Membrane Science* 290.1-2 (2007), pages 173–181.

[72] J.S. Louie et al. “Effects of polyether–polyamide block copolymer coating on performance and fouling of reverse osmosis membranes”. In: *Journal of Membrane Science* 280.1–2 (2006), pages 762–770.

[73] X. Wei et al. “A novel method of surface modification on thin-film-composite reverse osmosis membrane by grafting hydantoin derivative”. In: *Journal of Membrane Science* 346.1 (2010), pages 152–162.

[74] M. Mulder. *Basic principles of membrane technology*. Kluwer Academic, 1991.

[75] L. Sidney and S. Srinivasa. “High flow porous membranes for separating water from saline solutions”. 3133132. US Patent 3,133,132. 1964.

[76] J.E. Cadotte. “Interfacially synthesized reverse osmosis membrane”. 4277344. US Patent. 1981.

[77] J.E. Cadotte et al. “Interfacial Synthesis in the Preparation of Reverse Osmosis Membranes”. In: *Journal of Macromolecular Science*. 1981.

[78] M.F.A. Goosen et al. “Fouling of Reverse Osmosis and Ultrafiltration Membranes: A Critical Review”. In: *Separation Science and Technology* 39.10 (2005), pages 2261–2297.

[79] J.S. Vrouwenvelder et al. “The Membrane Fouling Simulator: A practical tool for fouling prediction and control”. In: *Journal of Membrane Science* 281.1-2 (2006), pages 316–324.

[80] J. Vrouwenvelder et al. “Monitoring and control of biofouling in nanofiltration and reverse osmosis membranes”. In: (2008).

[81] S. Shirazi, C.J. Lin, and D. Chen. “Inorganic fouling of pressure-driven membrane processes — A critical review”. In: *Desalination* 250.1 (2010), pages 236–248.

[82] L. Song and K. Tay. “Advanced Membrane Fouling Characterization in Full-Scale Reverse Osmosis Processes”. In: *Membrane and Desalination Technologies*. Edited by Lawrence K. Wang et al. 13th edition. Handbook of Environmental Engineering. Humana Press, 2008, pages 101–134.

[83] J.S. Baker and Dudley L.Y. *Biofouling in membrane systems- A review*. Conference Paper. Sept. 1998.

[84] H.F. Ridgway et al. “Microbial fouling of reverse-osmosis membranes used in advanced wastewater treatment technology: chemical, bacteriological and ultrastructural analyses”. In: *Applied and environmental microbiology* 45.3 (1983), pages 1066–1084.

[85] R.P. Schneider et al. “Dynamics of organic carbon and of bacterial populations in a conventional pretreatment train of a reverse osmosis unit experiencing severe biofouling”. In: *Journal of Membrane Science* 266.1-2 (2005), pages 18–29.

[86] K. Tasaka et al. “Analysis of RO elements operated at more than 80 plants in Japan”. In: *Desalination* 96.1 (1994), pages 259–272.

[87] C.L. Chen et al. “Community structure of microbial biofilms associated with membrane-based water purification processes as revealed using a polyphasic approach”. In: *Applied Microbiology and Biotechnology* 63.4 (2004), pages 466–473.

[88] L.A. Bereschenko et al. “Molecular characterization of the bacterial communities in the different compartments of a full-scale reverse-osmosis water purification plant”. In: *Applied and environmental microbiology* 74.17 (2008), pages 5297–5304.

[89] H.C. Flemming et al. “Biofouling—the Achilles heel of membrane processes”. In: *Desalination* 113.2 (1997), pages 215–225.

[90] S. Tsuneda et al. “Extracellular polymeric substances responsible for bacterial adhesion onto solid surface”. In: *FEMS Microbiology Letters* 223.2 (2003), pages 287–292.

[91] J.W. Costerton, Philip S. Stewart, and E.P. Greenberg. “Bacterial biofilms: a common cause of persistent infections”. In: *Science* 284.5418 (1999), pages 1318–1322.

[92] J.S. Vrouwenvelder and D. van Der Kooij. “Integral diagnosis of fouling problems by analysing biomass and inorganic compounds in membrane elements used in water treatment”. In: *Water science and technology: water supply* (2003), pages 211–215.

[93] M.C. Van Loosdrecht et al. “Influence of interfaces on microbial activity”. In: *Microbiological Reviews* 54.1 (1990), pages 75–87.

[94] A. Gjaltema et al. “Adhesion and biofilm development on suspended carriers in airlift reactors: Hydrodynamic conditions versus surface characteristics”. In: *Biotechnology and bioengineering* 55.6 (1997), pages 880–889.

[95] O. Holm-Hansen and C.R. Booth. “The measurement of adenosine triphosphate in the ocean and its ecological significance”. In: *Limnology and Oceanography* (1966), pages 510–519.

[96] C. Coufort et al. “Cohesion and detachment in biofilm systems for different electron acceptor and donors”. In: *Water Science and Technology* 55.8-9 (2007), pages 421–428.

[97] S. Kim et al. “Biofouling of reverse osmosis membranes: Microbial quorum sensing and fouling propensity”. In: *Desalination* 247.1-3 (2009), pages 303–315.

[98] J.S. Vrouwenvelder et al. “Quantitative biofouling diagnosis in full scale nanofiltration and reverse osmosis installations”. In: *Water Research* 42.19 (2008), pages 4856–4868.

[99] J. Mansouri, S. Harrisson, and V. Chen. “Strategies for controlling biofouling in membrane filtration systems: challenges and opportunities”. In: *Journal of Materials Chemistry* 20.22 (2010), pages 4567–4586.

[100] D.A. Graf von der Schulenburg et al. “Nuclear magnetic resonance microscopy studies of membrane biofouling”. In: *Journal of Membrane Science* 323.1 (2008), pages 37–44.

[101] E.R. Cornelissen et al. “Periodic air/water cleaning for control of biofouling in spiral wound membrane elements”. In: *Journal of Membrane Science* 287.1 (2007), pages 94–101.

[102] J.S. Vrouwenvelder et al. “A critical flux to avoid biofouling of spiral wound nanofiltration and reverse osmosis membranes: Fact or fiction?” In: *Journal of Membrane Science* 326.1 (2009), pages 36–44.

[103] H.B. Winzeler and G. Belfort. “Enhanced performance for pressure-driven membrane processes: the argument for fluid instabilities”. In: *Journal of Membrane Science* 80.1 (1993), pages 35–47.

[104] G. Belfort, R.H. Davis, and A.L. Zydney. “The behavior of suspensions and macromolecular solutions in crossflow microfiltration”. In: *Journal of Membrane Science* 96.1 (1994), pages 1–58.

[105] P. Moulin et al. “Mass transfer improvement by secondary flows: Dean vortices in coiled tubular membranes”. In: *Journal of Membrane Science* 114.2 (1996), pages 235–244.

[106] S. Wasche, H. Horn, and D.C. Hempel. “Influence of growth conditions on biofilm development and mass transfer at the bulk/biofilm interface”. In: *Water Research* 36.19 (2002), pages 4775–4784.

[107] S. Wijeyekoon et al. “Effects of substrate loading rate on biofilm structure”. In: *Water Research* 38.10 (2004), pages 2479–2488.

[108] M.C.M. van Loosdrecht et al. “Biofilm structures”. In: *Water Science and Technology* 32.8 (1995), pages 35–43.

[109] B.M. Peyton. “Effects of shear stress and substrate loading rate on Pseudomonas aeruginosa biofilm thickness and density”. In: *Water Research* 30.1 (1996), pages 29–36.

[110] W.K. Kwok et al. “Influence of biomass production and detachment forces on biofilm structures in a biofilm airlift suspension reactor”. In: *Biotechnology and bioengineering* 58.4 (1998), pages 400–407.

[111] L.F. Melo and Bott T.R. “Biofouling in water systems”. In: *Experimental Thermal and Fluid Science* 14.4 (1997), pages 375–381.

[112] M.O. Pereira et al. “Effect of flow regime on the architecture of a Pseudomonas fluorescens biofilm”. In: *Biotechnology and bioengineering* 78.2 (2002), pages 164–171.

[113] J.J. Beun et al. “Aerobic granulation in a sequencing batch reactor”. In: *Water Research* 33.10 (1999), pages 2283–2290.

[114] M.J. Chen, Z. Zhang, and T.R. Bott. “Effects of operating conditions on the adhesive strength of Pseudomonas fluorescens biofilms in tubes”. In: *Colloids and Surfaces B: Biointerfaces* 43.2 (2005), pages 61–71.

[115] B. Purevdorj, J.W. Costerton, and P. Stoodley. “Influence of Hydrodynamics and Cell Signaling on the Structure and Behavior of Pseudomonas aeruginosa Biofilms”. In: *Applied and environmental microbiology* 68.9 (2002), pages 4457–4464.

[116] P.A. Araujo et al. “Impact of feed spacer and membrane modification by hydrophilic, bactericidal and biocidal coating on biofouling control”. In: *Desalination* 295.0 (2012), pages 1–10.

[117] J.S. Vrouwenvelder et al. “Impact of flow regime on pressure drop increase and biomass accumulation and morphology in membrane systems”. In: *Water Research* 44.3 (2010), pages 689–702.

[118] J.Y. Park, C.K. Choi, and J.J. Kim. “A study on dynamic separation of silica slurry using a rotating membrane filter 1. Experiments and filtrate fluxes”. In: *Journal of Membrane Science* 97 (1994), pages 263–273.

[119] L. Ding, C. Charcosset, and M.Y. Jaffrin. “Albumin recovery enhancement in membrane plasma fractionation using pulsatile flow”. In: *The International journal of artificial organs* 14.1 (1991), pages 61–65.

[120] Y. Wang et al. “Simulation of cross-flow filtration for baffled tubular channels and pulsatile flow”. In: *Journal of Membrane Science* 95.3 (1994), pages 243–258.

[121] W.S. Kim, J.K. Park, and H.N. Chang. “Mass transfer in a three-dimensional net-type turbulence promoter”. In: *International Journal of Heat and Mass Transfer* 30.6 (1987), pages 1183–1192.

[122] J. Balster, D.F. Stamatialis, and M. Wessling. “Towards spacer free electrodialysis”. In: *Journal of Membrane Science* 341.1-2 (2009), pages 131–138.

[123] K. Zhang, Z. Cui, and R.W. Field. “Effect of bubble size and frequency on mass transfer in flat sheet MBR”. In: *Journal of Membrane Science* 332.1-2 (2009), pages 30–37.

[124] S. Judd. *The MBR book: principles and applications of membrane bioreactors for water and wastewater treatment*. Elsevier, 2010.

[125] N.V. Ndinisa, A.G. Fane, and D.E. Wiley. “Fouling Control in a Submerged Flat Sheet Membrane System: Part I – Bubbling and Hydrodynamic Effects”. In: *Separation Science and Technology* 41.7 (2006), pages 1383–1409.

[126] N.V. Ndinisa et al. “Fouling Control in a Submerged Flat Sheet Membrane System: Part II—Two-Phase Flow Characterization and CFD Simulations”. In: *Separation Science and Technology* 41.7 (2006), pages 1411–1445.

[127] C. Fritzmann et al. “Microstructured spacers for submerged membrane filtration systems”. In: *Journal of Membrane Science* 446.0 (2013), pages 189–200.

[128] D. Kim et al. “Biocide application for controlling biofouling of SWRO membranes — an overview”. In: *Desalination* 238.1 (2009), pages 43–52.

[129] C. Whittaker, H. Ridgway, and B.H. Olson. “Evaluation of Cleaning Strategies for Removal of Biofilms from Reverse-Osmosis Membranes”. In: *Applied and environmental microbiology* 48.2 (1984), pages 395–403.

[130] A. Al-Amoudi and R.W. Lovitt. “Fouling strategies and the cleaning system of NF membranes and factors affecting cleaning efficiency”. In: *Journal of Membrane Science* 303.1-2 (2007), pages 4–28.

[131] E. Zondervan and B. Roffel. “Evaluation of different cleaning agents used for cleaning ultra filtration membranes fouled by surface water”. In: *Journal of Membrane Science* 304.1-2 (2007), pages 40–49.

[132] S. Patil, F. Harnisch, and U. Schroder. “Toxicity Response of Electroactive Microbial Biofilms-A Decisive Feature for Potential Biosensor and Power Source Applications”. In: *ChemPhysChem* 11.13 (2010), pages 2834–2837.

[133] S. Selvaraj et al. “Toxicity of free and various aminocarboxylic ligands sequestered copper(II) ions to Escherichia coli”. In: *Journal of Hazardous Materials* 166.2-3 (2009), pages 1403–1409.

[134] B.R. Kim et al. “Literature review-efficacy of various disinfectants against Legionella in water systems”. In: *Water Research* 36.18 (2002), pages 4433–4444.

[135] K. Garny, T.R. Neu, and H. Horn. “Sloughing and limited substrate conditions trigger filamentous growth in heterotrophic biofilms-Measurements in flow-through tube reactor”. In: *Chemical Engineering Science* 64.11 (2009), pages 2723–2732.

[136] R.P. Carnahan, Bolin L., and Suratt W. “Biofouling of PVD-1 reverse osmosis elements in the water treatment plant of the City of Dunedin, Florida”. In: *Desalination* 102.1 (1995), pages 235–244.

[137] Z. Cui and T. Taha. “Enhancement of ultrafiltration using gas sparging: a comparison of different membrane modules”. In: *Journal of Chemical Technology & Biotechnology* 78.2-3 (2003), pages 249–253.

[138] J.Q.J.C. Verberk et al. “Hydraulic distribution of water and air over a membrane module using AirFlush”. In: *Water Supply* 2.2 (2002), pages 297–304.

[139] L. Tijhuis et al. “Influence of detachment, substrate loading and reactor scale on the formation of biofilms in airlift reactors”. In: *Applied Microbiology and Biotechnology* 45.1 (1996), pages 7–17.

[140] J.W.N.M. Kappelhof et al. “An in situ biofouling monitor for membrane systems”. In: *Water science and technology: water supply* (2003), pages 205–210.

[141] P. Willems et al. “Use of Particle Imaging Velocimetry to measure liquid velocity profiles in liquid and liquid/gas flows through spacer filled channels”. In: *Journal of Membrane Science* 362.1-2 (2010), pages 143–153.

[142] I.S. Ngene et al. “Particle deposition and biofilm formation on microstructured membranes”. In: *Journal of Membrane Science* 364.1-2 (2010), pages 43–51.

[143] T.S. Coffey. “Diet Coke and Mentos: What is really behind this physical reaction?” In: *American Journal of Physics* 76.6 (2008), pages 551–557.

[144] R. Hausman, T. Gullinkala, and I.C. Escobar. “Development of copper-charged polypropylene feedspacers for biofouling control”. In: *Journal of Membrane Science* 358.1-2 (2010), pages 114–121.

[145] H. Winters and L. Isquith. “A critical evaluation of pretreatment to control fouling in open seawater reverse osmosis—has it been a success?” In: *In Proceedings of the International Desalination Association World Congress on Desalination and Water Reuse*. Volume Vol. 1, pages 255–264.

[146] L.E. Applegate, C.W. Erkenbrecher, and H. Winters. “New chloroamine process to control aftergrowth and biofouling in permasepR B-10 RO surface seawater plants”. In: *Desalination* 74 (1989), pages 51–67.

[147] H. Winters. “Twenty years experience in seawater reverse osmosis and how chemicals in pretreatment affect fouling of membranes”. In: *Desalination* 110.1-2 (1997), pages 93–96.

[148] M. Wilf. “Effect of new generation of low pressure, high salt rejection membranes on power consumption of RO systems”. In: *American Water Works Association Membrane Technology Conference, New Orleans, LA*. 1997.

[149] A.J. Karabelas. "Key issues for improving the design and operation of spiral-wound membrane modules in desalination plants". In: *Desalination and Water Treatment* 52.10-12 (2014), pages 1820–1832.

[150] M. Wilf and C. Bartels. "Optimization of seawater RO systems design". In: *Desalination* 173.1 (2005), pages 1–12.

[151] ROchemicals. *Reverse Osmosis Systems*. URL: http://reverseosmosischemicals.com/reverse-osmosis-guides/reverse-osmosis-glossary-terms/net-driving-pressure-reverse-osmosis-systems.

[152] A.R. Da Costa, A.G. Fane, and D.E. Wiley. "Spacer characterization and pressure drop modelling in spacer-filled channels for ultrafiltration". In: *Journal of Membrane Science* 87.1-2 (1994), pages 79–98.

[153] A.H. Haidari, S.G.J. Heijman, and W.G.J. van der Meer. "Visualization of hydraulic conditions inside the feed channel of Reverse Osmosis: A practical comparison of velocity between empty and spacer-filled channel". In: *Water Research* 106 (2016), pages 232–241.

[154] G. Belfort and G.A. Guter. "An experimental study of electrodialysis hydrodynamics". In: *Desalination* 10.3 (1972), pages 221–262.

[155] D.G. Thomas et al. "Turbulence promoters for hyperfiltration with dynamic membranes". In: *Environmental Science & Technology* 4.12 (1970), pages 1129–1136.

[156] W.G. Light and T.V. Tran. "Improvement of Thin-Channel Design for Pressure-Driven Membrane Systems". In: *Industrial & Engineering Chemistry Process Design and Development* 20.1 (1981), pages 33–40.

[157] A.R. Da Costa et al. "Optimal channel spacer design for ultrafiltration". In: *Journal of Membrane Science* 62.3 (1991), pages 275–291.

[158] S.V. Polyakov and F.N. Karelin. "Turbulence promoter geometry: its influence on salt rejection and pressure losses of a composite-membrane spiral would module". In: *Journal of Membrane Science* 75.3 (1992), pages 205–211.

[159] J. Schwinge et al. "Characterization of a zigzag spacer for ultrafiltration". In: *Journal of Membrane Science* 172.1-2 (2000), pages 19–31.

[160] J.J.S. Shen and R.F. Probstein. "Turbulence Promotion and Hydrodynamic Optimization in an Ultrafiltration Process". In: *Industrial & Engineering Chemistry Process Design and Development* 18.3 (1979), pages 547–554.

[161] P.A. Araújo et al. "The potential of standard and modified feed spacers for biofouling control". In: *Journal of Membrane Science* 403-404.0 (2012), pages 58–70.

[162] D.G. Thomas. "Forced Convection Mass Transfer in Hyperfiltration at High Fluxes". In: *Industrial and Engineering Chemistry Fundamentals* 12.4 (1973), pages 396–405.

[163] O. Kuroda, S. Takahashi, and M. Nomura. "Characteristics of flow and mass transfer rate in an electrodialyzer compartment including spacer". In: *Desalination* 46.1 (1983), pages 225–232.

[164] F. Schwager, P.M. Robertson, and N. Ibl. “The use of eddy promoters for the enhancement of mass transport in electrolytic cells”. In: *Electrochimica Acta* 25.12 (1980), pages 1655–1665.

[165] H. Chang et al. “CFD Study of Heat Transfer Enhanced Membrane Distillation Using Spacer-Filled Channels”. In: *Energy Procedia* 75 (2015), pages 3213–3219.

[166] P. Feron and G.S. Solt. “The influence of separators on hydrodynamics and mass transfer in narrow cells: Flow visualisation”. In: *Desalination* 84.1-3 (1991), pages 137–152.

[167] C.P. Koutsou, S.G. Yiantsios, and A.J. Karabelas. “Direct numerical simulation of flow in spacer-filled channels: Effect of spacer geometrical characteristics”. In: *Journal of Membrane Science* 291.1-2 (2007), pages 53–69.

[168] A.H. Haidari, S.G.J. Heijman, and W.G.J. van der Meer. “Effect of spacer configuration on hydraulic conditions using PIV”. 2017.

[169] J. Balster et al. “Multi-layer spacer geometries with improved mass transport”. In: *Journal of Membrane Science* 282.1-2 (2006), pages 351–361.

[170] F. Li et al. “Optimization of non-woven spacers by CFD and validation by experiments”. In: *Desalination* 146.1-3 (2002), pages 209–212.

[171] M.S. Isaacson and A.A. Sonin. “Sherwood Number and Friction Factor Correlations for Electrodialysis Systems, with Application to Process Optimization”. In: *Industrial & Engineering Chemistry Process Design and Development* 15.2 (1976), pages 313–321.

[172] R. Darby. *Chemical Engineering Fluid Mechanics, Revised and Expanded*. Taylor & Francis, 2001.

[173] P.J. Hickey and C.H. Gooding. “Proceedings of Sixth International Conference on Pervaporation Processes in the Chemical Industry”. In: *Pervaporation processes in the chemical industry*. Edited by Bakish Materials Corporation. Volume 06. Bakish Materials Corporation, 1992, pages 153–169.

[174] D. van Gauwbergen and J. Baeyens. “Macroscopic fluid flow conditions in spiral-wound membrane elements”. In: *Desalination* 110.3 (1997), pages 287–299.

[175] J.P. Du Plessis and M.R. Collins. “A new definition for laminar flow entrance lengths of straight ducts”. In: *N&O Joernaal* 25 (1992), pages 11–16.

[176] C. Berner, F. Durst, and D.M. Mceligot. “Flow around baffles”. In: *Journal of heat transfer* 106.4 (1984), pages 743–749.

[177] V. Geraldes, V. Semiao, and M.N. de Pinho. “Flow management in nanofiltration spiral wound modules with ladder-type spacers”. In: *Journal of Membrane Science* 203.1-2 (2002), pages 87–102.

[178] R.B. Bird, W.E. Stewart, and E.N. Lightfoot. *Transport Phenomena*. Wiley, 2007.

[179] E. Pellerin et al. “Turbulent transport in membrane modules by CFD simulation in two dimensions”. In: *Journal of Membrane Science* 100.2 (1995), pages 139–153.

[180] G.A. Fimbres-Weihs and D.E. Wiley. “Review of 3D-CFD modeling of flow and mass transfer in narrow spacer-filled channels in membrane modules”. In: *Chemical Engineering and Processing: Process Intensification* 49.7 (2010). Process Intensification on Intensified Transport by Complex Geometries, pages 759–781.

[181] F.R. Menter. “Two-equation eddy-viscosity turbulence models for engineering applications”. In: *AIAA Journal* 32.8 (1994), pages 1598–1605.

[182] A.A. Sonin and M.S. Isaacson. “Optimization of Flow Design in Forced Flow Electrochemical Systems, with Special Application to Electrodialysis”. In: *Industrial & Engineering Chemistry Process Design and Development* 13.3 (1974), pages 241–248.

[183] Y. Winograd, A. Solan, and M. Toren. “Mass transfer in narrow channels in the presence of turbulence promoters”. In: *Desalination* 13.2 (1973), pages 171–186.

[184] D.G. Thomas and J.S. Watson. “Hyperfiltration. Reduction of Concentration Polarization of Dynamically Formed Hyperfiltration Membranes by Detached Turbulence Promoters”. In: *Industrial & Engineering Chemistry Process Design and Development* 7.3 (1968), pages 397–401.

[185] D.G. Thomas and Watson J.S. *Hyperfiltration. Reduction of Concentration Polarization of Dynamically Formed Hyperfiltration Membranes by Detached Turbulence Promoters.* 1968.

[186] D.G. Thomas. “Estimation of Concentration Polarization for Ion-Exclusion Hyperfiltration Membranes with Turbulent Flow”. In: *Industrial & Engineering Chemistry Fundamentals* 11.3 (1972), pages 302–307.

[187] J.J.S. Shen and R.F. Probstein. “On the Prediction of Limiting Flux in Laminar Ultrafiltration of Macromolecular Solutions”. In: *Industrial & Engineering Chemistry Fundamentals* 16.4 (1977), pages 459–465.

[188] Y. Taniguchi. “An analysis of reverse osmosis characteristics of ROGA spiral-wound modules”. In: *Desalination* 25.1 (1978), pages 71–88.

[189] J.L.C. Santos et al. “Investigation of flow patterns and mass transfer in membrane module channels filled with flow-aligned spacers using computational fluid dynamics (CFD)”. In: *Journal of Membrane Science* 305.1–2 (2007), pages 103–117.

[190] H. Ohya and Y. Taniguchi. “An analysis of reverse osmotic characteristics of ROGA-4000 spiral-wound module”. In: *Desalination* 16.3 (1975), pages 359–373.

[191] Z. Cao, D.E. Wiley, and A.G. Fane. “CFD simulations of net-type turbulence promoters in a narrow channel”. In: *Journal of Membrane Science* 185.2 (2001), pages 157–176.

[192] J.S. Vrouwenvelder et al. “The Membrane Fouling Simulator as a new tool for biofouling control of spiral-wound membranes”. In: *Desalination* 204.1 (2007), pages 170–174.

[193] S.A. Creber et al. “Chemical cleaning of biofouling in reverse osmosis membranes evaluated using magnetic resonance imaging”. In: *Journal of Membrane Science* 362.1-2 (2010), pages 202–210.

[194] S. Avlonitis, W.T. Hanbury, and M.B. Boudinar. “Spiral wound modules performance. An analytical solution, part I.” In: *Desalination* 81.1 (1991), pages 191–208.

[195] S. Avlonitis, W.T. Hanbury, and M.B. Boudinar. “Spiral wound modules performance an analytical solution: Part II”. In: *Desalination* 89.3 (1993), pages 227–246.

[196] S.K. In and N.C. Ho. “The effect of turbulence promoters on mass transfer - numerical analysis and flow visualization”. In: *International Journal of Heat and Mass Transfer* 25.8 (1982), pages 1167–1181.

[197] V. Geraldes, V. Semiao, and M.N. de Pinho. “The effect of the ladder-type spacers configuration in NF spiral-wound modules on the concentration boundary layers disruption”. In: *Desalination* 146.1-3 (2002), pages 187–194.

[198] G.A.F. Weihs. “Numerical Simulation Studies of Mass Transfer under Steady and Unsteady Fluid Flow in Two- and Three-Dimensional Spacer-Filled Channels”. Thesis. 2008.

[199] R. Ghidossi, D. Veyret, and P. Moulin. “Computational fluid dynamics applied to membranes: State of the art and opportunities”. In: *Chemical Engineering and Processing: Process Intensification* 45.6 (2006), pages 437–454.

[200] C. Gaucher et al. “Hydrodynamics study in a plane ultrafiltration module using an electrochemical method and particle image velocimetry visualization”. In: *Experiments in Fluids* 32.3 (2002), pages 283–293.

[201] M. Raffel, C.E. Willert, and J. Kompenhans. *Particle Image Velocimetry: A Practical Guide*. Engineering online library. Springer, 1998.

[202] R.J. Adrian. “Twenty years of particle image velocimetry”. In: *Experiments in Fluids* 39.2 (2005), pages 159–169.

[203] M. Gimmelshtein and R. Semiat. “Investigation of flow next to membrane walls”. In: *Journal of Membrane Science* 264.1-2 (2005), pages 137–150.

[204] M. Oinuma, S. Sawada, and K. Yabe. “New pretreatment systems using membrane separation technology”. In: *Desalination* 98.1-3 (1994), pages 59–69.

[205] F. Li et al. “Novel spacers for mass transfer enhancement in membrane separations”. In: *Journal of Membrane Science* 253.1-2 (2005), pages 1–12.

[206] R.G. Chapman et al. “Polymeric Thin Films That Resist the Adsorption of Proteins and the Adhesion of Bacteria”. In: *Langmuir* 17.4 (2001), pages 1225–1233.

[207] A. Roosjen et al. “Inhibition of adhesion of yeasts and bacteria by poly(ethylene oxide)-brushes on glass in a parallel plate flow chamber”. In: *Microbiology* 149.11 (2003), pages 3239–3246.

[208] I. Cringus-Fundeanu et al. “Synthesis and Characterization of Surface-Grafted Polyacrylamide Brushes and Their Inhibition of Microbial Adhesion”. In: *Langmuir* 23.9 (2007). PMID: 17388616, pages 5120–5126.

[209] J.E. Raynor et al. “Controlling Cell Adhesion to Titanium: Functionalization of Poly[oligo(ethylene glycol)methacrylate] Brushes with Cell-Adhesive Peptides”. In: *Advanced Materials* 19.13 (2007), pages 1724–1728.

[210] A.M. Brzozowska et al. “On the stability of the polymer brushes formed by adsorption of Ionomer Complexes on hydrophilic and hydrophobic surfaces”. In: *Journal of Colloid and Interface Science* 353.2 (2011), pages 380–391.

[211] A.L. Ahmad et al. “Integrated CFD simulation of concentration polarization in narrow membrane channel”. In: *Computers & Chemical Engineering* 29.10 (2005), pages 2087–2095.

[212] T. Icoz and Y. Jaluria. “Design Optimization of Size and Geometry of Vortex Promoter in a Two-Dimensional Channel”. In: *Journal of Heat Transfer* 128.10 (2006), pages 1081–1092.

[213] M. Amokrane et al. “New spacer designs for the performance improvement of the zigzag spacer configuration in spiral-wound membrane modules”. In: *Desalination and Water Treatment* 57.12 (2016), pages 5266–5274.

[214] A.L. Ahmad and K.K. Lau. “Impact of different spacer filaments geometries on 2D unsteady hydrodynamics and concentration polarization in spiral wound membrane channel”. In: *Journal of Membrane Science* 286.1-2 (2006), pages 77–92.

[215] A.I. Radu et al. “Spacer geometry and particle deposition in spiral wound membrane feed channels”. In: *Water Research* 64 (2014), pages 160–176.

[216] Y. Chen, M. Fiebig, and N.K. Mitra. “Conjugate heat transfer of a finned oval tube with a punched longitudinal vortex generator in form of a delta wingletGÇöparametric investigations of the winglet”. In: *International Journal of Heat and Mass Transfer* 41.23 (1998), pages 3961–3978.

[217] G.A. Fimbres-Weihs and D.E. Wiley. “Numerical study of mass transfer in three-dimensional spacer-filled narrow channels with steady flow”. In: *Journal of Membrane Science* 306.1–2 (2007), pages 228–243.

[218] P.E.M. Majamaa K.and Aerts et al. “Industrial water reuse with integrated membrane system increases the sustainability of the chemical manufacturing”. In: *Desalination and Water Treatment* 18.1-3 (2010), pages 17–23.

[219] J. Schwinge, D.E. Wiley, and A.G. Fane. “Novel spacer design improves observed flux”. In: *Journal of Membrane Science* 229.1-2 (2004), pages 53–61.

[220] S.K. Karode and A. Kumar. “Flow visualization through spacer filled channels by computational fluid dynamics I.: Pressure drop and shear rate calculations for flat sheet geometry”. In: *Journal of Membrane Science* 193.1 (2001), pages 69–84.

[221] C.T. Crowe et al. “Multiphase Flows with Droplets and Particles”. In: Taylor & Francis, 1997.

[222] H. Klank et al. “PIV measurements in a microfluidic 3D-sheathing structure with three-dimensional flow behaviour”. In: *Journal of Micromechanics and Microengineering* 12.6 (2002), page 862.

[223] J.S. Vrouwenvelder et al. “Tools for fouling diagnosis of NF and RO membranes and assessment of the fouling potential of feed water”. In: *Desalination* 157.1–3 (2003). Desalination and the Environment: Fresh Water for all, pages 361–365.

[224] P. Schausberger et al. “Simulation of protein ultrafiltration using CFD: Comparison of concentration polarisation and fouling effects with filtration and protein adsorption experiments”. In: *Journal of Membrane Science* 337.1–2 (2009), pages 1–8.

[225] J. Schwinge et al. “Estimation of foulant deposition across the leaf of a spiral-wound module”. In: *Desalination* 146.1-3 (2002), pages 203–208.

[226] K.W.K. Yee, D.E. Wiley, and J. Bao. “A unified model of the time dependence of flux decline for the long-term ultrafiltration of whey”. In: *Journal of Membrane Science* 332.1–2 (2009), pages 69–80.

[227] W.L. Oberkampf and T.G. Trucano. “Verification and validation in computational fluid dynamics”. In: *Progress in Aerospace Sciences* 38.3 (2002), pages 209–272.

[228] F. Li et al. “Optimization of commercial net spacers in spiral wound membrane modules”. In: *Journal of Membrane Science* 208.1-2 (2002), pages 289–302.

[229] K.K. Lau et al. “Feed spacer mesh angle: 3D modeling, simulation and optimization based on unsteady hydrodynamic in spiral wound membrane channel”. In: *Journal of Membrane Science* 343.1-2 (2009), pages 16–33.

[230] Sz.S. Bucs et al. “Effect of different commercial feed spacers on biofouling of reverse osmosis membrane systems: A numerical study”. In: *Desalination* 343 (2014), pages 26–37.

[231] Y.Y. Liang et al. “CFD modelling of unsteady electro-osmotic permeate flux enhancement in membrane systems”. In: *Chemical Engineering Science* 146 (2016), pages 189–198.

[232] J.S. Vrouwenvelder et al. “Biofouling in spiral wound membrane systems: Three-dimensional CFD model based evaluation of experimental data”. In: *Journal of Membrane Science* 346.1 (2010), pages 71–85.

[233] L.B. de Chazournes. *Fresh Water in International Law*. 2013.

[234] C.M. Wong et al. *World’s top 10 rivers at risk*. Report. WWF Global Freshwater Programme, Mar. 2007.

[235] *Pressure drop membrane damage and biofouling the primary challenges in Reverse Osmosis*. 2016. URL: http://www.conwedplastics.com/files/2614/2834/6954/CWD_RO_Series_Primary_Challenges_in_Reverse_Osmosis.pdf.

[236] W.G.J. van der Meer and J.C. van Dijk. “Theoretical optimization of spiral-wound and capillary nanofiltration modules”. In: *Desalination* 113.2–3 (1997), pages 129–146.

[237] V. Geraldes, V. Semiao, and M.N. de Pinho. “Flow management in nanofiltration spiral wound modules with ladder-type spacers”. In: *Journal of Membrane Science* 203.1–2 (2002), pages 87–102.

[238] V. Geraldes, V. Semiao, and M.N. Pinho. “Hydrodynamics and concentration polarization in NF/RO spiral-wound modules with ladder-type spacers”. In: *Desalination* 157.1 (2003), pages 395–402.

[239] S.S. Bucs et al. “Effect of different commercial feed spacers on biofouling of reverse osmosis membrane systems: A numerical study”. In: *Desalination* 343 (2014), pages 26–37.

[240] B. McKeon et al. “Velocity, Vorticity and Mach Number”. In: *Springer Handbook of Experimental Fluid Mechanics*. Edited by Cameron Tropea, Alexander L. Yarin, and John F. Foss. Berlin, Heidelberg: Springer Berlin Heidelberg, 2007, pages 215–471.

[241] L.B. de Chazournes. *Fresh Water in International Law*. 2013.

[242] C.P. Koutsou, S.G. Yiantsios, and A.J. Karabelas. “A numerical and experimental study of mass transfer in spacer-filled channels: Effects of spacer geometrical characteristics and Schmidt number”. In: *Journal of Membrane Science* 326.1 (2009), pages 234–251.

[243] V. Yakhot and S.A. Orszag. “Renormalization group analysis of turbulence. I. Basic theory”. In: *Journal of Scientific Computing* 1.1 (1986), pages 3–51.

[244] J. Schwinge, D.E. Wiley, and D.F. Fletcher. “Simulation of Unsteady Flow and Vortex Shedding for Narrow Spacer-Filled Channels”. In: *Industrial & Engineering Chemistry Research* 42.20 (2003), pages 4962–4977.

Acknowledgements

At this point, it is apparent to me that the overwhelming work of making a technical setup, running the experiments and writing the results was impossible without the direct and indirect help and great support of my family, supervisors, colleagues, and friends. Of course, it would be impossible to name all parties and people who contributed to the creation of this work and therefore, I apologize profusely to anyone whose contribution may have been overlooked.
In the first place, I would like to acknowledge Vitens Water Company, the Netherlands, for funding this research. Certain individuals provided a foundation for making the setup, understand the results and writing of several papers. In this context, firstly, I would like to express my most sincere gratitude to my promoter, Professor Walter van de Meer from the Delft University of Technology and the CEO of Oasen Water Company, who provides me with required encouragement and advice and keep me motivated through this thesis. I am deeply grateful for his support and the belief he has shown in me.
I would also like to thank Doctor Bas Heijman of the Delft University of Technology for his guidance, insightful discussions and keeping me motivated.
In special occasions, I got scientific support from Professor Wim Uijttewaal and Doctor Cristian Picioreanu of the Delft University of Technology; Doctor Harry Timmer and Doctor Bastiaan Blankert of Oasen Water Company, whom I gratefully thank for their support.
I could not go on without mentioning my fellow students, co-workers, and friends at the Delft University of Technology, some of whom have come and gone, and some who are still there.
Making of the setup was possible without the help and support of many University staff. I would like to particularly thank Sander de Vree for his support and providing me with insightful, practical advice.
I would also like to thank Alex Olive and Doctor Jasmina Doekhi Bennani who helped me to make picture with Atomic Force Microscopy (AFM).

Finally, I would like to especially thank my wife, Sodabeh Banaei, whose patience has been endless, and her support everlasting, and my son, Amirali, for being a source of everyday motivation for all of my efforts in all aspects of the life.

Amir Hoseen Haidari
Delft, September 2017

Curriculum Vitæ

Amir Hoseen HAIDARI

21-03-1978	Born in Herat, Afghanistan

EDUCATION

2001–2002	Hogeschool Inholland Learning Dutch
2002–2006	Hogeschool van Amsterdam HBO Bachelor degree in Civil Engineering Followed the structural engineering Graduated on geo-technic construction and modeling
2006–2007	Leiden University Foundational courses on Persian literature and culture
2007–2017	Delft University of Technology
2007–2008	University bachelor degree in Civil engineering
2008–2011	MSc degree in Civil engineering Thesis: silica scaling in Reverse Osmosis (RO) for using RO as the pretreatment for Eutectic freeze crystallization
2011–2015	PhD *Thesis:* One Step Membrane Filtration: The first step *Promoter:* Prof. dr. W.G.J. van der Meer
2015–Now	Scientific coordinator Professional Doctorate Engineering (PDEng)
2015–Now	Scientific coordinator and lecturer online Membrane Professional Education (ProfEd)

List of Publications

7. **B.J. Gonzalez, S.G.J. Heijman, A.H. Haidari, L.C. Rietveld and D. van Halem**, *As(V) rejection by NF membranes for drinking water from high temperature sources*, submitted to Journal of Desalination

6. **A.H. Haidari, S.G.J. Heijman, W.G.J. and van der Meer**, *Permeate treatment of reverse osmosis:Scaling at high temperature*, submitted to Journal of Desalination

5. **A.H. Haidari, S.G.J. Heijman, W.G.J. and van der Meer**, *Spacers: the optimal design for reverse osmosis*, submitted to Journal of Separation and Purification Technology

4. **A.H. Haidari, S.G.J. Heijman, W.G.J. and van der Meer**, *Effect of spacer configuration on hydraulic conditions using PIV*, submitted to Journal of Membrane Science

3. **A.H. Haidari, S.G.J. Heijman, W.G.J. and van der Meer**, *Determining effects of spacer orientations on channel hydraulic conditions using PIV*, submitted to Journal of Membrane Science

2. **A.H. Haidari, S.G.J. Heijman, W.G.J. and van der Meer**, *Visualization of hydraulic conditions inside the feed channel of Reverse Osmosis: A practical comparison of velocity between empty and spacer-filled channel*, Journal of Water Research **106**, 232-241 (2016).

1. **A.H. Haidari, B. Blankert, H. Timmer, S.G.J. Heijman, W.G.J. and van der Meer** , *PURO: A unique RO-design for brackish groundwater treatment*, Journal of Desalination **403**, 208-216 (2017).

Amir Hoseen Haidari